POLYMER GEL: KINETIC, DYNAMIC STUDIES AND ITS APPLICATIONS AS BIOMATERIALS

Changjie Wang, B.S., M.S.

Dissertation Prepared for the Degree of

DOCTOR OF PHILOSOPHY

UNIVERSITY OF NORTH TEXAS

December 2003

APPROVED:

Zhibing Hu, Major Professor
William D. Deering, Committee Member
Paolo Grigolini, Committee Member
Samuel E. Matteson, Committee Member
Sandra L. Terrell, Interim Dean of the Robert B. Toulouse School of Graduate Studies

Wang, Changjie, Polymer Gels: Kinetics, Dynamics Studies and Their Applications as Biomaterials. Doctor of Philosophy (Physics), December 2003, 138 pp., 3 tables, 33 illustrations, reference list, 111 titles.

The polymer gels especially hydrogels have a very special structure and useful features such as unusual volume phase transition, compatibility with biological systems, and sensitivity to environmental stimuli (temperature, pH value, electric field, light and more), which lead to many potential applications in physical and biochemical fields.

This research includes: (1) the theoretical and experimental studies of polymer gels on swelling kinetics, spinodal decomposition, and solution convection in gel matrix; (2) applications of polymer gels in wound dressing, tissue-simulating optical phantom and gel display.

The kinetics of gel swelling has been theoretically analyzed by considering coupled motions of both solvent and polymer network. Analytical solutions of the solvent and the network movement are derived from collective diffusion equations for a long cylindrical and a large disk gel. Kinetics of spinodal decomposition of N-isopropylacrylamide (NIPA) polymer gel is investigated using turbidity and ultrasonic techniques. By probing movement of domains, a possible time-dependent gel structure in the spinodal decomposition region is presented. Theoretical studies of solution convection in gel matrix have been done and more analysis on dimensionless parameters is provided.

To enhance the drug uptake and release capacity of silicone rubber (SR), NIPA hydrogel particles have been incorporated into a SR membrane. This SR/NIPA

composite gel has promising attributes for wound dressing and other uses. Tissue-simulating optical phantom has been synthesized and studied using NIPA solution trapped inside a hydrogel. Polymer gels with engineered surface patterns were implemented. NIPA gel deposited on the surface of an acrylamide gel can be used as responsive gel display. A dynamically measurement technique of local shear modulus and swelling ratio of gel is presented based on an engineered periodic surface pattern as square array.

ACKNOWLEDGMENTS

The author gratefully acknowledges major professor Dr. Zhibing Hu for his guidance.

Special thanks are extended to Dr. Yong Li in Kimberly-Clark Co., for his fruitful discussion.

Appreciation and thanks to my family for consistent support in many ways.

Financial support for this research was provided by the U.S. Army Research Office and Petroleum Fund, administrated by the American Chemical Society.

TABLE OF CONTENTS

LIST OF TABLES

LIST OF ILLUSTRATIONS

Figure Page

CHAPTER 1

INTRODUCTION

A polymer gel is a network formed by cross-linked long chain molecules. Polymer gel is one category of polymer materials with a unique network structure. One gel is a molecule. It is normally immersed in a liquid medium. So a gel consists of two parts, crossed linked network and liquid filled inside the network. Its characteristic is between solid and liquid, depending on temperature and time scale. In higher temperature and slower time scale, gel behaves more like liquid. In lower temperature and faster time scale, gel behaves more like solid. In general, it has viscous behavior as liquid and also elastic behavior as solid, which is referred to as viscoelastic behavior.

If a gel has water as liquid medium inside network, it is referred to as hydrogel. Hydrogel is a very important type, and surely will be the most important type of gels as biomaterials because of its biocompatibility and unique structure. Actually, many biological organs are gels such as cornea, and vitreous humor that fills the interior of the

eye. Many organic materials are natural materials such as cellulose, jello, and bean curd. Originated from network structure, liquid associated, temperature or environment responsive, and time-scale dependent features, the uniqueness of gels makes them match the diversity and complicated responsiveness of biomaterials. Gel applications range from diapers, drug delivery, wound dressing, synthesized organs, food, display, polymer dispersed liquid crystal (PDLC), photonic crystal, to many more. This list will be extended as researches in gel extend.

This dissertation will focus on hydrogel including synthesis, kinetics, dynamics, characterization, and applications of polymer gel as biomaterials.

Chapter 2 analyzes swelling kinetics of gel in pure solution and polymer chain solution, and convection inside gel. Chapter 3 studies spinodal decomposition in N-isopropylacrylamide gel. Chapter 4 is on engineered gel surface pattern and applications. Chapter 5 focuses on synthesis and applications of two gel composites as biomaterial: silicone/N-Isopropylacrylamide (NIPA) gel for wound dressing and NIPA/polyacrylamide gel system as tissue-simulating optical phantom. Chapter 6 provides a brief summary.

1.1 GEL SWELLING KINETICS

Kinetics of gel swelling process has been an interesting topic because swelling behaviors are related to many applications ranging from controlled drug release to gel actuators.

Tanaka, Hocker and Benedek (THB) first derived the theory of swelling of gel networks from the theory of elasticity. In this work, the spectrum of light scattered from thermally excited displacement fluctuations in polyacrylamide gels was measured on the polarized scattered light. A theory for amplitude and time dependence of gel networks under thermal excitations was presented.

Tanaka and Fillmore have used that theory to describe the swelling kinetics of spherical gels, assuming that the shear modulus of the gel is negligible compared with the osmotic bulk modulus. They have found that the relaxation time is proportional to the square of linear size of the gel and inversely proportional to the collective diffusion constant of the network. The gel size dependence of swelling and gel volume phase transition reveals a globally associated behavior and a slow response of gels. Later, Peters and Candau, extended Tanaka and Fillmore's model for long cylindrical and large disk gels in which the shear modulus can not be neglected.

All these works had been done with an assumption that the motion of the solvent inside of gel network is zero. This assumption, however, is only true for spherical gels. In general, the motion of the solvent directly contributes to swelling kinetics. Except the case of spherical gels, the swelling process changes both bulk and shear energy of the polymer network. The solvent motion helps the gel to minimize the total energy. The motion field of solvent strongly depends on the geometry of the gel and plays an important role in friction force and swelling kinetics.

Recently, Li and Tanaka (L-T) have proposed a theory on gel swelling kinetics with arbitrary shapes. Instead of directly dealing with motion of both network and solvent, they decomposed the swelling process into two imaginary processes. The first

process is a pure network diffusion process described by a collective diffusion equation with zero solvent velocity. In the second process, the solvent moves together with the network so that the solvent velocity is the same as the network velocity.

Chapter 2.2 presents a theoretical analysis of kinetics of gel swelling and solvent motion by directly solving coupled motion between network and solvent for long cylindrical and large disk gels. It is also found that the solvent motion can be independently derived from L-T's isotropic condition (minimum shear energy) and continuity condition without solving the coupled collective diffusion equations.

1.2 GEL SWELLING IN POLYMER SOLUTION

In chapter 2.3, swelling of a long cylindrical gel in aqueous polymer solution has also been studied here theoretically and experimentally. In a polymer solution, polymer chains are long and randomly coiled and tangled. Statistically, randomly coiled chains are too larger compared to the mesh size of gel network. If a gel is immersed into polymer solution, polymers chains could not freely penetrate into gel network. So the surface of a gel in polymer solution is not free of stress. It is the partial pressure of polymer chains in the solution that acts on the surface of the gel network because the polymer chains can’t go in and out of network freely. In this case, the boundary condition should be modified. For the condition that the volume of the polymer solution is much great than the relative swelling volume of gel network, the partial pressure of polymer in solution should be a constant. Experiments were done, and the results are analyzed using the theony.

1.3 CONVECTION INSIDE GEL

In chapter 2.4, the topic is convection in polymer gel. Convection in horizontal layers has become one of the most basic and widely investigated topics in fluid dynamics. When a horizontal layer of fluid is heated from below, it may undergo Rayleigh-Benard convection due to intrinsic instability. As an analogous form of convection in porous media, convection can occur for a fluid-saturated matrix. Here we propose to study convection in polymer gel. A gel consists of both network and solvent. The solvent in a gel can be divided into two classes. One is free solvent that can move through a polymer network and the other is bound solvent that is bonded to the network and can't move freely against gel network. The relevant part to this research is the free solvent in gels. When a thin horizontal layer of gel is heated from below, a temperature difference is created across a layer of height d. We have derived the governing equations for the gel system and found that the dominant term is the friction between the fluid and the polymer network.

The friction coefficient of the gel can be adjusted by either changing the polymer network concentration or the environmental temperature. The temperature dependence of friction coefficient is particularly interesting. According to previous studies that the effective pore size becomes larger and appears to diverge as the gel approaches to its phase transition temperature. The friction coefficient between solvent and network is expected to be very small. Then the convection in the gel system would be equivalent or close to the convection in a liquid system.

1.4 SPINODAL DECOMPOSITION

In Chapter 3, spinodal decomposition has been studied. Spinodal decomposition remains as one of the most active areas in study of the phase transition and has been investigated extensively for various systems including polymer blends, binary liquids, polymeric liquids, and binary gases. Because the chemically crosslinked polymer gels have a unique structure with a three-dimensional network immersed in a solvent, spinodal decomposition in gels is constrained by the elasticity of the gel network. As a result, spinodal decomposition in gels could exhibit significant and interesting properties that are different from those in polymer solutions. Extensive studies of spinodal decomposition in polymer gels have been carried out including theoretical discussion of spinodal curves of a gel, the turbidity study of phase separation in polyethylene glycol methacrylate-glycol-water, and experimental observations of phase transition and the spinodal decomposition of gels.

The NIPA polymer gel is a model system that has a large, reversible volume change in response to environmental temperature changes under atmospheric pressure. Specifically, the NIPA gel in water is transparent and swollen at room temperature. Upon heating, the gel shrinks and eventually collapses at a critical temperature (T_c) of about 34 ^{0}C. The NIPA gel exhibits critical behavior similar to the Ising system. When a typical critical phase-transition system undergoes a transition from the one-phase state to the two-phase coexistent state along the critical isochore path, the spinodal decomposition occurs. The beginning of the spinodal decomposition in the NIPA gel is marked by the

transition from a transparent gel to a cloudy gel. The initial stages if spinodal decomposition in NIPA gels have been studied using light scattering, turbidity, and small-angle X-ray techniques and can be analyzed using Cahn-Hilliard-Cook (CHC) theory. The shrinking kinetics of the NIPA gel after it is heated from below T_c to above T_c have been studied in details by Hirose and coworkers. They correlated NIPA chemical composition (monomer concentration and crosslinker density) with shrinking kinetics and bubble formation in the gel surfaces.

All previous studies of spinodal decomposition in the NIPA gel have focused on the kinetics of gel-volume change. In this section, it is the aim to report that associated with volume shrinking in the spinodal decomposition regime, gel turbidity undergoes significant change. Comparing measurements from two well-separated windows opened with an ultrasonic probe (λ=150 μm) and a visible light probe (λ=550 nm), we propose a qualitative picture of structural evolution during the decomposition process. Better understanding of the spinodal decomposition in gels may lead to the development of new technologies ranging from smart windows and optical displays to ultrasonic attenuators.

1.5 ENGINEERED GEL SURFACE PATTERN AND APPLICATIONS

In chapter 4, engineered surface patterns are synthesized, studied, and their applications are demonstrated.

The surface structures of hydrogels play important roles for many potential applications in physical, chemical and biomedical fields. Extensive efforts have been directed to study the natural surface structure of gels. Surface patterns have been

observed during gel swelling or shrinking processes, and caused by mechanical instability and constraints. The study of these patterns can lead to better understanding of the formation and evolution of patterns found in biological systems. On the other hand, it is not only desirable but also vital to modify gel surfaces in order to better control interactions between the gel surfaces and environments that are required for many applications. This chapter will provide synthesis and application of engineered surface patterns on environmentally responsive polymer gels. The central idea is to precisely control the local properties of one gel surface by incorporating different materials onto given areas selected with a mask. The first example is a NIPA gel covered by a square array of gold using sputter-deposition method. The periodicity of the surface array can be continuously tuned by external stimuli such as temperature and electric field. The periodic array produced on the gel surface can serve as a grating for optical filter and sensors applications. Its applications include shear modulus and swelling ratio in a local area. The second example is to deposit NIPA polymer gel on the surface of an acrylamide gel. The pattern of the NIPA deposited area can be either visible or invisible by simply switching temperature above or below the low critical solution temperature (LCST) of the NIPA gel. Such gels can be used as displays and sensors.

1.6 COMPOSITE SILICON/HYDROGEL MEMBRANE

The unique properties of hydrogels include but not limit to the compatibilities with biological environment and spinodal decomposition. The composite materials made from hydrogel may inherit above unique properties of hydrogels and open a door for

broad options to modify, fine tune, and combine the properties of each components in the composite, so would provide more potential applications in biomedical area.

As a first example, NIPA gel was incorporated into silicone rubber to composite materials for wound dressing with improved and enhanced absorption than that of pure silicone in past usage.

A numerous of dressing have been applied to wounds in the past centuries with functions of protection, support and absorption. Among them are films, hydrocolloids, hydrogels, and composite dressing. A dressing is no longer a passive adjunct to healing, but is an active element of wound management. Silicone rubber is used in wound healing dressings, it has good strength and flexibility, and is generally considered to be biocompatible. The water impermeability of silicone rubber has been shown to reduce evaporation fluid loss and maintain the moisture level. However, the water absorption of silicone rubber is almost zero, which strongly limits silicone rubber from fully functioning as drug releasing wound dressing or for exudate absorption and so on.

In this study, NIPA hydrogel micro-particles were synthesized and incorporated into silicone rubber. The NIPA gel is hydrophilic and swells in water when $T<T_c$, which is about 34 ^{0}C. While $T>T_c$, NIPA gel becomes hydrophobic and collapses into a small volume. Such unusual properties suggest various applications including controlled drug delivery and sensors. In this SR/NIPA composite membrane, the absorption ability has been drastically enhanced. The composite gel can absorb water equal to about its dry weight. Furthermore, as a drug delivery system, this membrane's release rate changes due to changes of environmental temperature. The silicone/NIPA composite membrane will be studied in chapter 5.2.

1.7 TISSUE-SIMULATING OPTICAL PHANTOM

In both diagnostic and therapeutic applications of light in medicine, it is important to evaluate optical properties of tissues including absorption coefficient and reduced scattering coefficient. One of the challenging works in this area is to develop tissue-simulating turbid media (optical phantoms). Optical phantoms may be used to test and calibrate optical instruments or techniques.

In chapter 5.3, we report a new optical phantom that consists of an entrapped NIPA polymer solution and a host matrix of a PAAM hydrogel. NIPA polymer solution and blue destran were trapped inside PAAM gel matrix to form NIPA/PAAM gel system. The turbid optical properties of an NIPA/PAAM gel system can be tuned to simulate biological tissues.

The turbidity of a NIPA/PAAM gel system can be drastically changed by simply switching the temperature from below the low critical solution temperature of the NIPA around 33 °C to above. The absorption and scattering depends on samples with selected NIPA and blue dextran concentrations. It is found that the scattering of the optical phantom comes from the NIPA polymer chains and the absorption from the blue dextran. The turbid optical properties of an NIPA/PAAM gel system can be tuned to simulate biological tissues by optimizing compositions of NIPA and blue dextran and further modified by controlling temperature.

CHAPTER 2

SWELLING KINETICS OF POLYMER GELS AND CONVECTION

2.1 INTRODUCTION

In this chapter, gel swelling will be discussed kinetically and analyzed mathematically for gel in liquid as a major topic (section 2.1 and 2.2) and then followed by gel swelling in polymer solution (section 2.3). Finally a mathematically analysis for convection in gel network is given by section 2.4. Section 2.5 is a brief conclusion and section 2.6 is chapter references.

Kinetics of gel swelling process has attracted a considerable interest in the past decade. Many applications ranging from controlled drug release to gel actuators are directly related to swelling kinetics.[1-8]

The theory of the swelling of gels networks was first derived from the theory of elasticity by Tanaka, Hocker and Benedek (THB).[9] In this work, the spectrum of light scattered from thermally excited displacement fluctuations in polyacrylamide gels was measured on the

polarized scattered light. A theory for the amplitude and time dependence of the gel network under thermal excitations was presented. The theory and its prediction have an excellent agreement with the experimental results of the light scattering.

Tanaka and Fillmore[10] have used that theory to describe the swelling kinetics of spherical gels, assuming that the shear modulus of the gel is negligible compared with the osmotic bulk modulus. They have found that the relaxation time is proportional to the square of linear size of a gel and inversely proportional to the collective diffusion constant of the gel network. Later, Peters and Candau[11,12], extended Tanaka and Fillmore's model for long cylindrical and large disk gels in which the shear modulus can not be neglected.

All these works had been done with an assumption that the motion of the solvent inside of gel network is zero. This assumption, however, is only true for spherical gels. As first pointed out by Onuki, the motion of the solvent directly contributes to swelling kinetics.[13] Except the case of spherical gels, the swelling process changes both the bulk and shear energy of the polymer network. The solvent motion helps the gel system to minimize the total energy. The motion field of solvent strongly depends on the geometry of the gel and plays an important role in the friction force and the swelling kinetics.

Recently, Li and Tanaka (L-T) have proposed a theory[14-16] on gel swelling kinetics with arbitrary shapes. Instead of directly dealing with motion of both network and solvent, they decomposed the swelling process into two imaginary processes. The first process is a pure network diffusion process described by a collective diffusion equation with the zero solvent velocity. This process raises shear energy of the sample. In the second process, the solvent moves together with the network so that the solvent velocity is the same as the network velocity.

This process minimizes the total energy. The effect of solvent motion is therefore included in their second process.

Although analytical solutions describing the gel network swelling at the gel boundary have been derived by Li and Tanaka, it is not easy to visualize the solvent motion through their work. Some general frame works that consider motion of both gel network and solvent have been proposed by several groups[13,14], and some progress has been made for long cylindrical gels. This chapter presents theoretical analysis of kinetics of gel swelling and solvent motion by directly solving coupled motion between network and solvent for long cylindrical and large disk gels. It is also found that the solvent motion can be independently derived from L-T's isotropic condition (minimum shear energy) and continuity condition without solving the coupled collective diffusion equations.

Swelling of a long cylindrical gel in aqueous polymer solution has been studied as a continuation of swelling kinetics theoretically and experimentally. In a polymer solution, polymer chains are long and randomly coiled and tangled. Statistically, randomly coiled chains are too larger compared to the mesh size of gel network. If a gel is immersed into polymer solution, polymers chains could not freely penetrate into gel network. So the surface of a gel in polymer solution is not free of stress. It is the partial pressure of polymer chains in the solution that acts on the surface of the gel network because the polymer chains can't go in and out of network freely.

Convection in horizontal layers is one of the most basic and widely investigated topics in fluid dynamics. When a horizontal layer of fluid is heated from below, it may undergo Rayleigh-Benard convection due to intrinsic instability. As an analogous form of convection in porous

media, convection can occur for a fluid-saturated matrix. Convection may also occur in a polymer gel.

2.2 THEORY OF SWELLING KINETICS

2.2.1 Review of L-T's Theory

The collective diffusion equation is expressed as

$$f\frac{\partial \mathrm{u}}{\partial \mathrm{t}} = \nabla \bullet \sigma \qquad (2.1)$$

where f is the friction coefficient between the network and the solvent. **u(r,** t) is the displacement vector of a point **r** in the network from its final equilibrium location after the gel reaches equilibrium. σ is the stress tensor and is described by[17]

$$\sigma_{ik} = \mathrm{K}\nabla \bullet \mathrm{u}\,\delta_{\mathrm{ik}} + 2\mu(\mathrm{u}_{\mathrm{ik}} - \frac{1}{3}\nabla \bullet \mathrm{u}\,\delta_{\mathrm{ik}}) \qquad (2.2)$$

with

$$u_{ij} = \frac{1}{2}(\frac{\partial u_i}{\partial x_j} + \frac{\partial u_j}{\partial x_i}) \qquad (2.3)$$

where K and μ are bulk and shear modulus, respectively.

The governing equation for minimizing the shear energy in L-T's theory[14] is:

$$\delta F_{sh} = 0 \qquad (2.4)$$

where F_{sh} is the shear energy of a gel of arbitrary shape. The equation states that the change of the total shear energy in response to any small change in shape under the constant volume condition should be zero.

For a long cylindrical gel, they obtained the solution as

$$u_r(r,t) = \Delta \sum_{n=1}^{\infty} A_n e^{-D_e q_n^2 t} J_1(q_n r) \qquad (2.5)$$

where the coefficients A_n are determined by the initial condition. $\Delta(=u_r(a, 0))$ is defined as the total change of the radius of the gel. J_1 is the Bessel function of first order. α_n $(=q_n a)$ are eigenvalues determined by the boundary condition. D_e is the apparent collective diffusion coefficient, which is related to the kinetic process and determined by

$$\frac{\partial(D_e t)}{\partial t} = \frac{D}{1+\lambda} \qquad (2.6)$$

$$\lambda(r,t) = \frac{r}{2z}\left(\frac{\partial u_z}{\partial t}\right)/\left(\frac{\partial u_r}{\partial t}\right) \qquad (2.7)$$

where collective diffusion constant D is defined by $D=(K+4\mu/3)/f$. At the boundary of r=a, they obtained $D_e=2D/3$, and

$$u_r(r,t) = \Delta \sum_{n=1}^{\infty} B_n e^{-\frac{2}{3} D q_n^2 t} \qquad (2.8)$$

where $B_n=A_n J_1(q_n a)$. For a large disk gel the similar solution is obtained with $D_e=D/3$ at the boundary.

2.2.2 Basic Equations of the Theory

To include the solvent motion, eq 2.1 can be revised as following,

$$f\frac{\partial(\mathrm{u}-\mathrm{w})}{\partial \mathrm{t}}=\nabla\_\sigma \qquad (2.9)$$

or

$$\frac{\partial \mathrm{u}}{\partial \mathrm{t}}=\frac{\partial \mathrm{w}}{\partial \mathrm{t}}+\frac{1}{\mathrm{f}}\nabla\_\sigma \qquad (2.10)$$

where **w** is the displacement vector of the solvent. Eq 2.4 remains valid to relate the relative changes in both radial and axial directions.

The continuity requirement is given by the equation

$$(1-\phi)\nabla\bullet(\frac{\partial \mathrm{w}}{\partial \mathrm{t}})+\phi\nabla\bullet(\frac{\partial \mathrm{u}}{\partial \mathrm{t}})=0 \qquad (2.11)$$

where φ is the fractional volume of the gel network. For small φ, eq 2.11 can be simplified as

$$\nabla\bullet\frac{\partial \mathrm{w}}{\partial \mathrm{t}}=0 \qquad (2.12)$$

Eqs 2.10, 2.4 and 2.12 form a set of basic equations with the boundary condition

$$\sigma_{\mathrm{normal}}=0 \qquad (2.13)$$

where σ_{normal} is the normal stress on the gel surface**.** The initial condition is

$$\sigma_{ik}=\pi_0\delta_{ik} \qquad (2.14)$$

where π_0 is the osmotic pressure of the gel. The boundary condition for solvent is unnecessary due to the isotropic identity that can be derived out from eq 2.4.

2.2.3 Long Cylindrical Gels

Let us first turn our attention to the solution for a long cylindrical gel. Long cylinder model assumes that the diameter of the gel cylinder is much smaller than the

length of the gel. So the solution is not related to z due to symmetry. The displacements of the network and the solvent in such a system can be written as

$$u(r, t) = u_r(r, t)\, r_0 + u_z(r, t)\, z_0 \tag{2.15}$$

$$w(r, t) = w_r(r, t)\, r_0 + w_z(r, t)\, z_0 \tag{2.16}$$

where $\mathbf{r}_0$ and $\mathbf{z}_0$ are the unit vectors along the radial and axial directions respectively. In this case, deformation on the both ends of the gel cylinder is neglected. The changes in radial and axial directions are independent with each other. Using eqs. 2.15 and 2.16, eq 2.10 can be separated into two equations along the axial and radial directions, respectively.

$$\frac{\partial u_r}{\partial t} = \frac{\partial w_r}{\partial t} + D[\frac{1}{r}\frac{\partial}{\partial r}(r\frac{\partial u_r}{\partial r}) - \frac{1}{r^2}u_r] \tag{2.17}$$

$$\frac{\partial u_z}{\partial t} = \frac{\partial w_z}{\partial t} + D\frac{\partial^2 u_z}{\partial z^2} \tag{2.18}$$

The boundary condition for the long cylinder can be rewritten as

$$[\frac{\partial u_r}{\partial r} + (1 - 2R)(\frac{u_r}{a} + \frac{\partial u_z}{\partial z})]_{-r=a} = 0 \tag{2.19}$$

where R=μ/(K+4μ/3) is the ratio of the shear modulus to the longitudinal modulus. The restraint condition given in eq 2.4 produces the isotropic identity for the long cylinder,[14]

$$\frac{u_z(z, t)}{z} = \frac{u_r(a, t)}{a} \tag{2.20}$$

Combining eq 2.20 and the boundary condition of eq 2.19, we obtain

$$\frac{\partial u_r}{\partial r}_{-r=a} + 2(1 - 2R)\frac{u_r(a, t)}{a} = 0 \tag{2.21}$$

Substituting eq 2.20 into eq 2.18, we obtain

$$\frac{\partial w_z}{\partial t} = \frac{z}{a}\frac{\partial u_r(a,t)}{\partial t} \qquad (2.22)$$

The continuity requirement in eq 2.12 can be rewritten as

$$\frac{\partial}{\partial r}(\frac{\partial w_r}{\partial t}) + \frac{1}{r}(\frac{\partial w_r}{\partial t}) + \frac{\partial}{\partial z}(\frac{\partial w_z}{\partial t}) = 0 \qquad (2.23)$$

Substituting eq 2.22 into eq 2.23 gives the differential equation for $\partial w_r/\partial t$. We have solved this equation with natural boundary condition $\partial w_r/\partial t|_{r=0}=0$,

$$\frac{\partial w_r}{\partial t} = -\frac{r}{2a}\frac{\partial u_r(a,t)}{\partial t} \qquad (2.24)$$

It is clear from eq 2.22, eq 2.24 and eq 2.20 that the solvent velocity $\partial w_r/\partial t$, $\partial w_z/\partial t$ and the axial displacement of the network u_z are all related to the radial displacement of the network u_r. Let us now derive the analytical solution of u_r. Substituting eq 2.24 into eq 2.17,

$$\frac{\partial u_r}{\partial t} + \frac{r}{2a}\frac{\partial u_r(a,t)}{\partial t} - D[\frac{1}{r}\frac{\partial}{\partial r}(r\frac{\partial u_r}{\partial r}) - \frac{1}{r^2}u_r] = 0 \qquad (2.25)$$

The solution for eq 2.25 is the Bessel function of the first order. So u_r can be written as

$$u_r(r,t) = \Delta\sum_{n=1}^{\infty} T_n(t)J_1(q_n r) \qquad (2.26)$$

Here $u_r(r, t)$ is normalized to $u_r(a, 0)=\Delta$. Let us also expand $\partial w_r/\partial t$ in Bessel function of the first order,

$$\frac{\partial w_r(r,t)}{\partial t} = \Delta\sum_{n=1}^{\infty} F_n(t)J_1(q_n r) \qquad (2.27)$$

Substituting eq 2.26 and eq 2.27 to eq 2.25 and separating the variables t and r, we have

$$\frac{T_{n'}(t) - F_n(t)}{D T_n(t)} = - q_n^2 \qquad (2.28)$$

Solve eq 2.28 and obtain

$$T_n(t) = \left[A_n + \int_0^t F_n(x) e^{Dq_n^2 t} dx \right] e^{-Dq_n^2 t} \qquad (2.29)$$

where $q_n(=\alpha_n a)$ are determined by the boundary condition (eq 2.13), which can be rewritten as

$$\frac{\alpha_n J_0(\alpha_n)}{J_1(\alpha_n)} - 4R + 1 = 0 \qquad (2.30)$$

Substituting eq 2.29 to eq 2.26, we get

$$u_r(r,t) = \Delta \sum_{n=1}^{\infty} \left[A_n + \int_0^t F_n(x) e^{Dq_n^2 x} dx \right] e^{-Dq_n^2 t} J_1(q_n r) \qquad (2.31)$$

The initial condition in eq 2.14 for the long cylinder turns out to be $u_r(r, 0)=r/a$. Using this initial condition to eq 2.31 gives

$$\sum_{n=1}^{\infty} A_n J_1(q_n r) = \frac{r}{a} \qquad (2.32)$$

Using the orthogonal relations of Bessel functions, coefficients A_n can be determined,

$$A_n = \frac{2(3 - 4R)}{\alpha_n^2 - (4R - 1)(3 - 4R)} - \frac{1}{J_1(\alpha_n)} \qquad (2.33)$$

Substituting eq 2.32 for r/a in eq 2.24, then comparing it with eq 2.27 one can obtain the following,

$$F_n(t) = - \frac{A_n}{2\Delta} \frac{\partial u_r(a,t)}{\partial t} \qquad (2.34)$$

Insert eq 2.34 to eq 2.31,

$$u_r(r,t) = \sum_{n=1}^{\infty} A_n \left[\Delta - \frac{1}{2} \int_0^t \frac{\partial u_r(a,\tau)}{\partial \tau} e^{Dq_n^2 \tau} \right] e^{-Dq_n^2 t} J_1(q_n r) \qquad (2.35)$$

Let r=a in eq 2.35,

$$u_r(a,t) = \sum_{n=1}^{\infty} B_n \left[\Delta - \frac{1}{2} \int_0^t \frac{\partial u_r(a,\tau)}{\partial \tau} e^{Dq_n^2 \tau} \right] e^{-Dq_n^2 t} \qquad (2.36)$$

where $B_n=A_n J_1(\alpha_n)$. From eqs 2.35, 2.20, 2.22 and 2.24, one can see that motions of both network and solvent have been separately solved along the radial and the axial directions. These solutions are explicitly expressed as a function of $u_r(a, t)$ which is determined by eq 2.36. In the space distribution, the speed of solvent motion is proportional to -r/2a along the radial direction and z/a along the axial direction, respectively. The magnitude of the speed decreases to zero gradually with the increase of time.

Several special cases are given below. For $t<<\tau_1$ ($1/\tau_1=Dq_1^2$), $u_r(r, t)=\exp(DQ^2t/3)v_r$, where $Q^2=\sum B_i q_i^2$ and $v_r=\Delta\sum A_n \exp(-Dq_n^2 t) J_1(q_n r)$. For $t>>\tau_1$, $u_r(r, t)\propto\exp[-2Dq_1^2 t/(2+B_1)]J_1(q_1 r)$.

As bulk modulus K approaches zero, we have

$$u_r(r,t) = \Delta \frac{r}{a} e^{-\frac{2}{3} Dq_1^2 t} \qquad (2.37)$$

which is identical to eq 2.29 in L-T's theory[14] and valid for any t. This is obvious become shear modulus μ is relatives approaching to zero. so it is back to the situation without considering shear energy. Previous solutions for two special cases of $t<<\tau_1$ and $t>>\tau_1$ consistently turn into the same form of eq 2.37 using the relations $B_1=1$, $B_i=0$ and $A_i=0$ for $i>1$ as $K\rightarrow 0$.

2.2.4 Comparison with L-T's results

To compare the current results with previous work by L-T, we start to rewrite eq 2.17 as

$$\frac{\partial u_r}{\partial t}\left(1-\frac{\partial w_r/\partial t}{\partial u_r/\partial t}\right)=D\left[\frac{1}{r}\frac{\partial}{\partial r}\left(r\frac{\partial u_r}{\partial r}\right)-\frac{1}{r^2}u_r\right] \qquad (2.38)$$

Using eq 2.20 and eq 2.24, the λ parameter defined by L-T (eq 2.7) can be written as

$$\lambda(r,t)=-\left(\frac{\partial w_r}{\partial t}\right)/\left(\frac{\partial u_r}{\partial t}\right) \qquad (2.39)$$

Combining eq 2.38 and eq 2.39, we have

$$\frac{\partial u_r}{\partial t}=\frac{D}{1+\lambda}\left[\frac{1}{r}\frac{\partial}{\partial r}\left(r\frac{\partial u_r}{\partial r}\right)-\frac{u_r}{r^2}\right] \qquad (2.40)$$

where the apparent diffusion coefficient is reduced by a factor $1/(1+\lambda)=(\partial u_r/\partial t)/(\partial(u_r-w_r)/\partial t)$. This equation is similar to eq 2.10 in L-T's theory. [14] Since the motion of the solvent is in the opposite direction of $\partial u_r/\partial t$, the relative speed and displacement of network are increased by a factor $(1+\lambda)$ than that expected by pure diffusion theory. Compared with the results of pure diffusion theory, the friction force increases and the relaxation process slows down accordingly.

Eq 2.17 is the Bessel equation with a free term. This free term can be expanded into Bessel series. Let us write the solution for eq 2.40 in the form,[14]

$$u_r(r,t)=\Delta\sum_{n=1}^{\infty}A_n e^{-D_e q_n^2 t}J_1(q_n r) \qquad (2.41)$$

Comparing eq 2.41 and eq 2.35, we found that D_e is only a function of time t. Substituting $u_r(r,t)$ into eq 2.40, and comparing the coefficients of Bessel functions of the equation in the approximation that λ is independent of r, it comes to the following,

$$\frac{\partial(D_e t)}{\partial t} = \frac{D}{1+\lambda} \qquad (2.42)$$

This was derived by Li-Tanaka through a two-process approach using the same approximation. At K=0, λ is 1/2 and independent of r, so D_e=2D/3 from eq 2.42. It is in agreement with eq 2.37.

The difference of D_e/D between L-T's theory and the present theory is given below in Table 2.1. The detailed calculation for large disk is similar to that of long cylinder and will be given in section 2.2.6.

Table 2.1 The comparison between L-T's and the current results

	D_e/D (L-T's)	D_e/D (Present)
Sphere	1	1
Cylinder	2/3	$2/(2+B_1)$
Disk	1/3	$1/(1+2B_1)$

Where B_1 is related to the ratio of the shear modulus and longitudinal modulus. $B_1 = A_1J_1(\alpha_1)$ for a long cylindrical gel, and $B_1=A_1\sin\alpha_1$ for a large disk gel which will be discussed in details later. It is noted that the values of D_e/D in the present theory can be used not only at the boundary but also in the interior of gel, and are valid for $t>>\tau_1$, which corresponds to a single-exponential relaxation in swelling and shrinking processes.

When the bulk modulus approaches to zero, $B_1=1$; the values of D_e/D obtained from the present theory are the same as ones obtained from L-T's theory.

In Onuki's calculation,[18] he obtained the stress-free boundary condition at r=a as

$$\frac{\alpha_n J_0(\alpha_n)}{J_1(\alpha_n)} = 4R\frac{(e_- + e_-)}{(2e_- + e_-)} \tag{2.43}$$

The volume change $\nabla\bullet\mathbf{u}$ can be expressed as

$$\nabla_- u = \sum_{n=1}^{\infty} A_n \frac{\alpha_n}{a} J_0(\frac{\alpha_n r}{a}) e^{-\Omega_n t} \tag{2.44}$$

As K approaches infinity, $J_0(\alpha_n)=0$. Therefore, $\nabla\bullet\mathbf{u}=0$ at r=a.

From L-T's theory, $\nabla\bullet\mathbf{u}\,|_{r=a}=-\Delta(t/D)\sum(A_n/\tau_n)\exp(-D_e q_n^2 t)\ J_1(q_n a)(\ \partial D_e/\partial r)$, for $K\rightarrow\infty$; and $\partial D_e/\partial r=0$ because D_e is independent of r. Therefore, $\nabla\bullet\mathbf{u}=0$ for $K->\infty$ at r=a, in agreement with Onuki's result.

From the present theory, we used the same equation (eq 2.30) as L-T's for the boundary condition to determine eigenvalues α_n. The volume change can be expressed as

$$\nabla\bullet u = (\frac{\partial}{\partial r} + \frac{1}{r})u_r + \frac{\partial u_z}{\partial z}$$
$$= \Delta\sum_n T_n(t)\left[J_1(\alpha_n\frac{r}{a})\frac{\alpha_n}{a} + \frac{J_1(\alpha_n\frac{r}{a})}{r} + \frac{J_1(\alpha_n)}{a}\right] \tag{2.45}$$

From the relation of Bessel functions, $J'_1(x)=J_0(x)-J_1(x)/x$, we obtain

$$\nabla\bullet u = \Delta\sum_n \frac{T_n(t)}{a}[\alpha_n J_0(\alpha_n\frac{r}{a}) + J_1(\alpha_n)] \tag{2.46}$$

As $K\rightarrow\infty$, $\alpha_n J_0(\alpha_n)=\sim J_1(\alpha_n)$, we have

$$\nabla \bullet u = \frac{\Delta}{a}\sum_n T_n(t)\alpha_n[J_0(\alpha_n\frac{r}{a}) - J_0(\alpha_n)] \qquad (K-> \infty) \qquad (2.47)$$

Therefore, $\nabla \bullet \mathbf{u}=0$ for K->$\rightarrow\infty$ at r=a, in agreement with Onuki's result.

2.2.5 Velocity Field of Solvent

One of the major results from this generalized gel diffusion model is the motion of the solvent, as expressed by eq 2.22 and eq 2.24. Here we demonstrate that the radial and axial components of solvent motion can be derived from volume conservation and isotropic swelling conditions. Let us first consider the radial component according to volume conservation, the volume change (δV) during a period of time (δt) for a gel cylinder (with radius r and length 2xl at time t) is related with the solvent velocity relative to gel network (v) and the side area (S) by the expression

$$\delta V = v\, S\, \delta t \qquad (2.48)$$

where $\delta V=\pi r^2(2l)(2\delta r/r+\delta l/l)$, $v=\partial w_r/\partial t-\partial u_r/\partial t$, $S=2\pi r(2l)$, $\delta r=-\delta u_r(r, t)$ and $\delta l=-\delta u_z(l, t)$. Note that we have neglected the end effect. Combining the isotropic swelling condition eq 2.22, $\delta l/l=-\delta u_r(a, t)/a$ and eq 2.48, we obtain

$$\frac{\partial w_r}{\partial t} = -\frac{r}{2a}\frac{\partial u_r(a,t)}{\partial t} \qquad (2.49)$$

That is the same as eq 2.24. The axial component of solvent motion (eq 2.22) can be directly obtained through $\nabla\bullet(\partial \mathbf{w}/\partial t)=0$. Therefore, the solvent motion can be independently derived from L-T's isotropic condition and continuity condition without using the coupled collective diffusion equations.

Let us now discuss the solvent velocity field. Rewrite eq 2.22 and eq 2.24 as

$$\frac{\partial w_z(z,t)}{\partial t} = \frac{z}{a} f(t) \qquad (2.50)$$

$$\frac{\partial w_r(r,t)}{\partial t} = -\frac{r}{2a} f(t) \qquad (2.51)$$

where f(t) is $\partial u_r(a,t)/\partial t$ which decreases to zero as the time approaches infinity.

Figure 2.1 shows the solvent motion pattern according to eqs 2.50 and 2.51. The solvent always moves toward the inside along the radial direction and toward the ends along the axial directions. Due to the solvent motion, the relative velocity between the network and the solvent is $(1+\lambda)\partial u_r/\partial t$ in the radial direction, but zero in the axial direction. In L-T's approach, the zero relative motion in the axial direction is built based on the two-step process.

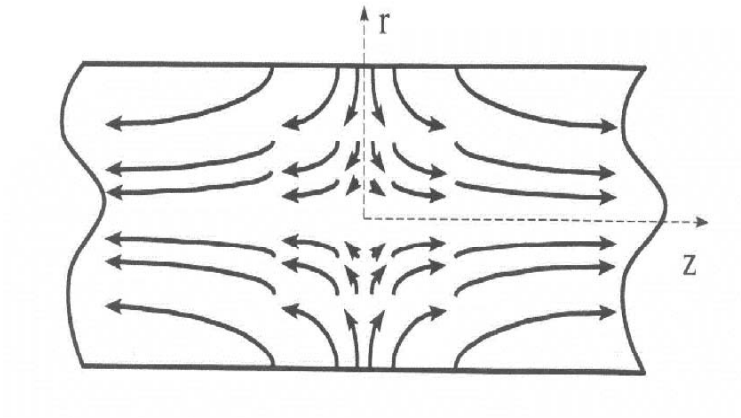

Figure 2.1. Solvent motion pattern for a long cylindrical gel in its swelling process. The drawing is scaled according to eqs 2.40 and 2.41.

The swelling process is controlled by elasticity and friction. The elastic force makes the whole gel network to swell until the stress tensor disappears everywhere inside gel. The friction force dissipates the elastic energy and slows down the swelling process. The collective diffusion coefficient D, which is proportional to the longitudinal elastic modulus ($K+4\mu/3$) and reversely proportional to the friction coefficient f, determines the swelling process. Taking the solvent motion into consideration, the apparent collective diffusion coefficient D_e is less than D by a factor of $1/(1+\lambda)$. Therefore, the whole swelling process is slower in the radial direction than it is expected based on the pure diffusion theory.

The numerical solution from eq 2.35 has been obtained. Figure 2.2 shows the normalized swelling displacement u_r/Δ versus normalized time $t/(a^2/D\alpha^2)$.

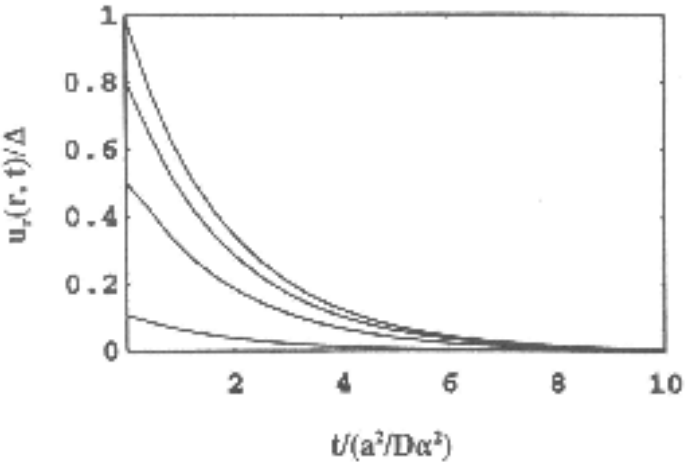

Figure 2.2. Typical curves for long cylindrical gel swelling. The displacement u_r (r,t) is drawn as a function of time t. The curves are corresponding to r/a = 0.1, 0.5, 0.8, 1 from the bottom to the top.

The network motion is coupled with solvent motion, resulting in gel swelling isotropically. Correspondingly, the time dependence of u_r cannot be described by exponential forms. The swelling ratio as a function of radial distance r/a is shown in Figure 2.3.

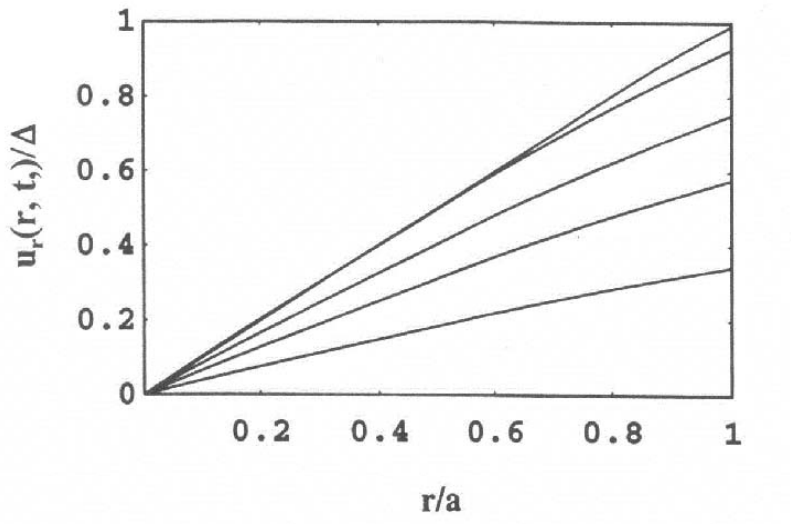

Figure 2.3. Typical curves for long cylindrical gel swelling. The displacement u_r (r,t) is drawn as a function of radius r. The curves are corresponding top $t/(a^2/Da^2) = 0, 0.1, 0.5, 1, 2$ from the top to the bottom.

From the figure, one can see that the swelling behavior is not only obtained at the boundary (r=a), but also inside gel (r<a). The previous work has only yielded the solutions at the boundary.[14-16]

It is noted that Onuki's theory[18] can lead to similar results about the solvent motion although calculations such as the boundary conditions and eigenfunctions employed by us and by Onuki are different. Some advantages of our approach: (a) Our work has modified and extended L-T's theory. (b) We have established that L-T's

consideration of isotropic condition and the continuity condition are equivalent to considering the motion of the solvent for long cylindrical and large disk gels. (c) We have obtained the detailed flow diagrams of the solvent in the gel network for long cylindrical gels and large disk gels. These diagrams could be experimentally tested.

2.2.6 Large Disks

The similar analysis can be also applied to a large disk gel. A large disk is defined such as its diameter is much larger than its length. The basic equations are

$$\frac{\partial \mathrm{u}}{\partial \mathrm{t}} = \frac{\partial \mathrm{w}}{\partial \mathrm{t}} + \mathrm{D}\nabla^2 \mathrm{u} \qquad (2.52)$$

$$\nabla \bullet \frac{\partial \mathrm{w}}{\partial \mathrm{t}} = 0 \qquad (2.53)$$

$$\frac{u_r(r,t)}{r} = \frac{u_z(a,t)}{a} \qquad (2.53)$$

where $u_z(z, t)$ is normalized to $u_z(a, 0)=\Delta$ and parameter a is the half thickness of the disk. The boundary condition is

$$[\frac{\partial u_z}{\partial z} + (1 - 2R)(\frac{u_r}{r} + \frac{\partial u_r}{\partial r})]|_{z=\pm h} = 0 \qquad (2.55)$$

And the initial condition is

$$u_z(z,0) = \pm\frac{z}{a}u_z(\pm a,0) \qquad (2.56)$$

Assuming that solvent movements in r and z directions are independent, we have,

$$\frac{\partial w_r(r,t)}{\partial t} = \frac{r}{a}\frac{\partial u_z(a,t)}{\partial t} \qquad (2.57)$$

$$\frac{\partial w_z(z,t)}{\partial t} = -2\frac{z}{a}\frac{\partial u_z(a,t)}{\partial t} \tag{2.58}$$

$$u_r(r,t) = \frac{r}{a}u_z(a,t) \tag{2.59}$$

$$u_z(z,t) = \sum_{n=1}^{\infty} A_n \left[\Delta - 2\int_0^t \frac{\partial u_z(a,\tau)}{\partial \tau} e^{-Dq_n^2\tau} d\tau \right] e^{-Dq_n^2 t} \sin(q_n z) \tag{2.60}$$

Here, $u_z(a, t)$ satisfies

$$u_z(a,t) = \sum_{n=1}^{\infty} A_n \left[\Delta - 2\int_0^t \frac{\partial u_z(a,\tau)}{\partial \tau} e^{-Dq_n^2\tau} d\tau \right] e^{-Dq_n^2 t} \sin(\alpha_n) \tag{2.61}$$

The eigenvalues α_n are determined by

$$R = \frac{1}{2} + \frac{1}{4}\alpha_n \cot(\alpha_n) \tag{2.62}$$

The coefficients A_n are given by initial condition,

$$A_n = \frac{4}{\alpha_n}\frac{\sin\alpha_n - \alpha_n\cos\alpha_n}{2\alpha_n - \sin(2\alpha_n)} \tag{2.63}$$

The solvent motion pattern is shown in Figure 2.4. The swelling ratio for a large disk gel as function of time t and axial distance z is shown in Figure 2.5 and Figure 2.6, respectively.

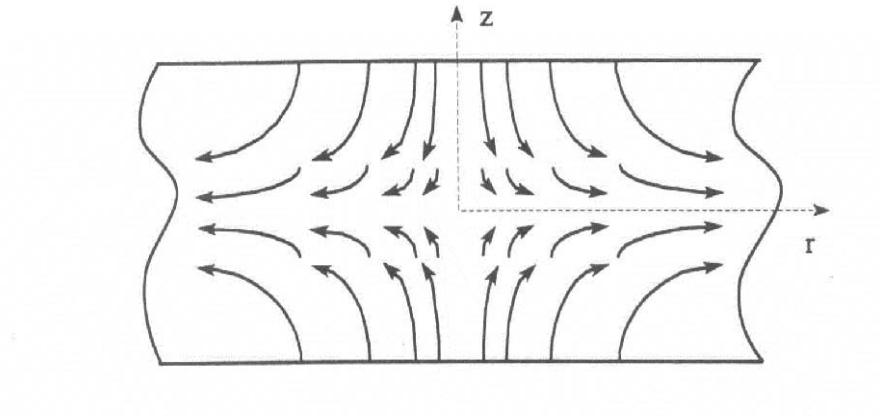

Figure 2.4. Solvent motion pattern for a large disk gel in its swelling process. The drawing is scaled according to eqs 2.53 and 2.59.

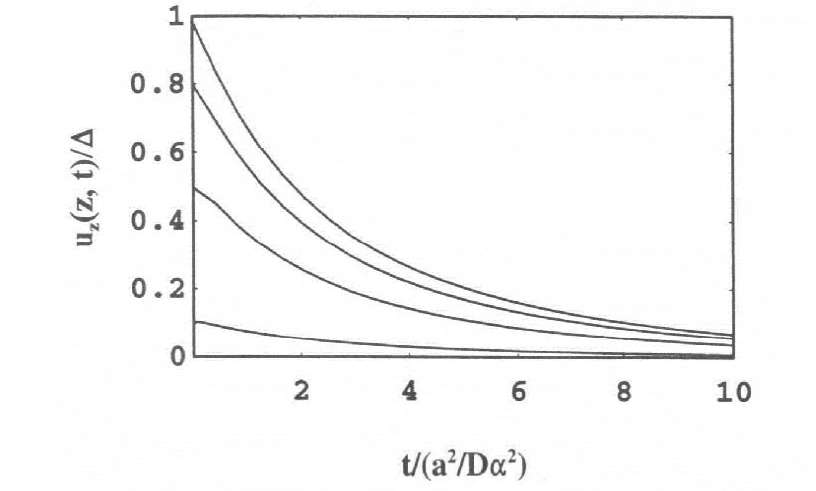

Figure 2.5. Typical swelling curves for a large disk gel. The displacement u_z (z,t) is drawn as a function of time t. The curves are corresponding to z/a = 0.1, 0.5, 0.8, 1 from the bottom to the top.

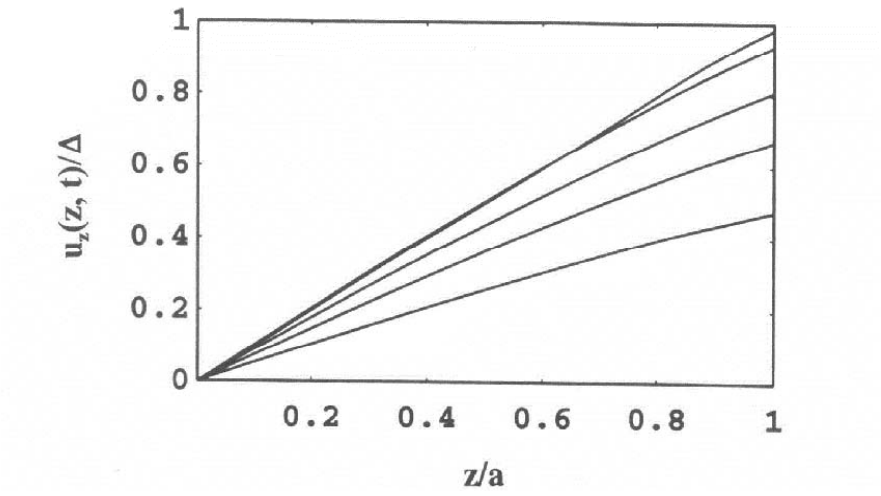

Figure 2.6. Typical swelling curves for a large disk gel. The displacement u_z (z,t) is drawn as a function of z. The curves are corresponding to $t/(a^2/Da^2) = 0, 0.1, 0.5, 1, 2$ from the top to the bottom.

The swelling behaviors of the large disk gel are similar to these of the long cylindrical gel as discussed in Section 2.2.5.

2.3 SWELLING AND SHRINKING OF GELS IN AQUEOUS POLYMER SOLUTION

2.3.1 Theoretical Analysis

Swelling of a long cylindrical gel (PAAM) in aqueous polymer solution, such as poly vinyl alcohol (PVA), has been studied here theoretically and experimentally. Eq. 2.1

for gel swelling still holds. However, **u** is the displacement of the gel relative to its final equilibrium position without stress on the surface.

In a polymer solution, polymer chains are long and randomly coiled and tangled. Statistically, randomly coiled chains are too larger compared to the mesh size of gel network. If a gel is immersed into polymer solution, polymers chains could not freely penetrate into gel network. So the surface of a gel in polymer solution is not free of stress. It is the partial pressure of polymer in the solution that acts on the surface of the gel network because the polymer can't go in and out of network freely. In this case, the boundary condition should be modified. For the condition that the volume of the polymer solution is much great than the relative swelling volume of gel network, the partial pressure of polymer in solution should be a constant. That is, the stress normal to the surface of gel network remains a finite constant. Therefore, the boundary condition of swelling gel network in polymer solution can be written as

$$\sigma_{normal} = P \qquad (on\ gel\ surface) \tag{2.64}$$

where P is a constant representing the partial pressure of polymer in solution. In the case of a long cylindrical gel, the above boundary condition at r=a is given by

$$\sigma_{rr} = M\,[\frac{\partial u_r}{\partial r} + (1-2R)(\frac{u_r}{r} + \frac{\partial u_z}{\partial z})] = P \tag{2.65}$$

and the initial condition remains as same as that for gels with free surface,

$$\frac{u_r(r,0)}{u_r(r,0)} = \frac{r}{a} \tag{2.66}$$

Here parameter 'a' corresponds to the radius of the cylindrical gel after the final equilibrium is reached in the pure water.

The isotropic assumption in eq 2.20 for an infinite long cylindrical gel still holds for the gel in a polymer solution. The general solution for the above problem is

$$u_r(r,t) = \frac{P}{3K} r + \Delta \sum_{n=1}^{\infty} A_{n'} J_1(q_n r) e^{-D_e(r,t) q_n^2 t} \qquad (2.67)$$

On the surface of the gel, r=a, $u_r=u_r(a,t)$, we have

$$u_r = \frac{Pa}{3K} + \Delta \sum_{n=1}^{\infty} A_{n'} J_1(\alpha_n) e^{-\frac{2}{3} D q_n^2 t} \qquad (2.68)$$

where $D_e(r, t)$ is the same as that with P=0. For r=a, D_e is equal to 2D/3. The eigenvalues $\alpha_n=q_n a$ satisfy eq 2.30 and have the same values. Therefore, the relaxation time parameters $\tau_n=a^2/(D_e\alpha_n^2)$ are the same as those for gels in pure water. The coefficients A_n' are expressed as

$$\begin{aligned} A_{n'} &= \frac{2(3-4R)}{\alpha_n^2 - (4R-1)(3-4R)} \bullet \frac{1}{J_1(\alpha_n)} \left(1 - \frac{a}{\Delta} \frac{P}{3K}\right) \\ &= A_n \left(1 - \frac{\Delta_r}{\Delta}\right) \end{aligned} \qquad (2.69)$$

where A_n is the normal coefficient in eq 2.33. Δ_r is an important parameter,

$$\begin{aligned} \Delta_r &= \frac{P a}{(3-4R)M} \\ &= \frac{P a}{3K} \end{aligned} \qquad (2.70)$$

which gives the difference of the final equilibrium radius between the same long cylindrical gel in pure water and in polymer solution. When $t\to\infty$, the gel in polymer solution reaches its new equilibrium position as $u_r(a, t\to\infty)=\Delta_r$. In pure water, Δ_r is zero as $u_r(a, t\to\infty)=0$. That means the final equilibrium radius of a gel in polymer solution will

be smaller than that in pure water by amount of Δ_r. Figure 2.7 shows the difference of the parameters Δ, Δ_r, a and $(\Delta-\Delta_r)$.

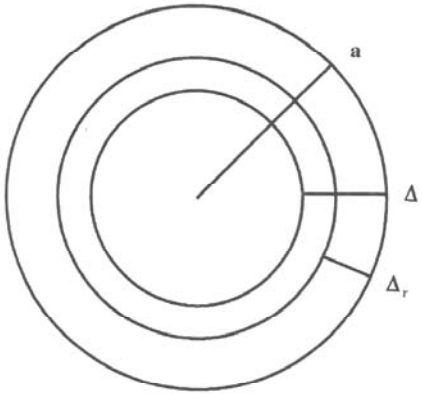

Figure 2.7. Crosectional view of a cylindrical gel in polymer solution, in which all parameters Δ, Δ_r, a and $(\Delta-\Delta_r)$ are labeled and identified.

Corresponding to different polymer concentrations, gels will swell into different equilibrium diameters. If $\Delta/\Delta_r=1$, then $A_n'=0$, the gel will not swell at all. If $\Delta/\Delta_r<1$, then $A_n'<0$, the gel will shrink by $(\Delta-\Delta_r)$. We consider the first term of the series in eq 2.68 which becomes dominant over the higher order terms at large t. The eq 2.68 can be expressed by

$$\ln(u_r - \Delta_r) = \ln[(\Delta - \Delta_r) A_1 J_1(\alpha_1)] - \frac{1}{\tau_1} t \qquad (2.71)$$

where $u_r-\Delta_r= (a-r)-(a-R)=R-r$, $\tau_1=a^2/(D\alpha^2)$. The curves for $\ln(u_r-\Delta_r)\sim t$ should be straight lines. The slopes of lines determine the relaxation times, which should be constant

according to eq 2.71 even the concentration of polymer chains and the surface pressure vary. The intercepts are a little different from each other according to their Δ_r, which depends on the gel surface pressure that is a function of the concentration of polymer, such as PVA in our experiment.

We also consider the gel shrinking from its equilibrium size in pure water to its new equilibrium size in polymer solution. The initial condition becomes $u_r|_{t=0}=0$. The general solution at t=0 now becomes

$$\Delta_r + \Delta \sum_{n=1}^{\infty} A_{n'} J_1(\alpha_n) = o \qquad (2.72)$$

$$A_{n'} = -\frac{\Delta_r}{\Delta} A_n \qquad (2.73)$$

At a large enough t, we have

$$\ln(\Delta_r - u_r) = \ln[\Delta_r A_1 J_1(\alpha_1)] - \frac{1}{\tau_1} t \qquad (2.74)$$

2.3.2 Experimental Results

Acrylamide gels of standard composition have been prepared in this experiment. The long cylindrical samples were made in glass tubings with 1.5 mm inner diameter. The aspect ratio of the long cylinder (length/diameter) was 30. The solutions were prepared with different concentrations of PVA, and were heated up to 95 ^{0}C. The concentration of the solution (wt) was defined by the relative weights of PVA to the solution. The swelling and shrinking of gels were measured by a microscope with accuracy of 5%.

The experimental results for gel swelling in solutions with concentration of PVA as 0%, 5wt%, and 10wt% are shown in Figure 2.8.

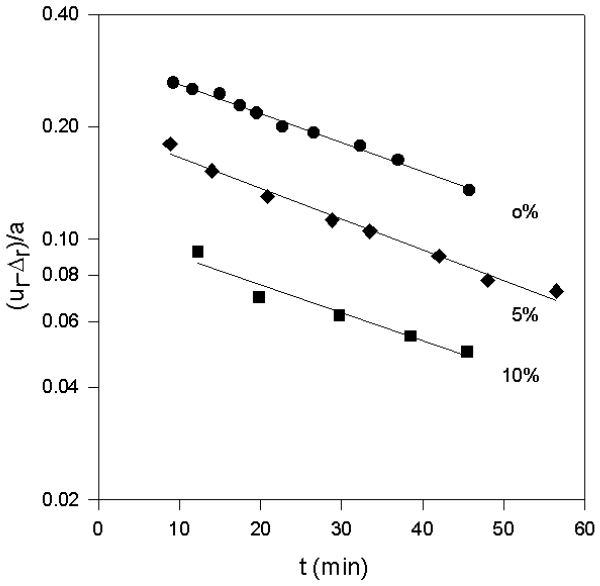

Figure 2.8. The experimental results of gel swelling in polymer solution with concentration of PVA as 0%, 5wt%, and 10wt%.

The swelling relaxation times are calculated as 53.4±5.8, 55±11, 62±21 min., respectively. The experimental results for gel shrinking in the solution with concentration of PVA as 1wt%, 5wt%, and 10wt% are shown in Figure 2.9.

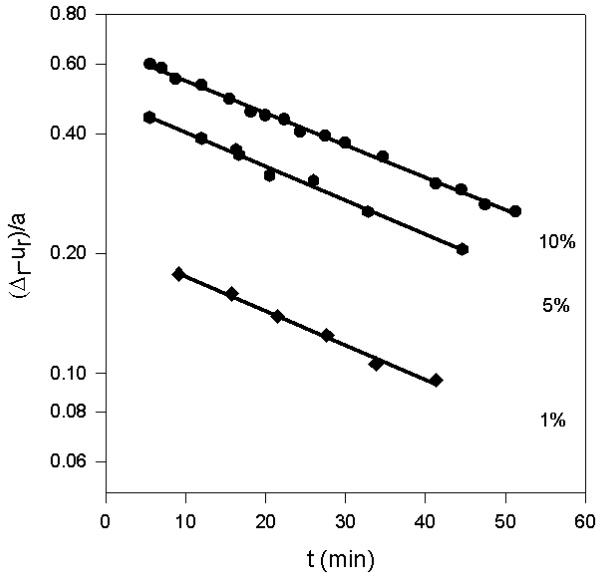

Figure 2.9. The experimental results of gel shrinking in polymer solution with concentration of PVA as 1 wt%, 5wt%, and 10wt%.

The shrinking relaxation times are 53.3±4.9, 51.2±3.1, 52.5±2.4 min. respectively. From above experiments, it is found that the swelling curves in Figure 2.8 have more fluctuation and the relaxation time have a little increase when the concentration of polymer increases. The most possible reason is that PVA in solution clogs water intake of the gel, resulting in decrease of effective surface area of the gel. Therefore the swelling process slows down. In the shrinking process, the water is flown out of the gel. Clogging effect is not significant. Therefore the relaxation times of gel shrinking in polymer solution with various PVA concentrations are the same within experimental error.

As the concentration of PVA in polymer solution increases, the partial pressure of PVA, which is the pressure acted on the surfaces of the gel, will increase. As a result, the radius of gel will decrease to a-Δ_p. Figure 2.10 shows the experimental results for Δ_r vs c where c is the concentration.

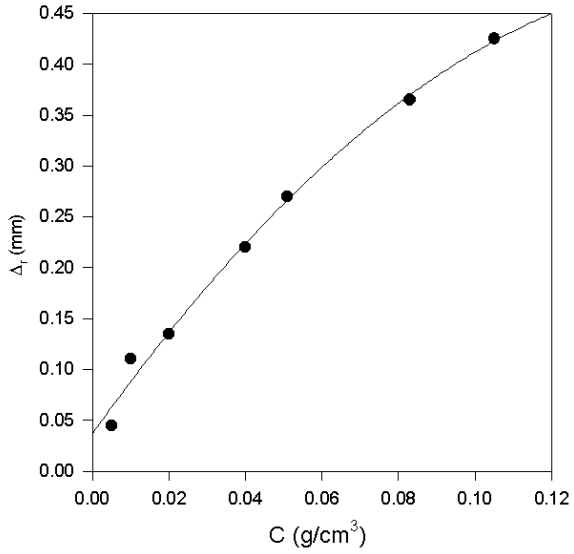

Figure 2.10. The experimental results of gel size over concentration of PVA solution as expressed as Δ_r vs c.

When the concentration is low, Δ_r is proportional to the concentration. The concentration c is expected to follow the equation Δ_r=aP/3K$\propto$P. A dilute polymer solution of PVA acts like an ideal gas in the limit of dilution.

The concentration dependence of the osmotic pressure for a dilute polymer solution[20-26] is usually written in form

$$\frac{\pi}{c} \approx \frac{RT}{M} + Bc \qquad (2.75)$$

where c is the concentration expressed in grams per unit volume. M is the average molecular weight of PVA. The osmotic pressure π of PVA is equal to the surface pressure P of the gel. Substituting eq 2.70 into eq 2.75, we have

$$\frac{\Delta_r}{c} = h + Bc \qquad (2.76)$$

$$h = \frac{a}{3K}\frac{RT}{M} \qquad (2.77)$$

Plotting $\Delta_r/c \sim c$ gives a straight line as showed in Figure 2.11. From the intercept h of the line we can find the bulk modulus of the acrylamide gel. Because K= aRT/(3hM), using a=1 mm, M=25 Kg/mol, T=295 K, h=0.66 cm^4/g, we obtain $K=4.9\times10^4 dyn/cm^2$, agreeing with previous report[27]. These results show an excellent agreement between our theoretical model and experiments.

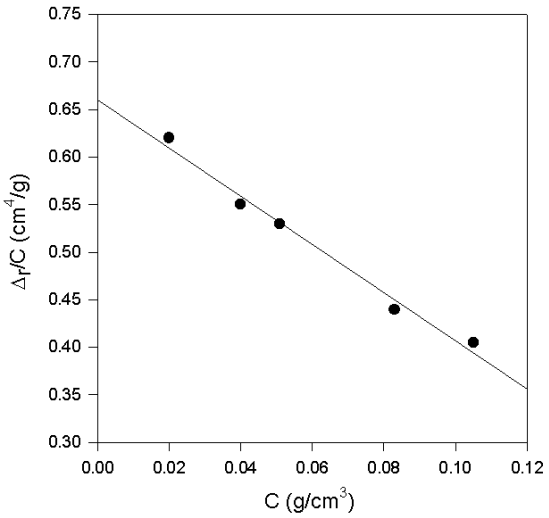

Figure 2.11. The experimental results of gel size over concentration of PVA solution as expressed as $\Delta_r/c \sim c$ where the bulk modulus of the gel can be calculated out from the intercept of the line.

2.4 CONVECTION IN POLYMER GELS

2.4.1 Background

Convection in horizontal layers has become one of the most basic and widely investigated topics in fluid dynamics[28,29]. When a horizontal layer of fluid is heated from below, it may undergo Rayleigh-Benard convection due to intrinsic instability. As an analogous form of convection in porous media, convection can occur for a fluid-saturated matrix[30,31]. In the laboratory, the matrix consists of a packing of spherical particles. Such convection is relevant to geothermal applications and to flow in soils.

Here we propose to study convection in polymer gel. A gel consists of both network and solvent. The solvent in a gel can be divided into two classes. One is free solvent that can move through a polymer network and the other is bound water that is bonded to the network and can't move freely against gel network. The relevant part to this research is the free water in gels. When a thin horizontal layer of gel is heated from below, a temperature difference ΔT is created across a layer of height d. We have derived the governing equations for the gel system and found that the dominant term is the friction between the fluid and the polymer network.

The friction coefficient of the gel can be adjusted by either changing the polymer network concentration or the environmental temperature. The temperature dependence of friction coefficient is particularly interesting. According to previous studies by Tanaka group in MIT,[32] as the gel approaches to its phase transition temperature, the effective pore size becomes larger and appears to diverge. The friction coefficient between solvent

and network is expected to be very small. Then the convection in the gel system would be equivalent or close to the convection in a water system.

2.4.2 The Governing Equation

The convection phenomena of fluid flow in polymer gel network are different from the convection of a free fluid in many aspects such as the convection pattern and the condition for convection onset.

Three governing equations for general convection in the Boussinesq approximation[28] are given below. Boussinesq approximation supposed that the fluid has a constant heat capacity per unit volume, ρC_p.

The first is the continuity equation

$$\nabla \bullet \mathrm{u} = 0 \qquad (2.78)$$

and the second is the Boussinesq dynamical equation

$$\frac{\partial \vec{\mathrm{u}}}{\partial \mathrm{t}} + \vec{\mathrm{u}} \bullet \nabla \vec{\mathrm{u}} = -\frac{1}{\rho}\nabla \mathrm{P} + \nu \nabla^2 \vec{\mathrm{u}} - \vec{\mathrm{g}}\alpha\Delta \mathrm{T} \qquad (2.79)$$

and the third is the thermal equation

$$\frac{\partial T}{\partial t} + \mathrm{u} \bullet \nabla \mathrm{T} = \kappa \nabla^2 \mathrm{T} + \frac{\mathrm{J}}{\rho \mathrm{C_p}} \qquad (2.80)$$

Where **u** is the velocity of the fluid and

α: the coeffidient of expansion of the fluid.

ν: kinematic viscosity of fluid, $\nu=\mu/\rho$.

κ: thermal diffusivity of fluid, $\kappa=K/(\rho C_p)$.

μ: the viscosity of fluid.

K: thermal conductivity of fluid.

ρ: the density of fluid.

C_p: specific heat at constant pressure.

g: the gravitional acceleration.

The Boussinesq dynamical equation is nothing but the Navier-Stokes equation except for the buoyance force term $-g\alpha\Delta T$, which is the force that drives the convection. As for a free convection, if heating from bottom, the warmer, light fluid on the bottom prefers to go up, the cooler, heavy one on the top prefers to sink.

As for a gel network, we should consider the friction force between the solvent and the gel network. Therefore, we need to add a new term in the form of $-f\mathbf{u}$ to the Boussinesq dynamical equation as

$$\frac{\partial u}{\partial t} + u \bullet \nabla u = -\frac{1}{\rho}\nabla P + \nu \nabla^2 u - \frac{f}{\rho} u - g\alpha\Delta T \qquad (2.81)$$

Where f is the friction coefficient between the fluid and the gel network. This new friction term, represents the tendency to prevent the convection, similar to the initia term $\mathbf{u}\bullet\nabla\mathbf{u}$, the viscous term $\nu\nabla^2\mathbf{u}$ in the same equation and the conduction term $\kappa\nabla^2 T$ in the thermal equation. Therefore, for a steady convection in a polymer gel without internal heat generation, time related term and heat generation term are gone. The governing

equations for convection in gel network on the Boussinesq approximation can be rewritten as

$$\nabla \bullet u = 0 \tag{2.78}$$

$$u \bullet \nabla u = -\frac{1}{\rho}\nabla P + \nu \nabla^2 u - \frac{f}{\rho} u - g\alpha \Delta T \tag{2.82}$$

$$u \bullet \nabla T = \kappa \nabla^2 T \tag{2.83}$$

2.4.3 Dimensionless Numbers

According to the Π theorem[29], if the governing equations are rewritten in the dimensionless form, the number of variables is reduced by m that is the number of fundamental units involved in the phenomenon. Hence, the whole dynamical system is determined by the fewer dimensionless variables. For the convection system here, let us introduce the relevant dimensionless variable. Some of them are related with each other.

1. Prandtl number:

$$P_r = \frac{\nu}{\kappa} \tag{2.84}$$

is defined as the ratio of two fluid properties (kinematics viscosity to thermal diffusivity). P_r is a property of the fluid instead of the particular flow. Gases have values of the Prandtl number around but a little less than 1. Most liquids have values greater than 1 but by widely varying amounts. Water has Prandtl number around 6 at room temperature.

2. Grashof number:

$$G_r = \frac{g\alpha \Delta T L^3}{\nu^2} \tag{2.85}$$

is defined as the ratio of the inertia and the viscous force. The parameter L is a length scale. That is the distance between which the convection would occur. For a sheet of gel for our interesting in convection, it is the thickness of the gel. Small Grashof number implies negligible inertia forces. In a typical case that water flows between two large horizontal plate, we have g=980 cm/sec^2, α=2x10^{-4}/^{0}C, v=1.8x10^{-2} cm^2/sec, ΔT=0.1 ^{0}C, L=5 mm and G_r= 7.6. It is found that the dynamical similarity depends on two non-dimensional parameters P_r and G_r.

3. Rayleigh number:

It is necessary to know which processes are important for temperature distribution in convection.

$$R_a = \frac{g\alpha\Delta T L^3}{\nu\kappa} \qquad (2.86)$$

which is defined as the ratio between the advection term $\mathbf{u}\bullet\nabla$T and the conduction term $\kappa\nabla^2$T. R_a is related to the above two numbers as $R_a=P_rG_r$ when G_r is small. For water convection in horizontal layers, the onset of the convection is given by R_a=1706[28].

4. Network numbers:

For the convection dynamics in the polymer gel, we need to introduce other two dimensionless numbers. N_1 is defined by the ratio of the gel network friction force and the viscous force that is

$$N_1 = \frac{f L^2}{\rho\nu} \qquad (2.87)$$

In our case, L=5 mm, ρ=1 g/mm^3, v=1.8x10^{-6}m^2/sec, f=5x10^{11} dyn$\bullet$sec$\bullet$cm^{-4} (see chapter references 9 and 33), and N_1=7x10^9>>1. Therefore, the viscous force can be neglected.

The dominant force against convection in gel system is the friction force between the network and solvent.

N_2 is defined as the ratio of the friction term to the inertia term:

$$N_2 = \frac{\alpha \rho^2 g \Delta T}{f^2 L} \qquad (2.88)$$

Gel number N_2 is related to G_r and N_1 as $N_2=N_1^2/G_r$. Using typical values for a horizontal convection in a gel, we have $N_2=6.4\text{x}10^{18}>>1$. From calculations of gel numbers N_1 and N_2, we know that both inertia and viscous terms can be omitted. The dynamical equation for steady flow (eq 2.82) is thus simplified to

$$-\nabla P - f\text{u} - \text{g}\alpha\rho\Delta\text{T} = 0 \qquad (2.89)$$

That would be similar to the dynamical equation for convection in porous media[30,31].

2.4.4 Nusselt Number and Gel Rayleigh Number

Nusselt number is defined as the ratio of the actual heat transfer to the heat transfer that would occur if the fluid remained at rest.

$$N_u = \frac{HL}{\text{K}(T_2 - T_1)} \qquad (2.90)$$

where H is defined as the rate of transfer per unit area. The onset of convection is thus marked by N_u increasing above unity.

Due to $N_2>>1$, the dominant force against the convection is the network friction force instead of the viscous force. Therefore, the Rayleigh number should be replaced by a new dimensionless number. From the original defination, Rayleigh number is the ratio of the advection term to the conduction term,

$$R_a = \frac{|\mathrm{u} \bullet \nabla \mathrm{T}|}{|\kappa \nabla^2 \mathrm{T}|} \sim \frac{L}{\kappa} \mathrm{U} \qquad (2.91)$$

But now the velocity of the fluid in convection is controlled by following two factors: buoyance force and network friction force: fU~αρgΔT. Therefore U~αρgΔT/f and the Rayleigh number for a gel system, based on eq 2.91, would be

$$R_a = \frac{\alpha g \rho \Delta T L}{\kappa f} \qquad (2.92)$$

By measuring N_u (eq 2.90) as a function of Ra (eq 2.92) for a gel system we can determine the critical value of the Rayleigh number R_{ac} at which the onset of the convection starts.

Also it is possible to calculate R_{ac} theoretically using the equations 2.78, 2.83 and 2.89 for a given system and boundary conditions, and compare it with the experimental value.

2.4.5 Discussion on the Friction Coefficient

From above analysis, we know that the friction coefficient plays an important role for determing onset of the convection in a gel system. It is interesting to note that the friction coefficient can be easily changed in the gel. In fact, the friction coefficient f depends on the total concentration of polymer of the gels, including both the main constituent and crosslinkers. The experimental results indicate that the concentration dependence of the friction coefficient is expressed by a power law relationship[33],

$$f \propto \phi^{3/2} \qquad (2.93)$$

In order to observe the phenomena of the convection in the polymer gel, one of the ways is to decrease the network concentration to obtain a large R_a.

According Tanaka and Tokita's studies, the friction coefficient also strongly depends on the temperature[33,34] when temperature approaches the phase transition. For a good solvent, the friction coefficient is inversely proportional to the square of the average mesh size of the network (assumed to be related linearly to the correlation length ξ of the gel),

$$f \propto \frac{1}{\xi^2} \qquad (2.94)$$

Tokita and Tanaka predict that the density fluctuation of a gel appears to diverge as the temperature approaches the spinodal temperature. On the spinodal line, the friction coefficient of a gel is expected to vanish. If the above prediction is true, the convection is expected to be free convection as in pure solution around the spinodal temperature T_c.

When f is near zero or much smaller, then the viscous force is dominant over the friction force. As a result, the Rayleigh number will take the original form as in eq 2.86. Once R_a is above the crucial point R_a=1706, the convection is still expected to exist. It could be predicted that the convection in gel network would have more chance to occur around phase transition than other temperature. One more thing for experimentally studies of convection in gel networks, phase transition temperature really depends on a local network structure. The non-uniformity of the gel network structure could disperse the phase transition temperature into a relatively broad range. Thus the critical phenomena would be weaker than expected.

The experimental studies on the convection in the polymer gel may help to understand both the characteristic of the convection in the polymer gel and the temperature dependence of the friction coefficient and may reveal even more novel phenomena. Further, convection in porous gel could be another interesting topic.

2.5 CONCLUSION

In this work on kinetics of gel swelling, we have extended Li and Tanaka's study by including the motions of both the solvent and the gel network. Using the new swelling equations, we have calculated the solvent velocity field and studied the swelling process of the network for a long cylindrical and a large disk gel. The motion patterns of solvent have been obtained. The results for network kinetics are obtained without using L-T′s two processes approach. We have found that the swelling processing is slower than expected based on the pure diffusion theory. From analytical solutions of our generalized gel swelling equations, we can obtain gel swelling behavior not only at the surface but also in the interior of gels**.** Analysis presented here could be used for many cases where non-spherical gels are used and in many applications such as drug delivery for better understanding.

We modified the equations for gel in pure liquid and extended to gel swelling and shrinking in polymer solution. Gels have smaller equilibrium diameters in polymer solution (such as PVA) than that in pure liquid (such as water). The equilibrium diameter of gel decreases with increase of the PVA concentration. We have calculated an important parameter Δ_r. If $\Delta_r>\Delta$, gels will shrink from their initial states. If $\Delta_r=\Delta$, gels will keep their diameters unchanged. The partial pressure of PVA is quadratically related

to its concentration in dilute polymer solution. The swelling of gels in polymer solution is slowed down by PVA clogging water intake of gels**.** The relaxation times of gels shrinking in polymer solution with various concentrations are not different within experimental error. The experimental results are in excellent agreement with the theory.

The convection in gel network is analyzed for the first time up to my knowledge. We modified the governing equations of the convection to accommodate the convection in gel network. Two network numbers were proposed as new dimensionless parameters in controlling the convection in gel networks. The analysis predicts the friction between solvent and gel network is the dominant force against convection. Approaching to spinodal decomposition of gel would lead to more chance for the convection to occur even though the convection has less chance otherwise. Further theoretically and experimentally researches on the convection on gel network would help for better understanding the interaction between gel network and solvent, and also for applications such as thermal conductivity of gel.

2.6 CHAPTER REFERENCES

[1] Tanaka, T. Am. Chem. Soc. Symp. **1992**, 480, 1.

[2] Li, Y.; Tanaka, T. Ann. Rev. Mater. Sci. **1992,** 22, 243.

[3] Shibayama, M.; Tanaka, T. Adv. Polym. Sci. **1993,** 109, 1 .

[4] Hoffman, A. S. J. Controlled Release, **1987**, 6, 297.

[5] Peppas, N. A.; Langer, R. Science **1994,** 263, 1715.

[6] Osada, Y.; Okuzaki, H.; Hori, H. Nature **1992**, 355, 242.

[7] Hu, Z.; Zhang, X.; Li, Y. Science **1995**, 269, 525.

[8] Kajiwara, K. et al. Polymer Gels; Plenum Press: New York and London, 1990.

[9] Tanaka, T.; Hocker L.; Benedek, G. J. Chem. Phys. **1973**, 59, 5151.

[10] Tanaka, T.; Fillmore, D. J. Chem. Phys. **1979**, 70, 1214.

[11] Peters, A.; Candau, S. J. Macromolecules **1986**, 19, 1952.

[12] Peters, A.; Candau, S. J. Macromolecules **1988**, 21, 2278.

[13] Onuki**,** A. Dynamics and Statistics of Patterns; World Science, 1989.

[14] Li, Y.; Tanaka, T. J. Chem. Phys. **1990,** 92, 1365.

[15] Li, Y.; Tanaka, T. Springer Proceedings in Physics, Heidelberg, **1990,** 52, 44.

[16] Li, Y.; Tanaka, T. Polymer Gels; Plenum Press: New York, 1991.

[17] Landau, L. D.; Lifshitz, E. M. Theory of Elasticity; Pergamon press: Oxford, 1986.

[18] Onuki**,** A.; Adv. Polym. Sci. **1993**, 109, 97.

[19] Zrinyi, M.; Rosta, J.; Horkay, F. Macromolecules **1993**, 26, 3097**.**

[20] Flory, P. J. Principles of Polymer Chemistry, Cornell University Press, Itaaca, N.Y., **1953**.

[21] Vink, H. Europ. Polym. J. **1971**, 7, 1411.

[22] Vink, H. Europ. Polym. J. **1974**, 10, 149.

[23] Cherayil, B. J. et al. Macromolecules **1986**, 19, 2770.

[24] Vasilevskaya, V. V. Macromolecules **1992**, 25, 384.

[25] Merkle G. et al., Macromolecules **1993**, 26, 2736.

[26] Silberberg-Bouhnik M. et al., J. Polym. Science **1995**, 33, 2269

[27] Li, Y. Ph. D. Thesis, MIT, unpublished **1989**

[28] Tritton, D.J. Physical Fluid Dynamics, 2nd ed. Oxford, Oxford University Press, England, **1989**.

[29] Eskinazi, S. Principles of Fluid Mechanics. 2th Edition, Allyn and Bacon, Boston, **1968**.

[30] Shattuck, M. D.; Behringer, R. P.; Jonson, G. A.; Georgiadis, J. G.; Phys. Rev. Lett., **1995**, 73,1934.

[31] Howle, L.; Behringer, R. P.; Georgiadis, J. G. Nature, **1993**, 362, 230.

[32] Tanaka, T.; Ishiwata, S.; Ishimoto, C.; Phys. Rev. Lett., **1977**, 38, 14.

[33] Tokita, M. Adv. Polym. Sci., **1992**, 110, 27.

[34] Matsuo, E. S.; Tanaka, T. J. Chem. Phys., **1988**, 89,1695.

CHAPTER 3

SPINODAL DECOMPOSITION IN N-ISOPROPYLACRYLAMIDE GEL

3.1 INTRODUCTION

Spinodal decomposition remains as one of the most active areas in the study of the phase transition[1] and has been investigated extensively for various systems including polymer blends[2,3], binary liquids[4], polymeric liquids[5], and binary gases[6]. Because chemically crosslinked polymer gels have a unique structure with a three-dimensional network immersed in a solvent, spinodal decomposition in gels is constrained by the elasticity of the gel network.[7] As a result, spinodal decomposition in gels could exhibit significant and interesting properties that are different from those in polymer solutions. Extensive studies of spinodal decomposition in polymer gels have been carried out including theoretical discussion of spinodal curves of a gel,[7~9] turbidity study

of phase separation in polyethylene glycol methacrylate-glycol-water,[10] and experimental observations of phase transition and the spinodal decomposition of gels.[11, 12]

The N-isopropylacrylamide (NIPA) polymer gel is a model system that has a large, reversible volume change in response to environmental temperature changes under atmospheric pressure.[13] Specifically, the NIPA gel in water is transparent and swollen at room temperature. Upon heating, the gel shrinks and eventually collapses at a critical temperature (T_c) of about 34 ^{0}C.[13] The NIPA gel exhibits critical behavior similar to the Ising system.[14] When a typical critical phase-transition system undergoes a transition from the one-phase state to the two-phase coexistent state along the critical isochore path, the spinodal decomposition occurs.[15] The beginning of the spinodal decomposition in a NIPA gel is marked by a transition from a transparent gel to a cloundy gel. The initial stages of spinodal decomposition in NIPA gels have been studied using light scattering,[16-18] turbidity,[15, 18] and small-angle X-ray[19] techniques and can be analyzed using Cahn-Hilliard-Cook (CHC) theory.[20] The shrinking kinetics of the NIPA gel after it is heated from below T_c to above T_c has been studied in details by Hirose and coworkers.[21, 22] They correlated NIPA chemical composition (monomer concentration and crosslinker density) with shrinking kinetics and bubble formation in the gel surfaces.

All previous studies of spinodal decomposition in the NIPA gel have focused on the kinetics of gel-volume change. In this section, it is the aim to report that associated with volume shrinking in the spinodal decomposition regime, gel turbidity undergoes significant change. Comparing measurements from two well-separated windows opened with an ultrasonic probe (λ=150 μm) and a visible light probe (λ=550 nm), we propose a qualitative picture of structural evolution during the decomposition process. Better understanding of the spinodal decomposition

in gels may lead to the development of new technologies ranging from smart windows[23] and optical displays[24] to ultrasonic attenuators.[25]

3.2 EXPERIMENTAL

The NIPA gel samples were prepared by free-radical polymerization[13]. A mixture of 7.8 g of N-isopropylacrylamide, 133 mg of methylenebisacrylamide (BIS) as cross-linker, and 240 μL tetramethylethylenediamine (TEMED) as accelerator, was dissolved in 100 mL of deionized and distilled water. Nitrogen gas was bubbled through the solution to remove dissolved oxygen. Then 40 mg ammonium persulfate (APS) was added to the solution to initiate gelation. Thin films of the solution were cast between two micro-slides with a fixed separation of 1 mm for turbidity measurement. A cylindrical gel was made by casting the pregel solution in a glass tube with a diameter of 1 cm. The sample were left untouched for about 12 hours before being transferred into a water bath to swell at room temperature.

Upon the increase of temperature, the gel shrank and eventually collapsed to a condensed phase at a T_c of about 34 ^{0}C. The spinodal decomposition of the gel can be induced by quenching the sample from a constant temperature below T_c to various temperature above T_c. The beginning of the spinodal decomposition was marked by a transition from a transparent gel to a cloudy gel.

The turbidity of gel samples was monitored by a spectrophotometer (Spectronic 301, Milton Roy Ltd.) operating at the wavelength of 555 nm. The temperature of samples was controlled by a circulation water bath (Brinkman Lauda Super RM-6) with an accuracy of $\pm$ 0.05

^{0}C. The temperatures at both the sample cell and the circulator were monitored by temperature sensors. In addition, a thermal bath was used to provide the initial temperature of the sample before it was quenched into the two-phase region inside the spectrometer sample holder.

The transmitted light intensity I_t and the incident intensity I_0 are related by the sample turbidity A and thickness L,

$$\frac{I_t}{I_0} = e^{-AL} \qquad (3.1)$$

The light absorption (=$\log(I_t/I_0)$) of gel sample was monitored by a spectrophotometer operating at a wavelength of 555 nm. Multiplying the absorption by a factor of ln(10)/L performed the conversion from absorption to turbidity.

The ultrasonic attenuation of NIPA gel samples was measured by a computer-controlled ultrasonic system (MBS-8000, METEC Instruments, Inc.). A ceramic transducer with a fundamental frequency of 10 MHz was used to generate a longitudinal ultrasonic wave with a wavelength of around 150 μm in the NIPA gel. The attenuation (α) was calculated from $\alpha=(1/d)20\log(A_2/A_1)$ where d is the thickness of the sample, and A_1 and A_2 are the amplitudes of the first and second echo, respectively. The cylindrical gel samples were immersed in water in an aluminum cell and placed between the transducer and the bottom of the cell with fixed space (0.8 mm here). The transducer was fixed properly to ensure it was in good contact with the sample and there was no air between them. Because the aluminum had much higher acoustic impedance than water, it could effectively reflect the acoustic wave in the bottom of the cell. The sample temperature was monitored using a self-built temperature-control device.

Design of experiments involved careful choice of a set of gel sizes and time scales of temperature ramping. Optical absorption and ultrasonic attenuation were both employed as two

windows to visualize gel structures and their evolution each with different micro-scale. Both optical absorption and ultrasonic attenuation are induced by gel's non-uniformity in relevant scale and the interaction between microstructure and optical wave or ultrasonic wave.

3.3 RESULTS AND DISCUSSION

Accompanied with the volume shrinkage at transition stage, NIPA's turbidity increases drastically, which is believed to be induced by the phase separation.[33, 34] Dense phase domains which are regions with more dense gel network density, and dilute phase domains which are regions with less gel network density are built up inside gel. It is this heterogeneous structure that scatters and absorbs light and makes the sample opaque. Li, Wang, and Hu presented a detailed study on such phase separation of NIPA gels.[15] Phase separation and turbidity enhancement in the phase transition stage are explained as follows. When the gel is quenched, due to the inherent inhomogeneities in the network structure, some regions have a stronger tendency to collapse than others. Initially, polymer chains aggregate to form bundles in concentrated regions. Since the system is unable to release water quickly, the water content in the nearby dilute regions increases. Further dilution of the already diluted region does not require much energy. Therefore, once some diluted regions are formed, they will be further diluted to facilitate the collapsing of the concentrated regions. So dense regions and dilute regions are formed in the gel. Excess water is kept in dilute domains compared to the complete shrunken and stable state.

This picture explains what really happens in NIPA gels. One thing seems puzzling. If such a heterogeneous structure, or in term of domain, is formed due to quick heating and slow water releasing, this implies that slow process or long enough time will make results different and the following statement might be true. In a slow enough heating process, the gel system has sufficient time to expel out excess water in a quasi-static process. No domains are formed in such case. There will be no opaque above the transition temperature correspondingly. Slow heating process could impede the opaque after phase transition. But no such or similar result was reported before. Furthermore, if an already opaque sample is kept at certain temperature above transition temperature long enough, excess water in dilute domains could be expelled out, then the domains disappear, the gel shrinks, and the opaque would also disappear accordingly. But the previous experiments showed that the opaque stays even after gel samples have totally shrunken. If the opaque was originated from the domains, how could the opaque still stay after the domains have disappeared?

To answer all above questions and fully understand dynamics of gel's domain, well-designed experiments have been carried out in our laboratory. These experiments did bring out interesting results. One of the experiments, designed with a long waiting time at temperature above T_s, showed the gel transition from the opaque to the clearing. It should be pointed out that that the clearing of the opaque does not simultaneously come out with volume change. The clearing takes much longer time than that of volume change. For example, one piece of NIPA sample of about 1.2 mm thickness at 34.4 ^{0}C took about 24 hours to get complete shrunk, but took about 80 hours to be clear. So the experiments implied at least two things. First, the opaque

is induced by a kind of metastable structure. Second, the opaque clearing and the volume shrinking are not synchronized in same dynamical processes.

Our further experimental results in ultrasonic attenuation, temperature dependence and sample size dependence of transition time from the opaque to the clearing greatly improved the understanding of the mechanism of opaque and phase separation of NIPA through transition stage. The experimental results are presented and analyzed in the following sections of this chapter. A new hypothesis is also proposed. The hypothetical theory and experimental results are consistent. NIPA gels were used as a model system. The all presented data were collected from NIPA gels. The results could be extended to similar systems. Many phenomena and concepts of spinodal decomposition in gels would be more general. Further experiments are necessary for confirmation and clarification. Bear the following facts in mind, the phase transition in local area of a gel is related to the solvent moving into or out from this local area, so is related to the whole gel system. Such globalization of the phase transition in gel system is a key to understand the uniqueness of gel turbidity and spinodal decomposition.

3.3.1 Optical Turbidity under Fast Heating Rate

Terms “fast” in this section and “slow” in the next section are relative to each other. Figure 3.1 shows the turbidity versus temperature for the NIPA gel with thickness of 1.2 mm at room temperature. The sample was heated from 33.3 ^{0}C up to 35.1 ^{0}C with an average heating rate of 0.1 ^{0}C every twenty minutes. The turbidity increases drastically while the sample temperature is approaching to the transition temperature T_s. In another word, the sample becomes

opaque at T_s. Then the opaque state stays when the sample temperature is above T_s. This result shows how the opaque is induced. In Fig. 3.1 is shown the above result of the turbidity as a function of temperature. The turbidity shoots up at T_s and stays at a high opaque level after the gel sample has totally shrunken above T_s even the heating process is slow enough to provide sufficient time for gel to shrink during the transition,

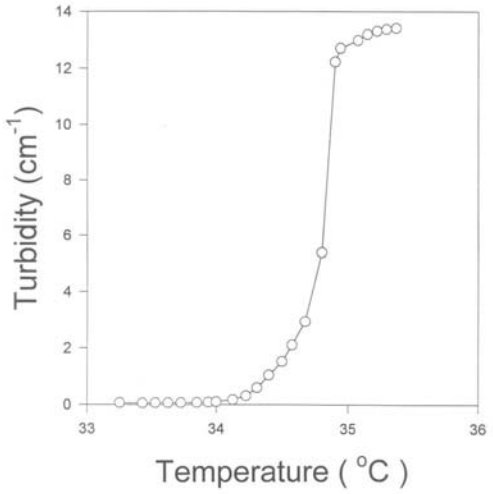

Figure 3.1. A NIPA gel sample, of 1.2 mm thickness, was heated from 33.3 ^{0}C up to 35.1 ^{0}C with an average heating rate of 0.1 ^{0}C every twenty minutes. The turbidity increases drastically at T_s and the sample became opaque. Then the opaque remains above T_s. Even the heating process is slow enough to provide sufficient time for gel shrinking. The opaque still remains after the gel sample has totally shrunken above T_s.

3.3.2 Optical Turbidity vs Slow Heating Rate

The same NIPA gel sample, of 1.2 mm thickness, was heated from 33.2 ^{0}C up to 34.6 ^{0}C very slowly compared to the above experiment in section 3.3.1. Each step waits long enough time until the sample reaches its thermal equilibrium. Step width varies according to how far away

from phase transition temperature T_s. Around T_s, typical temperature increment each step is 0.01 ^{0}C. Each step waits about ten hours or even more before another step taken. The turbidity shoots up at T_s due to strong fluctuation of gel density at the transition point. Then turbidity drops down when the temperature is increased above T_s, leaving a turbidity peak at T_s. That means the sample is clear again above T_s. This result, shown in Fig. 3.2, is different from the result of the first experiment in Fig. 3.1.

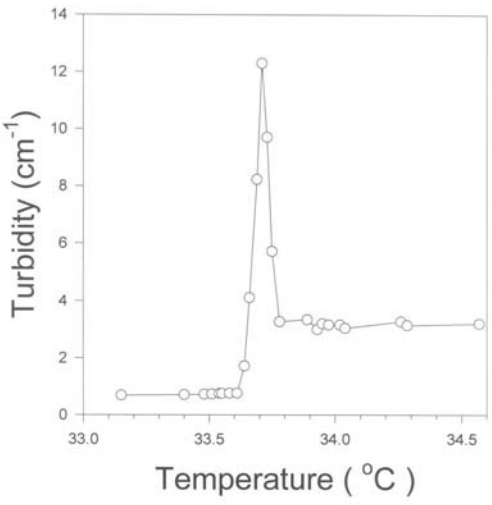

Figure 3.2. The same NIPA gel sample as in Fig. 3.1, of 1.2 mm thickness, was heated from 33.2 ^{0}C up to 34.6 ^{0}C very slowly. Each step waits long enough time until the sample reaches its thermal equilibrium. Step width varies according to how far away from phase transition temperature T_s. Around T_s, typical temperature increment each step is 0.01 ^{0}C. Each step waits about ten hours or even more before another step taken. The turbidity is recorded as the function of temperature.

3.3.3 Opaque Clearing

It is implied that the opaque state is not favored in term of free energy above T_s from the fact of

the turbidity shooting at T_s and depression above T_s (shown in Fig. 3.2) in a slow heating process. It is also implied that the opaque state is frozen above T_s in fast heating from the fact of the shooting of the turbidity at T_s and the retention of the turbidity above T_s (shown in Fig. 3.1) in a fast heating process. On the other hand, it suggests that the frozen opaque might be freed and the frozen gel might turn into the clearing state if such frozen opaque gel above T_s waits long enough time. It is confirmed by another experiment shown in Fig. 3.3. The same sample, as used in Fig. 3.1 and Fig. 3.2, of 1.2 mm thickness, was warmed up to 34.4 ^{0}C and kept at that temperature. The turbidity was recorded as a function of time t.

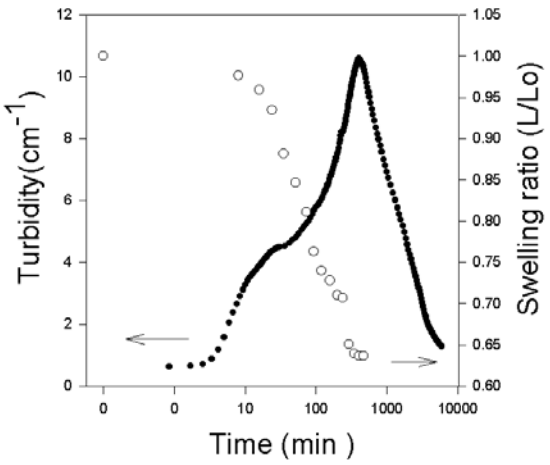

Figure 3.3. The turbidity, swelling ratio, and structure of the NIPA gel as a function of time. A room temperature NIPA gel of 1.2 mm thickness (the same sample as in Fig. 3.1) was quenched into 34.4 ^{o} C and kept at that temperature for measurements. Open circles are for the swelling ratio, where L_o is the length at room temperature, and solid circles are for the turbidity

The result is shown in Fig. 3.3. The turbidity goes down and the opaque clear out at last. The results of the experiment were reported for the first time by our group and clean off a lot of confusions. The swelling ratio was also recorded simultaneously as a function of time.

3.3.4 Ultrasonic Attenuation vs Fast Heating

Ultrasonic method is also employed to study phase transition of gels. The most content of hydrogel is water. Water forms a continuous phase in a gel system. The gel network is only very small fraction by volume. The velocity of ultrasonic longitudinal wave is mainly determined by water. But ultrasonic attenuation in gel system has a major contribution from gel network because of its non-uniform structure. Ultrasonic attenuation in gel system would give us more information about the structure and its evolution of gels over phase transition.

The sample was 1.2 cm in diameter and 2.0 cm in height at fully swollen state in room temperature. The measurement was carried out when the NIPA gel was warmed up from room temperature with an average heating rate of 1 ^{0}C per hour and the slowest rate of 1 ^{0}C every 2.5 hours on the transition stage around 34-35 ^{0}C. The ultrasonic attenuation (circles) is plotted as a function of temperature in Fig. 3.4. The swelling ratio (squares) of the NIPA gel is plotted against temperature. It is clearly that the sample volume was not significantly changed. Along with that, a higher attenuation state is reached at T_s and stays above the transition temperature T_s. The volume change was quenched since the temperature ramping is so fast. The high attenuation

above T_s implies that non-uniform structure was frozen along with the volume quench. It is this non-uniform structure that induced high attenuation.

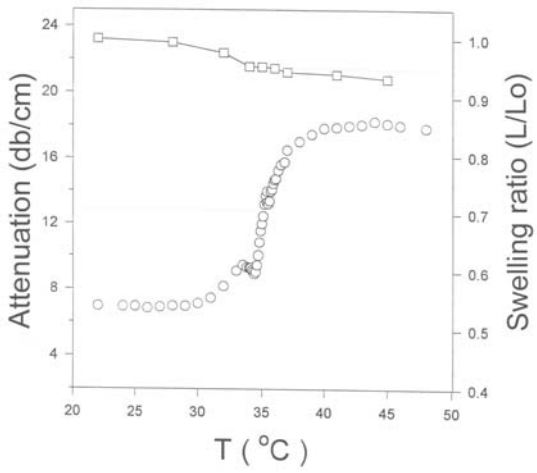

Figure 3.4. The sample was 1.2 cm in diameter and 2.0 cm in height at fully swollen state in room temperature. The measurement was carried out when the NIPA gel was warmed up from room temperature with an average heating rate of 1 ^{0}C per hour and the slowest rate of 1 ^{0}C every 2.5 hours on the transition stage around 34~35 ^{0}C. The ultrasonic attenuation (circles) is plotted as a function of temperature. The swelling ratio (squares) of the NIPA gel is plotted also as a function of the temperature..

3.3.5 Ultrasonic Attenuation of Mediate Heating

The dimensions of NIPA gel were the same as these of the sample in Fig. 3.4. The NIPA gel was slowly warmed up to 36 ^{0}C step by step. The heating rate is about 0.1 ^{0}C per day. The acoustic attenuation exhibits a very narrow peak at around 34 ^{0}C. The sample completely shrank and was opaque above 34 ^{0}C. The result is shown in Fig. 3.5. Please be aware of that the

temperature ramping is much slower than that of the sample in Fig. 3.4 so that the volume shrunk and high attenuation of ultrasonic wave is depressed above T_s. But the ramping rate is not slow enough to free the high opaque state (high turbidity of light).

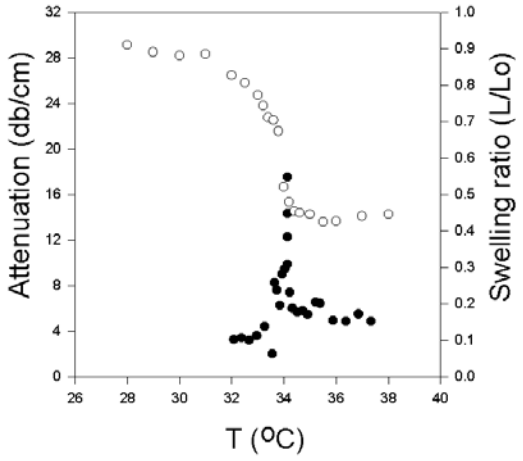

Figure 3.5. The Sample dimensions were the same as ones in Fig. 3.4. The NIPA gel was slowly warmed to 36 ^{0}C step by step. The heating rate is about 0.1 ^{0}C per day. The acoustic attenuation exhibits a very narrow peak at around 34 ^{0}C. The sample completely shrank and was opaque above 34 ^{0}C.

3.4 DYNAMICAL PROCESSES AND GEL STRUCTURE

As we briefly discussed in section 3.3, the experiments in Fig. 3.1 and Fig. 3.2 suggest that the opaque state induced at T_s by the density fluctuation will be depressed if the temperature ramping is slow enough and otherwise would be frozen above T_s. Furthermore, the frozen opaque state above T_s could be freed and the gel then become clear if the dwell time is long

enough. An example is the situation shown in Fig. 3.3. The similar situation happens to the ultrasonic attenuation and volume shrinking in a gel system such as the examples in Fig. 3.4 and Fig. 3.5. But the non-synchronized sequences between optical turbidity and ultrasonic attenuation indicate that they are either involved different gel structure dynamics or are related to the different spatial scales of the same gel structure dynamics so to be expressed in different time scales.

Combining above points, in addition to Li-Wang-Hu's hypothesis[15], following understanding and visualization of the dynamics of gel optical turbidity and ultrasonic attenuation is proposed.

When a sample is heated up to certain temperature above T_s, the whole gel system is going to shrink. If heating process is slow enough, it will assure that the sample shrinks in the thermal quasi-static process. The optical turbidity will shoot up at T_s as a peak due to enhanced fluctuation at transition stage. Passing over that point, the opaque is cleared (see Fig. 3.2).

In a fast heating process, the system is unable to release water quickly to respond the temperature change. The enhanced density fluctuation at transition stage could be favored in term of free energy under the condition that excess water is still inside gel network. Some dense regions are formed which is in a relative lower free energy. The other dilute regions are also formed correspondingly, which dose not increase the free energy the same much due to soften elastic modulus at transition stage. Over all, the free energy of the whole system is lowered by such heterogeneous structure, called domains, than that of homogeneous one. When the system

temperature is higher than T_s, the domain structure survives, and the opaque state also stays as a sequence of the domain structure. Such a dynamical process is referred to as phase separation.

When a NIPA gel sample (1.2 mm thickness for example) is quenched from room temperature to 34.4^o C, the turbidity and the swelling ratio were recorded as a function of time in Fig. 3.3. And structures of the NIPA gel are visualized in schematic diagrams Fig. 3.6 A to E. The turbidity, ultrasonic attenuation and volume change may be related to the time-dependent structure of the gel as shown in Fig 3.6 A to E.

NIPA polymer chains can bond to water through hydrogen bonds. This preferential interaction allows the gel to swell at room temperature. As a result, the NIPA gel is in a homogeneous, fully swollen phase (low polymer concentration) and is transparent to visible light and ultrasonic waves [Fig. 3.6A].

The spinodal decomposition of the gel is induced by quenching the sample from room temperature to the temperature above the phase transition point. Here, hydrogen bonds are broken by thermal energy. Interaction between polymer chains becomes dominant so that the gel tends to shrink. Because it is impossible to repel all excess water from the network quickly, the interior of the sample is initially under constant volume conditions, that is, the thermodynamic path is an isochore (constant volume). Because of the inherent spatial inhomogeneities (lightly cross linked and heavily cross linked regions) have a stronger tendency to collapse than others, resulting in the formation of dense and dilute domains with different network concentrations. For convenience, we have only marked dilute domains in Figure 3.6B and will refer to them as domains.

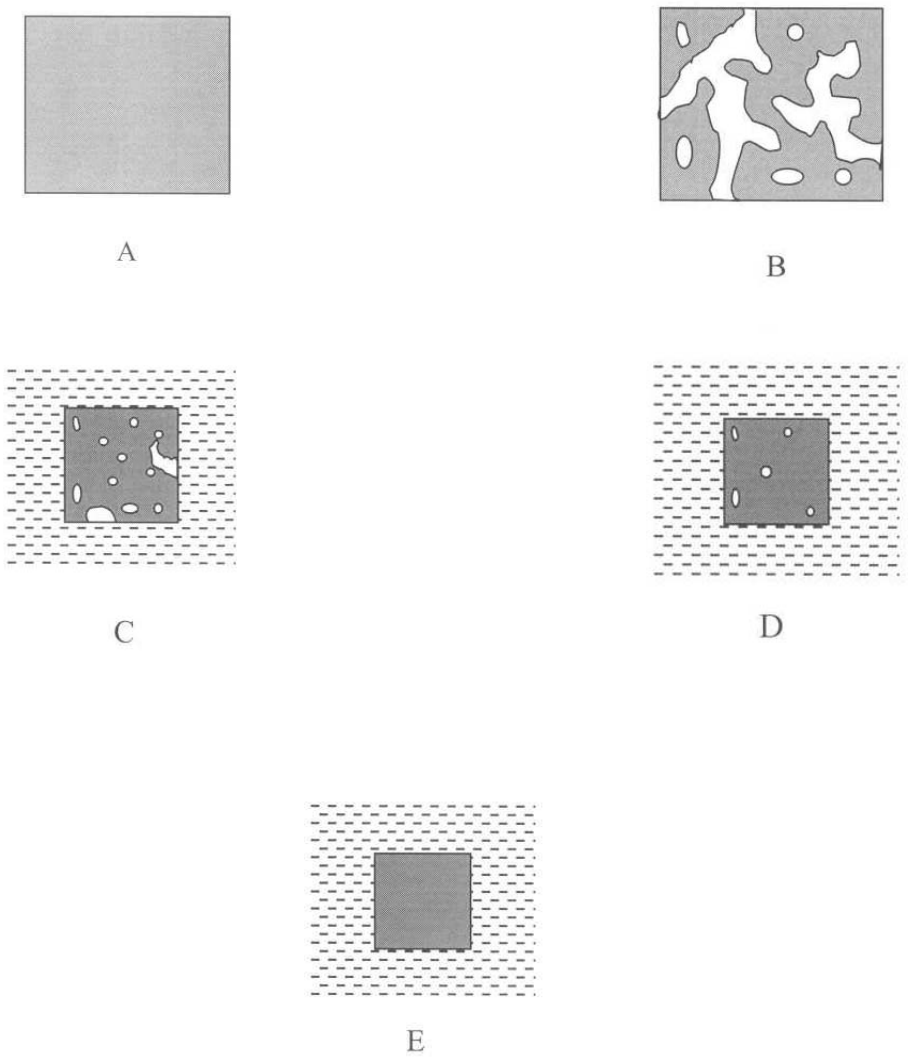

Figure 3.6. Sketches of the gel structures: (A) a homogeneous, transparent, swollen gel in water at room temperature, and (B) after the sample is quenched to $T > T_c$, the gel forms a domain structure. White areas indicate dilute domains with a broad size distribution. (C) Large-sized domains diffuse out first. (D) Small-sized domains diffuse out second. (E) The gel finally becomes transparent and collapsed with a high network concentration (shaded area).

Figure 3.6C suggests that there may be a broad size distribution of domains as revealed by ultrasonic and turbidity measurements. In general, an inhomogeneity will scatter acoustic or electromagnetic waves if it differs in modulus or refractive index from the surrounding medium. The scattering also depends on the wavelength relative to the size of the inhomogeneity. Because waves are scattered strongly by inhomogeneous structures having feature sizes close to the wavelengths (from 0.1 to 10λ), we may probe the movement of large-sized domains around the ultrasonic wavelength of 150 μm and small-sized domains close to the visible light wavelength around 555 nm. Direct evidence that ultrasonic waves and visible light probe different structures is that during the gel-shrinking process the turbidity remained large, whereas ultrasonic attenuation decreased to a small value. Because the formation of domain structure only involves the local arrangement of the network without changing the volume, the time required is short. This is why the turbidity and ultrasonic attenuation initially increase rapidly after the sample is quenched to $T > T_c$.

After the initial volume-frozen period, the gel starts to shrink with time. As the gel collapses almost completely and the ultrasonic attenuation approaches a small value, the turbidity remains at a high value. This indicates that on the average the large-sized domains diffuse out from the gel network faster than the small-sized domains do. This may be originated from the fact that the large-sized domains have better chances to connect to each other and to the external water as shown in Figure 3.6C. The solvent can easily move out of the gel at its boundary that is in contact with the solvent.

With an even longer waiting period, the turbidity of the gel starts to decreases. This process is very slow and may be associated with movements of small-sized domains that have

only a small fraction, by volume, but are responsible for scattering light as shown in Figure 3.6D. This slow kinetics is associated with very small concentration gradients and very small deformation which provide force to squeeze the solvent out of the gel. Upon extinction comes a homogeneous, transparent collapsed gel with high network concentration (shaded area) at $T > T_c$ as shown in Figure 3.6-E.

3.5 DOMAIN STRUCTURE

Now the morphology of domains is in our interesting to help understanding the optical turbidity and ultrasonic attenuation. The domain should not be too large in size. Since polymer chains are cross-linked into network, a large size domain will increase elastic energy a lot and so offset the benefit from the hydrophobic energy. But the distribution of domain size could be very broad. Let us focus on dilute domains, which are regions with excess water inside. When domain is referred to afterwards in this chapter, it means and represents dilute domain.

In a contrast to light turbidity, the ultrasonic attenuation comes up with gel shrinking, from Fig. 3.4 and Fig. 3.5. So it is assumed that the ultrasonic attenuation is induced by large domain structure considering the wavelength of the ultrasonic wave is 150 μm. As to light wavelength, it is in the order of 1 μm. It might be concluded that the opaque is induced by small domains. This gives us an idea that large domains are related to the gel volume change and ultrasonic attenuation. The small domains are related to light turbidity. Large domains and small domains behave differently.

The two types of domains, large size domains and small size domains, are distinguished qualitatively, due to their behaviors and functions. Statistically, most large domains are connected or are easy to be connected. It is supported indirectly by a swelling test of the porous NIPA gel prepared using phase separation,[35] in which porous space corresponds to dilute domains. Fast swelling and shrinking of such samples suggests that they are connected, or, in another word, continuous in space. So the excess water inside these domains is supposed to be released in a way described by the collective diffusion equations which Tanaka used to describe gel's shrinking and swelling with a relative large amplitude.[31] Roughly, they also obey scaling law as $\tau_1 \propto a^2/D$ where τ_1 is the characteristic time of gel swelling, a is the initial linear size (shortest) of gel sample and D is collective diffusion coefficient which is related to elastic modulus (bulk modulus K and shear modulus μ) and friction coefficient between water and gel network f. It is this type of domains that contribute to volume change in gel shrinking. So the process of volume shrinking obeys $\tau_1 \propto a^2/D$. Here $D \sim 10^{-7}$ cm^2/sec for our NIPA sample. A sample of 1 mm thickness will take about 24 hours to be totally shrunken.

Most domains are not connected to each other in gel. These domains are isolated by normal regions where no phase separation occurs. It is reasonable assumption and understandable that the most isolated domains are of small size. Their motion is not governed by Tanaka's diffusion equation due to their isolated environment. The domains may move around inside gel. The domains do not release extra water and uniformly distribute its network only because they are in favor of the free energy. It is the same reason that leads to phase separation and non-uniform structure. As soon as an isolated domain moves to the surface of the gel sample, it will release excess water and then disappear. It is these isolated, small size domains that

contributes to light scattering and absorption and so to the opaque of the gel sample. The disappearing of such domains on the surface of gel sample marks the clearing of the opaque of gel. Considering the experiment results, it is assumed that the size of such domains ranges below 1 μm. The size of continuous and large domains ranges about between 1 μm to 20 μm.

3.5.1 Brownian Motions

As an isolated domain "feels" the same pressure along all directions around it in that local region, it can change its position only in thermal fluctuation. But it cannot disappear inside of gel because the excess water is still there if excluding the case of domains merging. So the isolated domains move randomly. Their random motion can be described by Brownian motion.[36] If an isolated domain moves to the surface of the sample, the excess water will be released, and this domain disappears. The theory of Brownian motion gives the average squared displacement of an isolated domain from its origin as a function of time τ,

$$\overline{(\Delta X)^2} \propto D_d \tau \qquad (3.2)$$

where D_d is the diffusion coefficient of such isolated domains. On the average, the isolated domains in the center of the spherical sample moves to the surface of the spherical sample with radius a and disappear in the time,

$$\tau_2 = \frac{a^2}{2 D_d} \qquad (3.3)$$

Statistically, all isolated domains in the sample will move to the surface and disappear before that time. That means the sample will be clear at τ_2. The result is roughly same no matter what

shape of gel is. The parameter a can be understood as gel sample's shortest size. By coincidence, it obeys the same scaling law of size squared. But D_d is a different coefficient from collective diffusion coefficient D for gel shrinking.

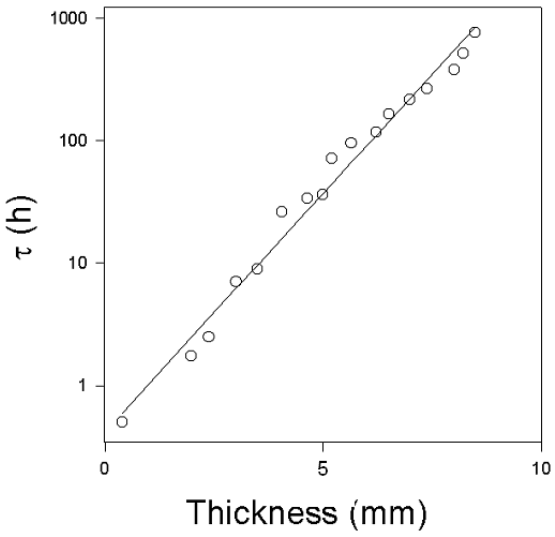

Figure 3.7. The clearing time of the opaque of NIPA gel as the function of sample thickness. All measurements were carried out at temperature 34.3 ^{0}C.

The experimental data of clearing time as the function sample thickness is drawn in Fig. 3.7. The fitting result gives $\tau_2 \propto a^{1.95\pm0.1}$. And $D_d \cong 3.8\times10^{-8}$ cm^2/sec at 34.3 ^{0}C. D_d is small than D in the tested temperature range. The volume shrinking is faster than turbidity clearing. This would explain the Eq. 3.2.

3.5.2 Activation Energy

Besides, isolated small domains may need an extra energy to overcome the elastic deformation while they are moving. So this process is associated with an activation energy ΔE. Obviously ΔE is the function of the elastic modulus. It is expected that

$$D_d = D_{d0} e^{-\Delta E / K_B T} \tag{3.4}$$

where K_B is Boltzman constant, T is absolute temperature.

If the above-assumed mechanism is correct, it can also be checked by experiments. Put Eq. 3.3 back into Eq. 3.2, one has,

$$\tau_2 = \frac{a^2}{2D_{d0}} e^{\frac{\Delta E}{k_B T}} \tag{3.5}$$

The time of opaque clearing increases exponentially with ΔE. At transition temperature, activation energy ΔE is trivial due to nearly zero elastic modulus. For small $\Delta T = T - T_s$, it is also true that $\Delta E \propto \Delta T$ approximately and $\Delta E/(K_B T) \cong \Delta E/(K_B T_s)$. At the range far away from T_s, elastic modulus gradually becomes nearly constant, so ΔE also becomes a constant. For a given sample, one has

$$\ln \tau_2 \approx \frac{\Delta E}{K_B T} + C \tag{3.6}$$

The experimental result for temperature dependence of clearing time is shown on Fig. 3.8. τ increases in exponential way along with temperature. $\Delta E/(K_B T)$ varies in the expected way as analyzed above. Again theory and experiments are in excellent agreement. Data fitting shows that $\Delta E \cong 0.14$ eV at 35.5 ^{0}C and $D_{do} \cong 4.8 \times 10^{-7}$ cm^2/sec.

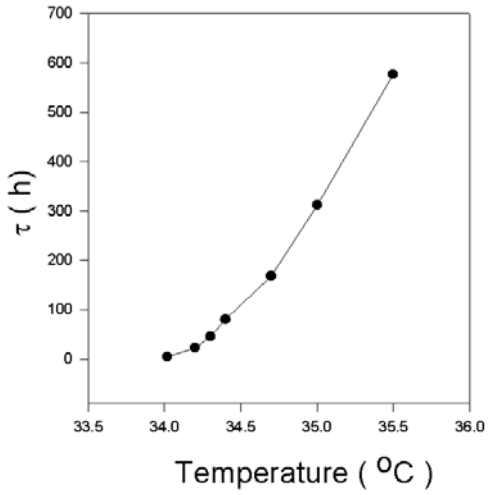

Figure 3.8. The clearing time of the opaque of NIPA gel as the function of temperature. The thickness of the sample was 1.2 mm.

3.5.3 The Kinetics of the Turbidity Clearing

Theoretically, the opaque clearing is not simply mono-exponential function of time. Suppose a sample is in arbitrary shape, considering the Brownian motion of domains, the problem can be treated as a diffusion process with diffusion coefficient D_d in infinite space. The number density of domains at time t at position **r** is $\phi(t, \mathbf{r})$. The initial condition is

$\phi(t=0,|\mathbf{r}|<a)$=constant, $\phi(t=0,|\mathbf{r}|>a)=0$. Assume the absorption is proportional to the total numbers of domains inside of gel. The absorption at time t is,

$$I_t \propto \int_V \phi(\bar{r},t)dV \qquad (3.7)$$

Turbidity is $A= (1/L)\ln(I/I_t)$ as mentioned before. For any given sample, it is complicated. But detailed studies of turbidity kinetics in several special cases like large film would help us understand domain diffusion much better.

3.6 CONCLUSIONS

NIPA gel undergoes volume phase transition around 34 ^{0}C. The light turbidity has a jump at that temperature. Usually the opaque remains even after sample are totally shrunken. Our experiment shown that the turbidity can disappear if the sample stay long enough at that temperature or even never show up at higher temperature if it is heated quite slowly. The kinetics of turbidity reveals the mechanism of domains induced in phase separation and improves our understanding of both opaque and phase separation at transition stage.

NIPA gel's domain structure is meta-stable. It is induced by quick dynamical process. Slow heating will suppress the showing up of opaque above the transition temperature. Domains could be formed in phase separation only if heating process is quick and could disappear if the time is long enough. But these domains have a very broad distribution in size. Large size and continuous domains, which is responsible for volume change of sample, release the excess water in a scaling law $\tau_1 \propto a^2/D$; small size and isolated domains, which is responsible for the opaque of sample, will disappear in the way $\tau_2 \propto (a^2/D_{d0})\exp(\Delta E/(K_B T))$. Kinetics of light absorption is $I_t \propto \int_V \varphi(\mathbf{r}, t)dV$.

3.7 CHAPTER REFERENCES

[1] Gunton, I. D.; Miguel, M. S.; Sahni, P. S. In Phase Transition and Critical Phenomena, Edited by Domb, C and Lebowitz, J. L. Academic, NY, **1983**, 8.

[2] Wiltzius, P.; Bates, F. S.; Heffner, W. R. Phys. Rev. Lett. **1988**, 60, 1538.

[3] Bates, F. S.; Wiltzius, P. J. Chem. Phys. **1989**, 91, 3258.

[4] Kielhorn, L.; Muthukumar, M. J Chem Phys **1999**, 110, 4079.

[5] Tanaka, H.; Sigehuzi, T. Phys. Rev. Lett. **1995**, 75, 874.

[6] Dhont, J. K. G. J Chem Phys **1996**, 105, 5112.

[7] Onuki, A.; Puri, S. Phys Rev E: Stat Phys Plasmas Fluids Relat Interdiscip Top **1999**, 59, 1331.

[8] (a) Borchard, W. Ber Bunsen-Ges Phys Chem **1977**, 81, 989; (b) Borchard, W. Eyr Polym J **1978**, 14, 661.

[9] Dusek, K.; Prins, W. Adv Polym Sci **1969**, 6, 1.

[10] Sedlacek, B. Collect Czech Chem Commun **1967**, 32, 1308.

[11] Tanaka, T. Phys. Rev. Lett. **1978**, 40, 820.

[12] Sato Matsuo, E.; Tanaka, T. J Chem Phys **1988**, 89, 1695.

[13] Hirotsu, S.; Hirokawa, Y.;Tanaka, T. J. Chem. Phys. **1987**, 87, 1392.

[14] Li, Y.; Tanaka, T.; J Chem Phys. **1989**, 90, 5161.

[15] Li, Y.; Wang, G.; Hu, Z. Macromolecules, **1995**, 28, 4194.

[16] Otake, K.; Inomata, H.; Yagi, Y.; konno, M.; Saito, S. Polym Commun **1989**, 30, 203.

[17] Inomata, H.; Yagi, Y.; Saito, S. Macromolecules, **1991**, 24, 3962.

[18] Bansil, R.; Liao, G.; Falus, P. Physica, **1996**, A 231, 346.

[19] Liao, G.; Xie, Y.; Ludwig, K. F.; Bansil, R.; Gallagher, P. Phys Rev E: Stat Phys Plasmas Fluids Relat Interdiscip Top **1999**, 60, 4473.

[20] Cahn, J. W.; Hilliard, J. H. J. Chem. Phys. **1958**, 28, 258; Cook, H. E. Acta Metall. **1970,** 18, 297.

[21] Hirose, H.; Shibayama, M. Macromolrcules **1998**, 31, 5336.

[22] Shibayama, M.; Nagai, K. Macromolrcules **1999**, 32, 7461.

[23] Dagani, R. Chem Eng News **1997**, 75, 26.

[24] Hu, Z.; Chen, U.; Wang, C.; Zheng, Y.; Li, Y. Nature, **1998**, 393, 149.

[25] Yuan, Kai.; Hu, Z.; Li, Y. Appl Phys Lett **1999**, 74, 2233

[26] Chen, G.; Hoffman, A. S. Macromol. Rapid Comm. **1995,** 16, 175.

[27] Weissman, J. M.; Sunkara, H. B.; Tse, A. S.; Asher, S. A. Science, **1996**, 274, 959.

[28] Papadakis, E. P. In Methods of Experimental Physics: Ultrasonic; Edmonds, P. D., Ed.; Academic: New York, **1981**, 19, 237.

[29] Eck, W.; Wilson, H. R.; Cantow, H. J. Adv Mater **1995**, 7, 800.

[30] Mills, N. J. In Encyclopedia of Polymer Science and Engineering; Mark H. F., Ed., Wiley: New York, **1988**, 10, 493

[31] Tanaka, T.; Hocker, L.; Benedek, G. J. Chem. Phys **1973**, 59. 5151

[32] Li, Y.; Tanaka, T. J. Chem. Phys. **1990**, 92, 1365.

[33] Heskins, M.; Guillet, J. E. J. Macromolec. Sci. Chem. **1969**, 2, 1441.

[34] Fujishige, S.; Kubota, K.; Ando, I. J. Phys. Chem. **1989**, 93, 3311.

[35] Gehrke, S. H. Adv. Polym. Sci., **1993**, 110,80.

[36] P. K. Pathria, Statistical Mechanics, Pergamont Press, New York, (1989)

CHAPTER 4

STUDIES AND APPLICATIONS OF ENGINEERED GEL SURFACE PATTERN

4.1 INTRODUCTION

The surface structures of hydrogels play important roles for many potential applications in physical, chemical and biomedical fields. Extensive efforts have been directed to study the natural surface structure of gels. Surface patterns have been observed during gel swelling or shrinking processes, and are caused by mechanical instability and constraints.[1-5] The study of these patterns can lead to better understanding of the formation and evolution of patterns found in biological systems. On the other hand, it is not only desirable but also vital to modify gel surfaces in order to better control interactions between the gel surfaces and environments that are required for many applications.[6-7] This chapter will provide synthesis and application of engineered surface patterns on environmentally responsive polymer gels. The central idea is to precisely control the local properties of the one gel surface by incorporating different materials

onto given areas selected with a mask. The first example is a N-isopropylacrylamide (NIPA) gel covered by a square array of gold using sputter-deposition method. The periodicity of the surface array can be continuously tuned by external stimuli such as temperature and electric field. The periodic array produced on the gel surface can serve as a grating for optical filter and sensors applications. The emphasis is on its applications. The second example is to deposit NIPA polymer gel on the surface of an acrylamide gel. The pattern of the NIPA deposited area can be either visible or invisible by simply switching temperature above or below the low critical solution temperature (LCST) of the NIPA gel. Such gels can be used as displays and sensors. This chapter will illustrate how to synthesize engineered pattern on gel surface and their applications. Section 4.2 provides background. Section 4.3 focuses on shear modulus and swelling ratio measurement using engineered periodic surface patterns. Section 4.4 is about built-in patterns on a two-gel system. Section 4.5 gives a brief summary and section 4.6 is for chapter references.

4.2 BACKGROUND

In general, polymer gels have two types of surface patterns, natural surface patterns and engineered surface patterns, where the natural patterns are induced from uniform polymer gel materials but the engineered surface patterns are produced by designed non-uniform structure.

Polymer gels present unique natural surface patterns due to following factors such as crosslinked network structure, interaction between polymer gel network and solvent, and global movement of solvent. A crosslinked gel links chemically or physically

polymer chains into a three dimensional topological structure and allows its chains to move in a local and limited range which is compatible to its topological structure. The interaction between polymer network and solvent, combined with temperature makes free energy of the whole gel system favors the mixing of polymer chains and solvent in one situation and favors the separation of the solvent from polymer chains in another situation such as higher temperature or lower temperature. Further, mixing and separation are constrained by the network structure of polymer gels as mentioned earlier. In addition, the solvent holding inside gel network could move under any local changes such as temperature or electric field. However, the solvent movement is global, which involves global flowing of the solvent (until a fraction of the solvent inside gel flows out of the gel network or vise verse) and rearrangement of the gel network. Global movement dramatically slows down flowing and rearranging process from almost instant response to slow viscoelastic behavior for bulk polymer gels in long time scale. The interaction between polymer gel network and solvent is a reason why the gel changes its configuration. And the constrain from network structure and global movement make shrinking, swelling or volume transition very slow. As a result, a gel could take non-uniform bulk structure (such as in spinodal decomposition), shape change, and surface deformation to instantly decrease the free energy. This non-uniform structure could be meta-stable state, or even unstable state. Thus induced non-uniform structure are natural patterns.

In this chapter, our focus is on engineered surface patterns and their applications. The importance of the engineered surface patterns relies on their applications. There are diverse possibilities and options for preparing and designing engineered surface patterns

of polymer gels due to almost infinite choices of polymer gels in terms of structure (such as copolymer gel, and interpenetrating polymer gels), material (such as NIPA, PAMM, poly-vinylalcohol (PVA), agarose, silicone, and cellulose), and extendibility of gel structure by changing ratio of cross-linker to monomer, solvent, gelation temperature, and gelation methods including suspension. Two methods for preparing engineered surface patterns were first implemented. Their applications will be described and analyzed for illustration. More examples of preparing engineered surface patterns will be discussed.

4.3 SHEAR MODULUS AND SWELLING RATIO MEASUREMENT USING PERIODICAL PATTERNS

4.3.1 Surface Pattern and Diffraction Pattern

Let us first discuss the surface patterns produced using sputtering-deposition technique. N-isopropylacrylamide gel slabs were made by free radical polymerization. Pregel solution includes following materials: 7.8 g of N-isopropylacrylamide, 133 mg of methylene-bis-acrylamide (crosslinker), and 240 μl tetra-methyl-ethylene-diamine (accelerator), and 100 ml of deionized water with all above materials dissolved in. The pregel solution was nitrogen-gas bubbled about thirty minutes for oxygen-free, which is required for proper polymerization. The polymerization was initiated by adding 40 mg of ammonium persulfate (APS). The polymerized NIPA gel was soaked in water more than 24 hours to wash out chemical residues and then gradually dried.

Then the gel sample was coated by sputtering deposition using square mesh grids as masks, which have bar width of 6 μm and the mesh hole width of 19 μm. The sputtering chamber was pumped to the vacuum of 0.04 mbar in argon gas. Argon molecules, inside the sputtering chamber, were ionized using voltage of 2.5 kV. The deposition time is about 3.5 min and the gold thickness is approximately 53 nm. The affinity between gold and the polymer gel may be due to the interaction between the lone pair electron of the amine group in the NIPA gel and the empty orbitals of gold[8], and to entrapment of gold in the gel. The samples were maintained in a circulation water bath for constant temperature.

Thus prepared gel has a periodic surface pattern and could be used as a two-dimensional grating. The coated surface arrays have a periodic square structure. Many other structural arrays may be synthesized, including round, rectangular, hexagonal, and even non-periodic by utilizing different masks. The width of the slits and the number of the slits per unit area of the gel surface grating can be changed by external stimuli such as temperature and electric field. As the periodicity of the gel surface pattern changes in responsive to the external stimuli, the diffraction angle, or diffraction pattern changes accordingly. The gel grating has potential for applications in optical filter and sensors, and optical communications. When monochromatic light shines on periodic patterned surface and passes through slits between gold spot, the diffraction pattern will be formed. And the gel grating is tunable by temperature. The experiment data shown that temperature-induced change in the diffraction pattern was reversible. The consistence was verified up to at least seven thermal cycles. Several different samples were synthesized and tested, and their diffraction patterns were reproducible as well. We have

also successfully tuned the periodicity of the surface array of an ionic NIPA gel by applying an electric field. The electric field caused migration of positive counter ions and water inside NIPA gel toward the negative electrode and resulted in volume shrinkage.[9]

4.3.2 Mechanism of Shear Modulus Measurement of Gels using Tunable Grating

One of the applications of the periodical surface patterns is to measure the shear modulus of polymer gels, which is hard to measure. The measurement of shear modulus is especially challenging in following two situations. The first is measuring shear modulus in-situ while the gel undergoes responsive changes such as shrinking or swelling. Traditional measurement includes pressure over shear deformation, in which shear modulus could not be measured in situ. In the second situation, when the gel experiences inhomogeneous deformation in the environment of non-uniform thermal field, or polymer gel itself is intrinsically inhomogeneous, then localized measurement of shear modulus is a proper way to get most accurate gel information, while the traditional methods only yield a shear modulus as an average value over a bulk gel. The proposed method using a gel with a periodic surface pattern could measure local shear modulus of a small area depending on optical beam size. When a gel is inhomogeneous-deformed or is intrinsically inhomogeneous, it is especially an effective way to know if there is any change of shear modulus from center to edge or corner of a gel film or if a geometrical restriction and boundary condition will impact on shear modulus.

To illustrate this concept and feasibility, N-isopropylacrylamide gels with periodical gold surface pattern were prepared using the method mentioned in section

4.3.1. We will describe how to locally trace and measure shear modulus of a hydrogel with an engineered surface pattern. An engineered surface pattern can serve as a responsive 2-D optical grating in this method. Aiming a He-Ne laser beam on a gel surface yields a diffraction pattern on a screen. Any swelling or shrinking of the gel can be measured and traced by continuously recording and analysis of the corresponding diffraction pattern. Specifically, this diffraction pattern responses only to a local area of less then 1 mm^2 where the laser beam shines through. This method provides an efficient way for local measurement and dynamical trace of shear modulus, swelling kinetics and other mechanical properties of gels.

In addition to shear modulus measurement, an engineered gel grating could be used in all following applications: swelling measurement including swelling ratio, swelling rate, local swelling, anisotropy swelling, and inhomogeneous swelling; display including color diffraction pattern, and electric field modulated display using ionic gel; gel grating including ion gel grating, interaction between gel grating diffraction pattern and ultrasonic interaction, and tunable optical grating which could be used for optical coupling in fiber optics, sensor, or even in information optics which further extends to thermal-controllable frequency filter, logic components in an optical digital system such as an optical computer. If a periodical pattern is made into three dimensions and incorporated into bulk gel, then applications such as optical crystal could also be implemented, and can be used as a tunable optical filter or absorber.

4.3.3 Experiment Setup for Measurement

With automatic imaging system to collect diffraction pattern data, and a computer system to extract pattern parameters, and convert diffraction pattern to gel dimensional parameters, shear modulus of a gel under test could be in-situ measured, and dynamically traced for certain applications. The setup described below is one embodiment to illustrate how a tunable polymer grating is implemented to measure shear modulus. A gold-coated NIPA gel film was totally soaked in a water bath and hang up to a stand in one end as shown in Figure 4.1.

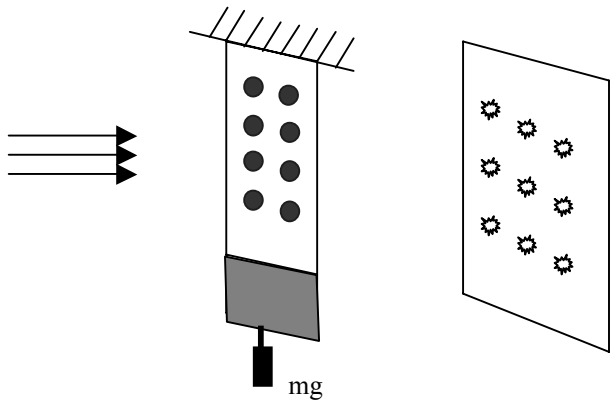

Figure 4.1. A setup for shear modulus measurement using a gel with a periodic surface pattern.

A hooker was attached to the bottom end of gel film for weights. Self-made weights were attached onto the hooker with fully carefulness one by one. A laser beam was shone on gel, and a diffraction pattern was produced on a screen. Pictures of corresponding diffraction pattern with an one-centimeter mark were taken by a camera.

The diffraction pictures were measured and calculated to determine gel deformation and the shear modulus of NIPA gel.

4.3.4 Mathematical Model

A mathematical model for shear modulus measurement will be deducted and presented below. It is assumed that a square pattern is used for periodic pattern. In such pattern, all gold spots are aligned in x direction, and the distance between the centers of the neighbor spots is constant d (referred to as optical constant). Also, all gold dots are aligned in y direction where y is perpendicular to x direction, and the distance between the centers of the neighbor dots is the same constant d. If the gel can be hanged in such a way that x direction is horizontal and y direction is vertical, then the calculation would be very straightforward. Further assumptions include that a parallel coherent light beam is used to shine onto a gel surface and the light beam is perpendicular to the gel surface. λ_w is the wavelength of the light beam, L is the distance from the gel surface to the screen where the diffraction pattern is displayed. The diffraction pattern is also a square pattern accordingly. Then the distance between neighbor spots in the diffraction pattern can be referred to as w and is related to the experimental setup as below,

$$w = L\frac{\lambda_w}{d} \tag{4.1}$$

where λ (not wavelength λ_w) is be defined as relative deformation and expressed as,

$$\lambda = \frac{d}{d_0} \tag{4.1}$$

where d_0 and d are optical constants without stress and with stress along y direction, respectively. Accordingly,

$$d = L\frac{\lambda_w}{w} \tag{4.2}$$

$$d_0 = L\frac{\lambda_w}{w_0} \tag{4.3}$$

Combine eqs. 4.1, 4.2, and 4.3,

$$\lambda = \frac{w_0}{w} \tag{4.4}$$

By measuring geometrical changes in diffraction pattern, the strain could be extracted through eq. 4.4. Since applied force f is known, shear modulus μ can be easily obtained using the following equation[17],

$$f = A_0\mu\left(\lambda - \frac{1}{\lambda^2}\right) \tag{4.5}$$

where A_0 is cross sectional area which is perpendicular to the direction of the applied force, The subscript '0' stands for initial value before any stress is applied. f is a force applied to a gel. In our experiment, f is gravity force of weights offset by buoyancy.

$$f = m(1 - \frac{\delta_w}{\delta})g = m'g \tag{4.6}$$

where δ_w, and δ are density of water and weights respectively.

In general, a coated gel could not be easily aligned such that two major optical directions in the patterned gel surface match both horizontal and vertical directions, so a more general mathematical model is introduced below for further application in shear modulus measurement. When a periodic-coated gel is stretched by weights vertically (in

y direction), the gel will swell along y direction and shrink horizontally (in x-direction) . Assume that relative swelling ratio in x direction is α where the relative swelling ratio is defined as the ratio of absolute increased length over the original whole length in x direction, and swelling ratio in y direction is β where the swelling ratio is defined as the ratio of absolute increased length over the original whole length in y direction. Referring to Fig.4.2, assume that x_0 is the original length between two points on gel in x-direction before any stress is applied and x is the current length between the two points after shrinking under stress in x-direction. Similarly in y-direction, y_0 is the original length between two points on gel in y-direction before any stress is applied and y is the current length between the two points after swelling under stress in y-direction. And the angle between r_1 and r_2 is θ.

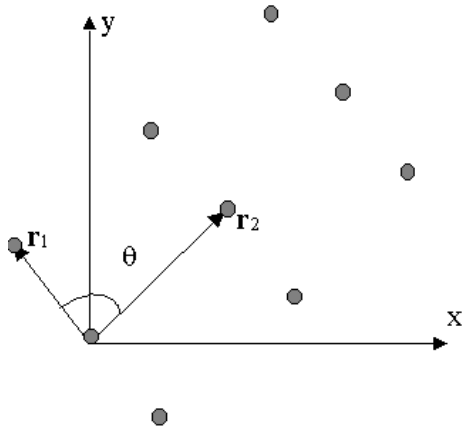

Figure 4.2. A schematic view of a gel with an engineered periodic surface pattern.

Two equations can be set up and expressed as below,

$$X = (1+\alpha)X_o \tag{4.7}$$

$$Y = (1+\beta)Y_o \tag{4.8}$$

And

$$\mathbf{r}_{10} = X_{10}\,\mathbf{i} + Y_{10}\,\mathbf{j} \tag{4.9}$$

$$\mathbf{r}_1 = X_1\mathbf{i} + Y_1\,\mathbf{j}$$

$$= (1+\alpha)\,X_{10}\,\mathbf{i} + (1+\beta)\,Y_{10}\,\mathbf{j} \tag{4.10}$$

$$r_{20} = X_{20}\,\mathbf{i} + Y_{20}\,\mathbf{j} \tag{4.11}$$

$$r_2 = (1+\alpha)\,X_{20}\,\mathbf{i} + (1+\beta)\,Y_{20}\,\mathbf{j} \tag{4.12}$$

where r_1 and r_2 are constants of periodical pattern under stress along two major directions, respectively, while r_{10} and r_{20} are corresponding parameters before any stress is applied. Apparently,

$$r_{10}^{\,2} = X_{10}^{\,2} + Y_{10}^{\,2} \tag{4.13}$$

$$r_1^{\,2} = (1+\alpha)^{\,2}\,X_{10}^{\,2} + (1+\beta)^{\,2}\,Y_{10}^{\,2} \tag{4.14}$$

and

$$r_{20}^{\,2} = X_{20}^{\,2} + Y_{20}^{\,2} \tag{4.15}$$

$$r_2^{\,2} = (1+\alpha)^{\,2}\,X_{20}^{\,2} + (1+\beta)^{\,2}\,Y_{20}^{\,2} \tag{4.16}$$

Since $\mathbf{r}_{10}$ and $\mathbf{r}_{20}$ are perpendicular to each other, so

$$\mathbf{r}_{10} * \mathbf{r}_{20} = 0 \tag{4.17}$$

or in scalar equation,

$$X_{10}\,X_{20} + Y_{10}\,Y_{20} = 0 \tag{4.18}$$

and

$$r_1^* r_2 = r_1 r_2 \cos\theta \tag{4.19}$$

where θ is an angle between $\mathbf{r}_1$ and $\mathbf{r}_2$ and note that they are no more perpendicular after being stretched under applied stress. Eq. 4.19 can be transformed according to eqs. 4.7 ~eq. 4.18,

$$(1+\alpha)^2 X_{10} X_{20} + (1+\beta)^2 Y_{10} Y_{20} = r_1 r_2 \cos\theta \tag{4.20}$$

From eq. 4.9 and eq. 4.10,

$$X_{10}^2 = \frac{(1+\beta)^2 r_{10}^2 - r_1^2}{(1+\beta)^2 - (1+\alpha)^2} \tag{4.21}$$

$$Y_{10}^2 = \frac{r_1^2 - (1+\alpha)^2 r_{10}^2}{(1+\beta)^2 - (1+\alpha)^2} \tag{4.22}$$

From eq. 4.11 and eq. 4.12,

$$X_{20}^2 = \frac{(1+\beta)^2 r_{20}^2 - r_2^2}{(1+\beta)^2 - (1+\alpha)^2} \tag{4.23}$$

$$Y_{20}^2 = \frac{r_2^2 - (1+\alpha)^2 r_{20}^2}{(1+\beta)^2 - (1+\alpha)^2} \tag{4.24}$$

From eq. 4.18 to eq. 4.20.

$$r_1 r_2 \cos\theta = -[(1+\beta)^2 - (1+\alpha)^2] X_{10} X_{20} \tag{4.25}$$

$$r_1 r_2 \cos\theta = [(1+\beta)^2 - (1+\alpha)^2] Y_{10} Y_{20} \tag{4.26}$$

Let

$$U_\alpha = (1+\alpha)^2 \tag{4.27}$$

$$U_\beta = (1+\beta)^2 \tag{4.28}$$

$$\Delta_1 = \left(\frac{r_{10}}{r_1}\right)^2 \tag{4.29}$$

$$\Delta_2 = \left(\frac{r_{20}}{r_2}\right)^2 \tag{4.30}$$

$$\Delta_\theta = Cos^2 \Delta\theta \tag{4.31}$$

where $\Delta\theta = \theta - \frac{\pi}{2}$. Then eq. 4. 25 and 4.26 can be expressed as,

$$\Delta_1\Delta_2 U_\alpha{}^2 - (\Delta_1 + \Delta_2)U_\alpha + \Delta_\theta = 0 \tag{4.32}$$

$$\Delta_1\Delta_2 U_\beta{}^2 - (\Delta_1 + \Delta_2)U_\beta + \Delta_\theta = 0 \tag{4.33}$$

So U_α and U_β satisfy the same equation. Since stress is applied by weight in vertical direction, it can be assumed that

$\alpha<0$ (4.34)

$\beta>0$ (4.35)

$U_\alpha < 1$ (4.36)

$U_\beta > 1$ (4.37)

So

$$U_\alpha = \frac{1}{2}\left(\frac{1}{\Delta_1} + \frac{1}{\Delta_2}\right)\left[1 + \sqrt{1 - \frac{4\Delta_1\Delta_2\Delta_\theta}{(\Delta_1 + \Delta_2)^2}}\right] = (1+\alpha)^2 \tag{4.38}$$

$$U_\beta = \frac{1}{2}\left(\frac{1}{\Delta_1} + \frac{1}{\Delta_2}\right)\left[1 + \sqrt{1 - \frac{4\Delta_1\Delta_2\Delta_\theta}{(\Delta_1 + \Delta_2)^2}}\right] = (1+\beta)^2 \tag{4.39}$$

Assume a gel film is very thin and the relative change of the thickness is trivial compared to these of other two directions due to boundary effect. Thus $|\alpha| \cong |\beta|$, and

$$(\frac{1}{\Delta_1} + \frac{1}{\Delta_2}) \approx 2 \tag{4.40}$$

or

$$\left(\frac{r_1}{r_{10}}\right)^2 + \left(\frac{r_2}{r_{20}}\right)^2 \approx 2 \tag{4.41}$$

According to definition,

$$\lambda = \frac{y}{y_0} = 1 + \beta \tag{4.42}$$

And the shear modulus μ can be extracted from a curve according to eq.4.5. with an assumption $|\alpha||\beta| \cong 1$, then

$$(1+\alpha)^2 = 1 - \sqrt{1-\Delta_\theta} = 1 - |\sin\Delta\theta| \tag{4.43}$$

$$(1+\beta)^2 = 1 + \sqrt{1-\Delta_\theta} = 1 + |\sin\Delta\theta| \tag{4.44}$$

$$\lambda = 1 + \beta = (1+\sin\Delta\theta)^{1/2} \tag{4.45}$$

f $\Delta_\theta << 1$, *then*

$$(1+\alpha)^2 \approx 1 + 2\alpha = 1 - \sin\Delta\theta \tag{4.46}$$

$$(1+\beta)^2 \approx 1 + 2\beta = 1 + \sin\Delta\theta \tag{4.47}$$

$$\beta = \frac{1}{2}\sin\Delta\theta \cong \frac{1}{2}\Delta\theta \tag{4.48}$$

$$\lambda = 1 + \frac{\Delta\theta}{2} \tag{4.49}$$

According to diffraction optics, $\Delta\theta$ on gel surface pattern should be as same as $\Delta\theta$ in diffraction screen. By measuring $\Delta\theta$ in recorded diffraction pattern, relative swelling ratio and shear modulus information can be extracted from. Currently, we used camera to take pictures and manually measure angle change $\Delta\theta$.

4.3.5 Results

The above designed experiments have been done for NIPA gel. The parameters of the used NIPA sample are provided below, and 980 cm/s^2 is used for gravity acceleration.

d = 3.5 mm

w = 13.8 mm

$A_0 = w \times d = 0.48\ cm^2$

And the result of measurement is summarized in Table 4.1 where $\Delta\theta$ values were measured from pictures of diffraction patterns, and λ values were calculated from eq. 4.49.

A curve of f/A_0 vs $(\lambda\text{-}1/\lambda^2)$ was drawn in Fig. 4.3. And the shear modulus was extrapolated from the curve and found out that is about $4x10^4$ dyn/cm^2, which is in agreement with the results from other methods.

Table 4.1 Experimental data of applied force and deformations

$m'(g)$	f/A_0 (10^4xdyn/cm^2)	$\Delta\theta(\deg ree)$	$\Delta\theta(rad)$	λ	λ-1/λ^2
0	0	0	0	1	0
0.9	0.18	4	0.07	1.036	0.11
1.8	0.37	5.5	0.1	1.05	0.14
2.7	0.55	6.5	0.11	1.06	0.17
3.6	0.73	8	0.14	1.08	0.21
4.5	0.91	10	0.17	1.096	0.26
5.4	1.1	11	0.19	1.106	0.29
6.3	1.3	11.8	0.21	1.115	0.31
7.2	1.5	12.5	0.22	1.123	0.33
8.1	1.6	14	0.24	1.139	0.37
9.0	1.8	16	0.28	1.162	0.42

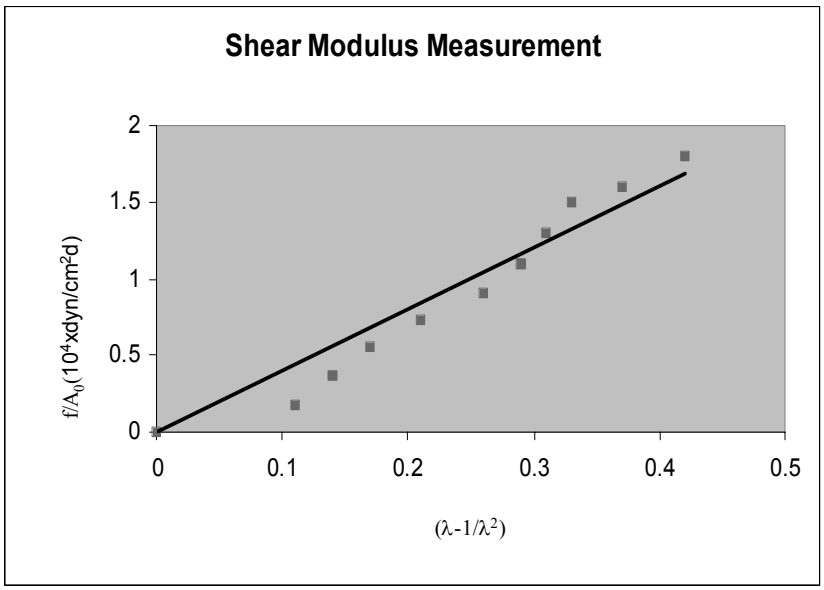

Figure 4.3. Stress over strain for a NIPA gel based on data in Table 4.1.

4.3.6 Measurement of Swelling Ratio

Swelling ratio can also be measured using a gel with periodic surface pattern by the same setup and experiment as that used in shear modulus measurement. Similar to shear modulus measurement, a swelling ratio measured from a gel with engineered surface pattern is related to a local area. So the current measurement is related to a local characteristic while traditional methods only yield an average swelling ratio over a bulk gel. The current method provides a way to study some interesting phenomena. For example, swelling ratio variation from gel center to edge or corner?

So far, we have done preliminary experiments to illustrate the feasibility and implementation of the current method. In an illustrated method, NIPA gels with periodic surface patterns were measured using the similar method as described in section 4.3.3 to section 4.3.4. Diffraction patterns of the gel were recorded for two states. The first state is dry gel state, the second state is wet gel soaked in water at given temperature. The results are compared with ones by direct measurement. These results are summarized in Table 4.2.

Table 4.2 Experimental data of applied force and deformations

Test condition	Sample number	1-D swelling Rate		3-D swelling Rate	
		Diffraction method	Direct measurement	Diffraction method	Direct measurement
22 °C	6-1	2.6	2.56	17.6	16.8
22 °C	8-8	1.54	1.54	3.7	3.7
22 °C	6-12	2.68	2.64	19.2	18.4
25 °C	7-9	2.4	2.4	14.5	14.5
29 °C	6-6	2.44	2.2	14.5	10.6
30 °C	6-18	2.08	2.16	9.0	10.1
30 °C-	8-17	1.24	1.42	1.9	2.9
32.5 °C	6-9	2	1.96	8	7.5
33.6 °C	6-13	1.72	1.64	5.1	4.4

4.4 BUILT-IN PATTERN ON A TWO-GEL SYSTEM

Another example of engineered surface patterns is accomplished by depositing one polymer gel (NIPA) to the surface of another polymer gel (polyacrylamide gel (PAAM)). The PAAM gel was made using the NIPA recipe with 7.8 g of N-isopropylacrylamide monomers replaced by 5 g of acrylamode monomers. The NIPA pre-gel solution had the same chemical composition as stated in the standard recipe except that the initiator APS was reduced by a factor of 0.33, and 4 mg riboflavin-5'-phosphate (UV photo-initiator) was added. The NIPA pre-solution was put on the surface of the PAAM gel.

The sample was then covered by a mask and illuminated by ultraviolet light for about 60 min. The NIPA solution gelled only at areas that were exposed to ultraviolet light. At these areas, an interpenetrating polymer network[14] of NIPA and PAAM was formed with an estimated depth about 0.5 mm.

Since both PAAM substrate and NIPA gel in the surface of the PAAM gel are transparent at room temperature, no surface structure can be observed as shown in Figure 4.4a. When the surface-engineered sample is warmed up to 37 ^{0}C, the NIPA-deposited areas become cloudy[15,16], while the PAAM gel remains in the transparent state. As a result, the outlined imaging (the NIPA-deposited areas) of a Texas map appears at the surface of the PAAM gel (Figure 4.4b). This map can be turned-on or turned–off by simply switching the temperature below or above the low critical solution temperature, T_c (=34 ^{0}C) of the NIPA gel. The switching time was approximately ten seconds, much shorter than that required for a shape memory gel[14].

To further demonstrate the potential of the gels with engineered surface patterns, a gel display consisting of a PAAM substrate with the NIPA gel filling the un-masked area was made and is immersed in water as shown in Fig. 4.5. At room temperature (Fig. 4.5a), both NIPA and PAAM gels were transparent and no pattern was observed. At 37^{o}C (Fig. 4.5b), the NIPA deposited area becomes cloudy and results in appearance of a solid imaging of a dinosaur. The gel display system demonstrated here is responsive to temperature. By changing the chemical composition of the gel, the gel displays can be responsive to other external stimuli such as salt concentration and infrared light. The image of a gel display can be clearly seen at any angles in contrasted to a well-established liquid crystal display that requires head-on viewing angles.

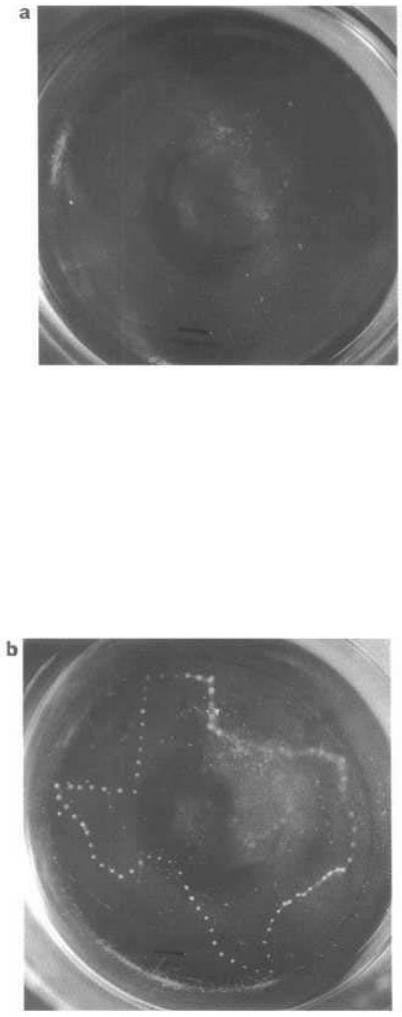

Figure. 4.4. (a) In room temperature, the NIPA deposited PAAM gel is transparent and no surface pattern exhibits. (b) When it is heated to above 37 ^{0}C, the outlined imaging of a Texas map appears. This is because the NIPA deposited areas become cloudy while PAAM gel remains transparent at that temperature. The whole process only takes approximately ten seconds. After the sample is cooled down, the map disappears. The process is fully reversible. The black bar indicates 1 cm.

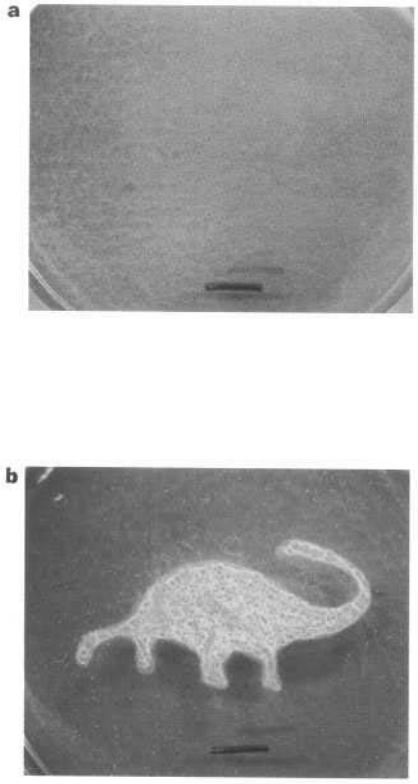

Figure 4.5. A gel display with a solid image. (a) In room temperature, the NIPA deposited PAAM gel is transparent and no surface pattern exhibit. (b) When it is heated to above 37 ^{0}C, the solid image of a dinosaur appears. The black bar indicates 1 cm.

4.5 CONCLUSION

Polymer gels with engineered surface patterns could be synthesized using different materials combination. In one implementation, non-polymer materials such as metal or dielectric materials could be incorporated onto gel surface with certain pattern. The patterns will always exist after a pre-designed pattern being transferred to a gel

surface. Since a gel is environmentally responsive, and can swell or shrink in response to temperature, polymer solution pressure, and electric field (for ionic gel), so gel surface pattern will change accordingly. A gel with such surface pattern can be used as sensors, responsive grating. Another example is gel/gel system where two or more than two types of gels (sometime, one of them could be polymer chains)are incorporated together. The first type gel is synthesized first, the second (or the rest for multi-gel system) type of gel can be incorporated into the first type of gel in different ways, and the second type of gel could undergo phase transition by environmental changes including temperature, polymer solution pressure, and electric field. The method of photo-induced crosslinking can be used to form the second type gel and a surface pattern will be transferred to the surface of this gel system. The gel system takes advantage of gel phase transition so the refractive indexes mismatch after phase transition, and a built-in pattern will show up. Applications include display, sensor, smart window curtain, and indicator.

The structure of a gel with an engineered surface pattern could include, surface coated and patterned by mask; two types of polymers with interpenetrating structure such as NIPA/PAAM composite gel system shown in this chapter, or the second type gel can be polymer chains which are physically trapped inside of the first type gel; Another possible option for future experiment could be a gel/gel system where the first type gel is a porous gel and the second type gel is trapped inside the porous space of the first type gel only. So the first gel may only function as porous matrix to hold the second gel. If such structure is formed only on surface of the matrix, then such surface patterned gel has an unique application due to its different mechanical characteristics, and swelling mechanism.

This method that incorporates a metal array to a hydrogel surface also opens a new avenue to make microelectrode array devices that can greatly enhance sensor performance. The combination of microelectrode arrays and smart gels has potential applications for ion chromatography[11], detecting enzyme activity[12], and monitoring cell electrical activity[13].

Another application could be soft microelectronics, similar to the current integrated circuits based on semiconductor materials and photolithography process. However soft microelectronics has other unique properties and advantages such as flexibility, bending, and resistant to pressure, mechanical shock. The soft microelectronics is based on soft polymer materials. Two types of materials shall be well developed and incorporated together: conductive polymer and dielectric polymer materials, which are already under intensive studies and developing over the world.

4.6 CHAPTER REFERENCES

[1] Tanaka, T., Sun, S. T., Hirokawa, Y., Katayama, S., Kucera, J., Hirose, Y. & Amiya, T. Nature **1987**, 325, 796.

[2] Sato-Matsuo, E. & Tanaka, T. Nature, **1992**, 358, 482.

[3] Li, Y., Li, C. & Hu, Z. J. Chem. Phys. **1994**, 100, 4637.

[4] Li, C., Hu, Z. & Li, Y. J. Chem. Phys. **1994**, 100, 4645.

[5] Suzuki, A., Yamazaki, M. & Kobiki, Y. J. Chem. Phys. **1996**, 104, 1751.

[6] Hoffman A. S. Macromol. Symp. **1996**, 101, 443.

[7] Peppas, N. A. & Langer, R. Science **1994**, 263, 1715.

[8] Grabar, K. C., Freeman, G. G., Hommer, M. B. & Natan, M. J. Anal. Chem. **1995**, 67, 735.

[9] Hirotsu, S. Japn. J. Appl. Phys. **1985**, 24, 396.

[10] Weissman, J. M., Sunkara, H. B., Tse, A. S. and & Asher, S. A. Science. **1996**, 274, 959.

[11] Imisides, M. D., John, R., & Wallace, G. G. Chemtech. **1996**, 26, 19.

[12] Wang, J. & Chen, Q. Anal. Chem. **1994**, 66, 1007.

[13] W. Nisch, J. Bock, U. Egert, H. Hammerle, and A. Mohr, Biosensors & Bioelectronics. **1994**, 9, 737.

[14] Hu, Z., Zhang, X., & Li, Y. Science. **1995**, 269, 525.

[15] Li, Y., G. Wang, G. & Hu, Z. Macromolecules. **1995**, 28, 4194.

[16] Bansil, R., Liao, G. & Falus, P. Physica A. **1996**, 231, 346.

[17] Treloar, L. R. G. The physics of rubber elasticity. Oxford, Clarendon Press, **1975**.

CHAPTER 5

COMPOSITE GEL MATERIALS FOR BIOMEDICAL APPLICATIONS

5.1 INTRODUCTION

The unique properties of hydrogels include but not limit to the compatibilities with biological environment and spinodal decomposition. The composite materials made from hydrogel may inherit above unique properties of hydrogels and open a door for broad options to modify, fine tune, and combine the properties of each component in the composite, so would provide more potential applications in biomedical area. In this chapter, two hydrogel composite materials were proposed for biomedical applications as examples. First, NIPA gel was incorporated into silicone rubber to form composite materials for wound dressing with improved and enhanced absorption than that of pure silicone in past usage. Second, NIPA polymer solution and blue destran were trapped inside PAAM gel matrix to form NIPA/PAAM gel system. The turbid optical properties of an NIPA/PAAM gel system can be tuned to simulate biological tissues by optimizing

compositions of NIPA and blue dextran and further modified by controlling the temperature. The silicone/NIPA composite membrane will be discussed and studied in section 2. NIPA/PAAM gel system will be covered in section 3. The section 4 is a brief conclusion. And the references are given in section 5.

5.2 CONTROLLED RELEASE FROM COMPOSITE SILICONE/HYDROGEL MEMBRANE

To enhance the drug uptake and release capacity of silicone rubber (SR), N-isoprylacrylamide (NIPA) hydrogel particles have been incorporated into a SR membrane. The NIPA particles were thoroughly blended with uncured SR with a certain ratio at room temperature. Then the mixture was cast in a petri-dish to 1 mm thickness and cured 10 hours at 90 ^{0}C. The SR/NIPA composite gel can absorb the water about equal to its dry weight. Brilliant blue, used as a mock drug, was loaded into the composite gel. Drug-release increased exponentially to a final value that is temperature dependent: low at $T>T_c$ and high at $T<T_c$. This is because the NIPA changes hydrophobic with temperature. Pulsed release in response to the temperature switching between 20 and 39 ^{0}C has been achieved. Drug uptake and release capability strongly depends on the structure of the composite gel. Optimum range of the NIPA composition is found to be from 75% to 87% by volume. In the cited range, the NIPA particles form an interconnected network that provides a channel for diffusion of drug solution. The SR/NIPA composite gel has promising attributes for wound dressing and other uses. In this section, the background on wound dressing will be given for better understanding the

current structure and its application (section 5.2.1) and then followed by materials and preparation method for silicone/NIPA composite material (section 5.2.2). Finally an analysis for the silicone/NIPA composite material is given in section 5.2.3. The optimized range for silicone/NIPA ratio is given for better performance as wound dressing according to the analysis.

5.2.1 Background

A numerous of dressing have been applied to wounds in the past centuries with functions of protection, support and absorption.[1] Currently many dressing types are available. Among them are films, hydrocolloids, hydrogels, and composite dressing.[1~4] These provide a wide variety of dressing based on wound type and individual case[4~5]. A dressing is no longer a passive adjunct to healing, but is an active element of wound management, aiming to remove necrotic tissue, eliminate infection, absorb excess exudate, maintain a moist wound surface, provide thermal insulation and protect the healing wound from trauma and bacterial invasion. [1~4]

Silicone rubber is used in wound healing dressings, it has good strength and flexibility, is generally considered to be biocompatible, and has gained acceptance in the management of hypertrophic and keloid scars.[6~10] Even though the mechanism is not completely understood, both physical and chemical effects are believed to be involved. The water impermeability of silicone rubber has been shown to reduce evaporation fluid loss and maintain the moisture level.[7] It has also been reported that Vitamin E added to a silicone rubber sheet improved wound healing over simple silicone gel.[6] However, the water absorption of silicone rubber is almost zero, which strongly limits silicone rubber

from fully functioning as drug releasing wound dressing or for exudate absorption and so on.

In this study, poly (N-isopropylacrylamide) (NIPA) hydrogel micro-particles were synthesized and incorporated into silicone rubber. The NIPA gel is hydrophilic and swells in water when $T<T_c$, which is about 34 ^{0}C. While $T>T_c$, NIPA gel becomes hydrophobic and collapses into a small volume.[11] Such unusual properties suggest various applications including controlled drug delivery[12-13] and sensors[14-15]. In this SR/NIPA composite membrane, the absorption ability has been drastically enhanced. The composite gel can absorb water equal to about its dry weight. Furthermore, as a drug delivery system, this membrane's release rate changes due to changes in environmental temperature.

5.2.2 Materials and Methods

The synthesis of composite silicone rubber membranes consisted mainly of two steps. First NIPA microgels were prepared. Then NIPA microgels were incorporated into the silicone gel.

NIPA microgels were prepared by the suspension method. A mixture of 7.8 g N-isopropylacrylamide monomers (Acros Organics), 133 mg of methylene-bis-acrylamide as crosslinker, and 240 µl tetra-methyl-ethylene-diamine as an accelerator (both from BIO-RAD Laboratories), were dissolved in 100 ml deionized and distilled water. Nitrogen gas was bubbled through the solution to remove dissolved oxygen. The polymerization was initiated by adding 40 mg of ammonium persulfate (Aldrich Chemical Company). This pre-

gel solution was poured into the prepared mixture of 300 g cyclohexane (EM Science) and 5 g sorbitan monooleate (Aldrich Chemical Company). The suspension was stirred and bubbled with nitrogen for about 3 hours and kept overnight. Afterward, NIPA particles were washed to remove cyclohexane and sorbitan monooleate. The optical microscope was used to check the NIPA gel particles. The average size of the NIPA gel particles was around 100 μm in diameter when fully swollen in water at room temperature. The NIPA microgels were found to swell below the lower critical solution temperature (LCST) T_c=34 ^{0}C and shrink above T_c, as expected. Thus, this composite membrane could be used to release drug under external stimuli such as temperature.

Implant grade liquid silicone rubber (LSR) 10:1 system was purchased from Applied Silicone Corporation. It is a two-part, pourable, dimethyl silicone elastomer, and is designed to mix with 10 parts base (part A) to 1 part crosslinker (part B). The mixture will cure to a high strength, clear and flexible elastomer. The NIPA microgels were thoroughly blended with uncured SR at room temperature. The concentration ratio of the NIPA over SR/NIPA by volume varied from 75% to 87%. After completely mixing with help of a centrifuge, the mixture was cast in a petri-dish to about 1 mm thickness and cured for 10 hours at 90 ^{0}C. The composite membrane was then washed with deionized water. By immersing the sample into warm water pf temperature =37 ^{0}C, the membrane would reversibly become opaque compared to its transparent state at room temperature. This demonstrated that the NIPA microgels were incorporated into the silicone rubber. The opacity is caused by the volume phase transition of the NIPA gel at 34°C.[16]

5.2.3 Results and Analysis

The water absorption of the SR/NIPA composite material is measured as a function of the NIPA ratio as shown in Fig. 5.1.

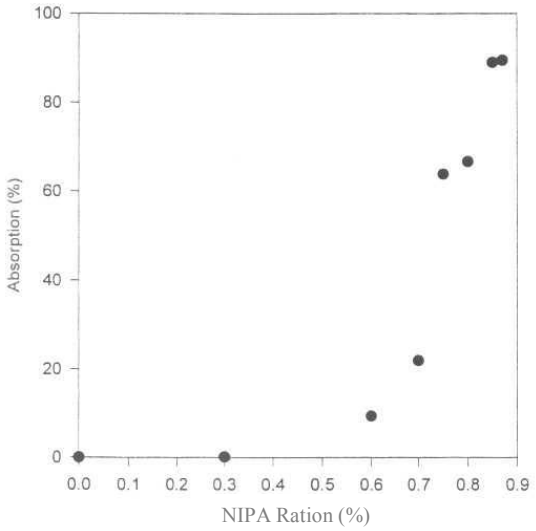

Figure 5.1. The water absorption of the silicone rubber/N-isopropylacrylamide (SR//NIPA) composite material was measured as a function of the ratio of NIPA particles incorporated over the composite material in volume. The threshold of absorption was identified at a ratio of approximately 75%.

The ratio is defined as the volume of the NIPA microgel to the volume of whole composite material (SR + NIPA) when the sample is prepared. If the ratio is lower than about 75%, the absorption is very low. If the ratio is higher than 90%, the silicone rubber

can no longer form a good matrix, resulting in poor mechanical strength. The threshold at which the water absorption exhibits a sharp increase is around 75% from the curve.

Water uptake of the composite membrane can be understood from the connectivity of both silicone rubber and NIPA microparticles. For lower ratios, NIPA microgels are not contacted to each other. That is, almost all NIPA microgel particles are isolated within the silicone rubber matrix. The permeability of such low ratio material is nearly zero considering the permeability of the silicone rubber is almost zero. As the concentration of NIPA microgel increases, neighboring microgels will begin to be in physical contact. As this continues to increase with increasing microgel concentration, soon a pathway is formed wherein most of the microgels are in physical contact. At this point, there is direct communication existing throughout the SR matrix including the surface. And water is readily absorbed from the surface and taken up within the SR matrix. This is described mathematically by the percolation theory, as described below.

Suppose the silicone rubber has a three-dimensional lattice of sites, and gel microparticles are contacted between every pair of neighboring sites with probability p. At a threshold value of p_c, one cluster will span the lattice, meaning that there is a connected path across the lattice through a single spanning cluster. Only above this threshold, the water uptake of the composite membrane becomes available. Using the percolation model in the three-dimensional site problem,[17] the threshold is found to be 74% under the assumption that all microgel particles are spherical and have the same size. Our experimental result is in good agreement with the theoretical one.

The water absorption kinetics was measured for a composite SR/NIPA membrane of 85% NIPA ratio with thickness of 0.65mm.

The results are shown in Fig. 5.2. The absolute absorption rate depends on the NIPA ratio, size of microgel particles and the thickness of the membrane.

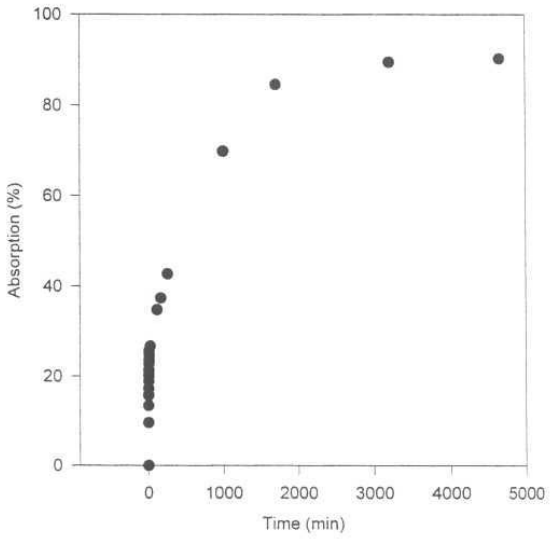

Figure 5.2. Water absorption of the composite membrane at 85% ratio, with a thickness of 0.65 mm, was measured as a function of time. The absorption time depends upon the ratio of NIPA to SR and the thickness of the composite membrane.

The mechanical strength of the composite material is much better than that of the NIPA gel. The shear modulus of the sample is measured by uniaxially stretching the sample with different weights (F) attached to its bottom. When the volume of the sample is kept constant, one can obtain[18]

$$F / A_0 = \mu(\lambda - 1/\lambda^2) \qquad (5.1)$$

where μ is the shear modulus and A_0 is the cross-sectional area of the undeformed sample. λ is the z-direction elongation ratio of the gel. By plotting F/A_0 vs $(\lambda-1/\lambda^2)$, the slope μ of the sample is obtained as shown in Figure 5.3. It is found that the shear modulus is $3.6x10^7$ dyn/cm^2 for the membrane with 87% NIPA. There is no significant difference for samples with NIPA ranging from 75% to 87%. Compared with pure NIPA gel's shear modulus of $2.2x10^4$ dyn/cm^2,[19] the mechanical strength of the composite membrane is drastically enhanced.

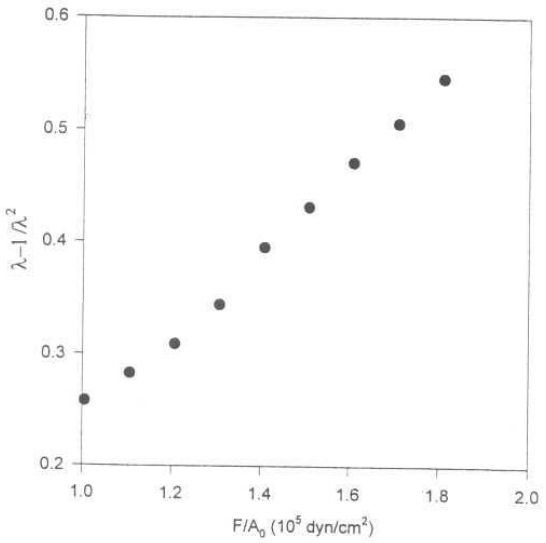

Figure 5.3. The shear modulus of the composite material was measured by the tensile method and found to be 3.6×10^5 dyn /cm^2 for the sample containing 85% NIPA.

The microscopic structures of samples were examined by a scanning electron microscope (SEM) as show in Figure 5.4. a & b. The sample was first dried and then

sputter-coated with gold to achieve satisfactory conductivity with minimum damage to the specimens. The coated specimens were observed in the scanning electron microscope (Model JSM-T300, JEOL). The scanning images were photographed on Polaroid PN/52 films. From the pictures, one can see that the NIPA microgel particles are trapped and exposed to the surface of silicone rubber membrane. The NIPA microgel particles must also be connected in a three dimensional cluster inside of the silicone as demonstrated by the absorption kinetics.

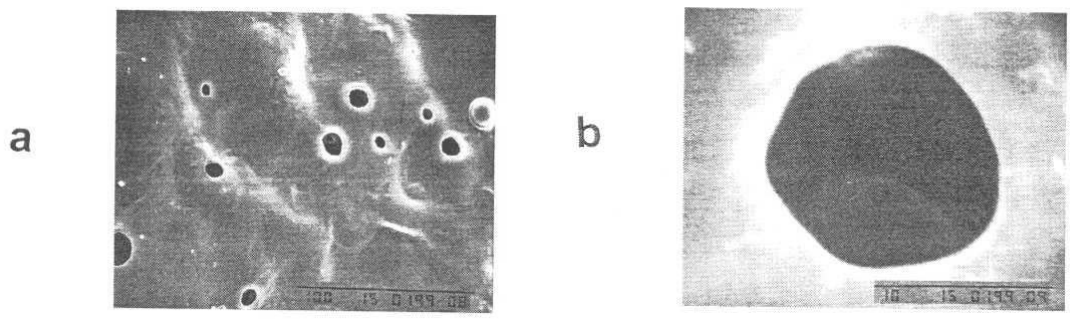

Figure 5.4. The surface of the composite membrane was studied by scanning electron microscopy. Samples were first dried and then coated with gold. (a) Attached inside the voids of silicone rubber are NIPA gel particle in the dehydrated state. (b) close-up of a singe NIPA particle embedded in the surface of the silicone rubber membrane.

Brilliant blue (Aldrich), used as a mock drug, was loaded into the composite membrane. The drug- loaded composite was then transferred to a water bath, whose temperature was controlled by a thermal controller. The brilliant blue was eventually released into water. The concentration of brilliant blue in the water bath was monitored

through the turbidity measurement by a spectrophotometer (Spectronic 301, Milton Roy Ltd.) operating at a wavelength of 555 nm. The result was shown in Fig. 5.5 with arbitrary unit. Drug release increased exponentially to a final value that is temperature dependent: low at $T>T_c$ and high at $T<T_c$, where T_c ($\approx$34 ^{0}C) is the low critical solution temperature (LCST). This is because the NIPA changes hydrophobicity with temperature. In such a thermo-sensitive system, hydrophobic drugs tend to be immobilized in the polymer network above T_c and diffuse out at temperature below T_c.[20] Pulsed release in response to the temperature switching between 20 ^{0}C and 39 ^{0}C has been achieved.

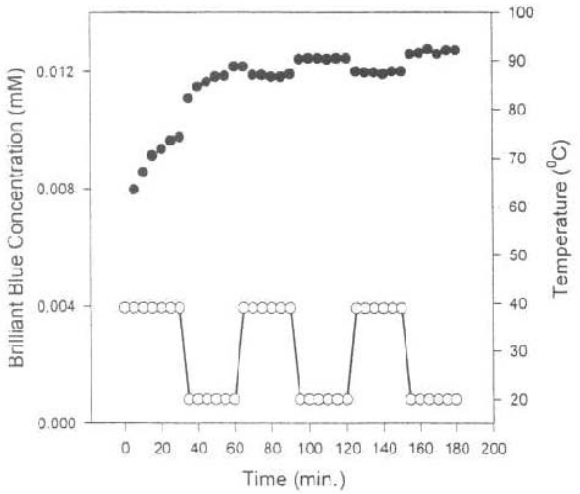

Figure 5.5. The composite membrane loaded with brilliant blue was transferred to a thermal bath. The concentration of brilliant blue in the bath was monitored by determining turbidity of the bath by using a spectrophotometer. Drug release increased exponentially to a final value that is temperature dependent.

Drug uptake and release capability strongly depends on the structure of the composite gel. Optimum range of the NIPA composition is found to be from 75% to 87% by volume. In the cited range, the NIPA particles form an interconnected network that provides a channel for diffusion of drug solution.

5.3 DEVELOPMENT OF TISSUE-SIMULATING OPTICAL PHANTOM: POLY-N-ISOPROPYLACRYLAMIDE SOLUTION ENTRAPPED INSIDE A HYDROGEL

The average turbid optical properties of NIPA polymer solution entrapped inside a polyacrylamide hydrogel (called a NIPA/PAAM gel system) were prepared and studied. The turbidity of such a system can be drastically changed by simply switching the temperature from below the low critical solution temperature of the NIPA around 33 °C to above. The absorption and scattering depends on samples with selected NIPA and blue dextran concentrations. It is found that the scattering of the optical phantom comes from the NIPA polymer chains and the absorption from the blue dextran. The turbid optical properties of an NIPA/PAAM gel system can be tuned to simulate biological tissues by optimizing compositions of NIPA and blue dextran and further modified by controlling the temperature.

5.3.1 Introduction

In both diagnostic and therapeutic applications of light in medicine, it is important to evaluate optical properties of tissues including the absorption coefficient and the

reduced scattering coefficient[21]. One of the challenging works in this area is to develop tissue-simulating turbid media (optical phantoms). Optical phantoms may be used to test and calibrate optical instruments or techniques. A typical optical phantom consists of de-ionized water mixed with minimally scattering Trypan blue dye as the absorbers and minimally absorbing polystyrene spheres as the scatterers[22].

In this study we report a new optical phantom that consists of an entrapped PNIPA polymer solution and a host matrix of a PAAM hydrogel. The PAAM hydrogel is transparent in the temperature range[23] that this study was carried out, and holds the NIPA solution so that the solution can be easily transported and handled in the laboratory. The NIPA polymer solution undergoes a phase transition from a hydrophilic to a hydrophobic structure rather abruptly at the LCST[24]. Below the LCST, NIPA is transparent and above the LCST, it becomes cloudy. The advantage of such an optical phantom is that its turbidity can be tuned reversibly by simply varying the temperature. For a neutral NIPA polymer solution, this LCST is found to be about 32 °C.[24, 25] By copolymerizing NIPA with acrylamide over the entire composition range, Taylor *et al* (1975)[26] and Hoffman *et al* (1987) research groups found that the LCST can be either up or down when the comonomer has respectively a smaller or larger group. Ability to shift the LCST of NIPA-like polymers provides excellent flexibility in tailoring transition for specific use[24].

The NIPA/PAAM gel system as a temperature-responsive turbid medium has potential to be used to dynamically simulate the turbid optical properties of biological tissues. For example, photocoagulation of biological tissues varies the optical properties of the tissues as the coagulation progresses. Current optical phantoms have static optical properties, which may not be varied once the phantoms are made. The new temperature-

responsive phantoms will have unique advantages for this type of simulations. Here, the average turbid optical properties of the NIPA/PAAM gel system were characterized using a multi-wavelength oblique-incidence reflectometer.

5.3.2 Sample Preparation

The samples were prepared in two steps. First, the NIPA polymer solution was obtained using free radical polymerization[24]. A mixture of 7.8 g of N-isopropylacrylamide and tetra-methyl-ethylene-diamine (240 μl) as an accelerator were dissolved in 100 ml of deionized and distilled water. Nitrogen gas was bubbled through the solution to remove dissolved oxygen. Then 40 mg ammonium persulfate was added to the solution as an initiator. The gelation process has been completed in about 30 minites. The sample was left in the reactor for overnight. Second, the NIPA solution was introduced into a pre-gel solution of acrylamide. The PAAM gel was made using the NIPA recipe with the 7.8 g of N-isopropylacrylamide monomers replaced by 5 g of acrylamide and 0.133 g of methylene-bis-acrylamide as a cross linker. The weight ratios between the PAAM and entrapped NIPA were 1:0.1 for phantom 1, 1:0.5 for phantom 3, and 1:0.1 with 0.05 g of blue dextran for phantom 2. The phantoms became opaque in either aqueous NaCl solution (>1.2 M) or a warm temperature bath (T>33 °C).

5.3.3 Optical Experiments

The experimental system for measuring the absorption coefficient and the reduced scattering coefficient of the optical phantom is described below. White light (Oriel, 75 W Xenon Arc Lamp) was delivered, and the diffuse reflectance was collected with a fiber

optic probe made from black delrin and 600 μm diameter, low-loss optical fibers. The source fiber was oriented at a 45° angle of incidence, and the nine collection fibers, arranged in a linear array, collected the diffuse reflectance. To correct for slight variations in collection efficiency from one detection fiber to the next, we calculated a correction factor for each fiber based on a calibration procedure using standard phantoms[27]. The detection system was composed of an imaging spectrograph (Oriel, Multispec 257), a CCD camera (Princeton Instrument Inc., 1530P), and a personal computer to automatically record the spectrum of the collected light through the wavelength range of 450 - 800 nm.

Phantom 1 [PAAM/NIPA 1:0.1], phantom 2 [PAAM/NIPA 1:0.1 with 0.05 g of blue dextran], and phantom 3 [PAAM/NIPA 1:0.5] were placed in a bath of water and heated to a temperature of approximately 60 °C for 1 hour until the phantoms were completely turbid. The fiber probe was aligned perpendicular to the surface of the phantoms. An exposed x-ray film was placed on top of the phantom to approximate a matched boundary condition for diffusion theory[28]. Ten measurements were performed, the absorption and reduced scattering spectra were evaluated for each diffusion reflectance measurement, and the results were averaged.

The turbidity (A) of the optical phantoms was obtained from the ratio of the transmitted light intensity (I_t) to the incident intensity (I_0), $A = -(1/L) \ln(I_t/I_o)$, where L is the length of the sample. The light transmission was measured by a spectrophotometer operating at the wavelength (λ) of 555 nm. An external water circulator controlled the temperature of the sample. In addition to the temperature sensor in the circulator, a thermocouple was placed inside the sample cell for temperature measurement. The cell

was sealed using a plastic film to prevent evaporation. The accuracy of the temperature measurement was estimated to be $\pm$0.5 °C.

5.3.4 Results

A typical result of turbidity as a function of temperature is shown in Fig. 5.6 for phantom 3. It is apparent that the turbidity of the sample increased drastically as the LCST about 33 °C. The optical properties of the phantoms presented below are all obtained at T = 60 °C at which the samples are in the high turbid state.

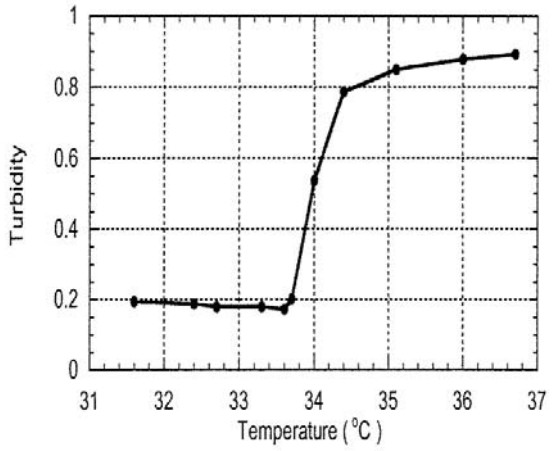

Figure 5.6. The turbidity of phantom 3 is plotted as a function of temperature. The low critical solution temperature is about 33° C, at which the turbidity exhibits a sharp increase.

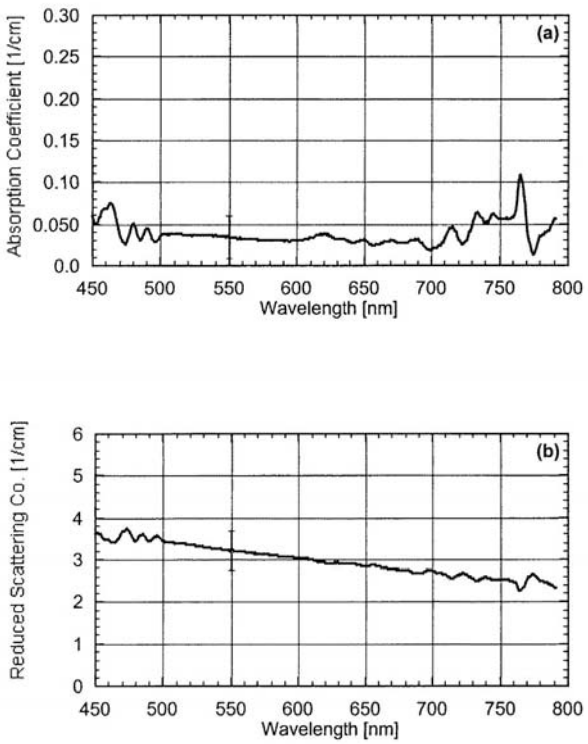

Figure 5.7. The average turbid optical properties of phantom 1 (PAAM:NIPA 1:0.1) at 60°C. (a) The absorption coefficient, u_a . (b) The reduced scattering coefficient, u'_s . The standard deviation error bar is plotted at 550 nm.

The average turbid optical properties of phantom 1 [PAAM/NIPA 1:0.1] are plotted in Fig 5.7. The absorption coefficient is negligible between 500 to 700 nm [Fig. 5.7a]. The reduced scattering coefficient decreased smoothly with an increase in wavelength [Fig. 5.7b]. In Fig. 5.8 we plot the average turbid optical properties of phantom 2 [PAAM/NIPA 1:0.1 with 0.05 g of blue dextran]. The absorption coefficient, μ_a, has a maximum of 0.63 cm^{-1} at 610 nm [Fig. 5.8a]. The reduced scattering coefficient also decreased smoothly with an increase in wavelength. In Fig. 5.9 we plot the average turbid optical properties of phantom 3 [PAAM/NIPA 1:0.5]. The absorption

between 500 to 700 nm was approximately 0.1 cm^{-1} [Fig. 5.9a]. The reduced scattering coefficient decreased very slightly with an increase in wavelength [Fig. 5.9b].

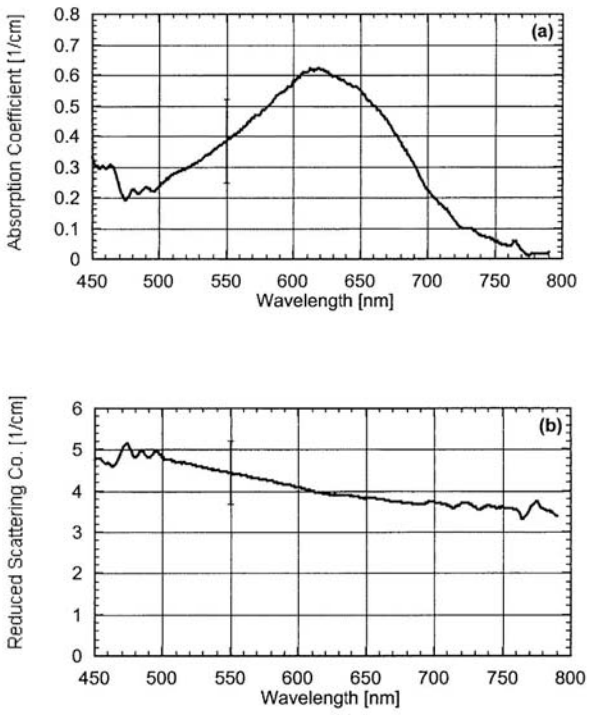

Figure 5.8. The average turbid optical properties of phantom 2 (PAAM:NIPA 1:0.1 with 0.05 g of blue dextran) at 60 ^{o}C. (a) The absorption coefficient, u_a . (b) The reduced scattering coefficient, u'_s . The standard deviation error bar is plotted at 550 nm.

The increase of approximately 1 cm^{-1} in reduced scattering of phantom 2 was probably caused by the blue dextran since phantom 2 and phantom 1 have the same PAAM/NIPA concentration. For phantom 3, we observed a much larger reduced scattering than the first phantom, but it was not 5 times larger as per concentration of NIPA. Finally, all three phantoms showed a similar trend in the reduced scattering spectra.

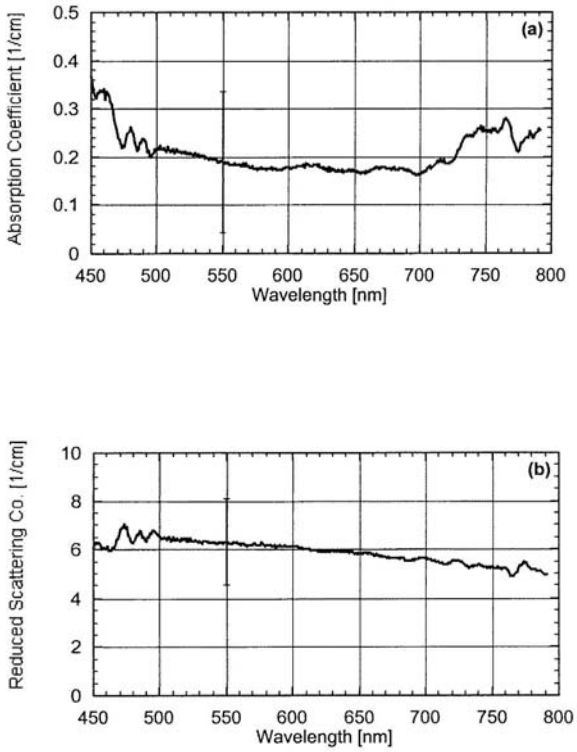

Figure 5.9. The average turbid optical properties of phantom 3 (PAAM:NIPA 1:0.5) at 60 ^{o}C. (a) The absorption coefficient, u_a . (b) The reduced scattering coefficient, u'_s . The standard deviation error bar is plotted at 550 nm.

5.3.5. Analysis

As a tissue-simulating turbid medium, the NIPA/PAAM gel system exhibits a unique property that its turbidity can be tuned by adjusting the external temperature as shown in Fig. 5.6. Here, the PAAM gel network as a host matrix has negligible contribution to light absorption and scattering, and is insensitive to the temperature. The temperature–dependence turbidity change comes from the linear NIPA polymer chains that are entrapped inside the PAAM gel. When these NIPA chains are heated, the

polymer molecular dimensions changes abruptly from a state of well-solved random coils at the temperature below the LCST (33 °C) to a state of tightly packed globular particles at the temperatures above. This is then followed by the onset of aggregation of individual polymer chains due to mainly the intermolecular interaction among the hydrophobic groups distributed on the surface of the resulting globular particles of the polymer in aqueous medium[29]. This spatial concentration fluctuation results in scattering light and reducing the transmission of visible light through the gel. The reduction of the transmission is quantified in terms of the sample turbidity. It is noted that the phase transition process between the transparent to the cloudy state in NIPA/PAAM gel system is completely reversible as a function of temperature.

The temperature-dependent turbidity of the NIPA entrapped system is similar to that of the free NIPA solution[24] and the pure NIPA gel[22]. However, the NIPA/gel undergoes the clear to cloudy transition near the LCST while its shape remains the same. In contrast, the NIPA solution does not have a shape, and the NIPA gel has to change its volume near the LCST. Therefore, the NIPA entrapped system is a better one for optical phantom applications.

Contribution from NIPA polymer to the reduction of transmitted light is mainly through the light scattering mechanism as revealed from large scattering coefficient but very small absorption coefficient (Figs. 5.7 and 5.9). Increase of the NIPA concentration can result in substantially increase of the reduced scattering coefficient. To enhance the optical absorption of the NIPA/PAAM phantom, blue dextran is introduced into the system. As shown in Fig. 5.8, the NIPA/PAAM gel system with blue dextran indeed exhibits a larger absorption coefficient. By selecting compositions of NIPA and blue

dextran, the scattering coefficient and absorption coefficient of the NIPA/PAAM gel system can be adjusted to simulate biological tissues. It is noted that the reduced scattering coefficient of the NIPA/PAAM gel system decreases with wavelength. This may indicate that the NIPA polymer chains aggregate to form clusters with a broad size distribution. When the wavelength becomes longer than the cluster sizes, the scattering coefficient decreases.

The temperature-dependent turbidity of this new type of gels will find many applications in optically simulating biological tissues. The optical properties of biological tissues are frequently found to vary dynamically. The variation of optical properties due to photocoagulation mentioned earlier is an example in laser therapeutics. The optical properties of hemoglobin vary with its oxygenation saturation, which is an important physiological parameter that changes with time or environment. The scattering coefficient of blood varies with the concentration of glucose because glucose modifies the refractive index of the interstitial fluid and thus changes the scattering cross section of the scatters. When a device or a technique is developed for applications involving this type of dynamic parameters, a dynamically variable phantom such as the one developed in this research is highly desired.

The dynamic phantoms may be useful in some other scenarios. Multiple static optical phantoms are sometimes made to check a device or technique for a range of optical properties. The temperature-dependent optical phantoms may be used instead, where the optical properties can be varied with arbitrary resolution. A single dynamic phantom will cover a wide range of optical properties. Using a temperature field, one

may produce a continuous distribution of optical properties in the phantoms, which would be difficult to accomplish using static phantoms.

5.4 CONCLUSION

The SR/NIPA composite gels combine the strength of the silicone rubber and the wettability of the NIPA gel. The hydrophobic SR provides strong mechanical support, while the hydrophilic NIPA hydrogel enhances the wettability of the system. The NIPA particles form an interconnected network that provides a channel for diffusion of drug solution. The composite membrane could be used to release drug under external stimuli such as temperature and pH and has promising attributes for wound dressing and other uses.

As a possible candidate for tissue-simulating phantoms, the turbid optical properties of the NIPA/PAAM gel system were investigated using a multi-wavelength oblique-incidence reflectometer. The turbidity of the NIPA/PAAM gel system can be easily changed by adjusting the sample temperature and NIPA concentration. It is found that the NIPA plays a crucial role in light scattering while the blue dextran determines the light absorption. The reduced scattering coefficient and absorption coefficient of the NIPA/PAAM gel system can be adjusted to simulate biological tissues by choosing the compositions of NIPA and blue dextran.

5.5 CHAPTER REFERENCES

[1] Hayward, P. G.; Morrison, W. A. Australian Prescriber, **1996**, 19, 11.

[2] Findlay, D. Australian Family Physician, **1993**, 23, 824.

[3] Ryan, T. J. Dermatologic Therapy, **1993**, 11, 207.

[4] Baranoski, S. Home Healthcare Nurse, **1999**, 17, 19.

[5] Hall, C. M. Geriatric Nursing, **1997**, 18, 266.

[6] Palmieri, B.; Gozzi, G. International Journal of Dermatology, **1995**, 34, 506.

[7] Clugston, P. A.; Vistnes, M. D.; Perry, L. C.; Maxwell, G. P. Annals of Plastic Surgery, 1995, 34, 12.

[8] Gold, M. H. Journal of the American Academy of Dermatology, **1994**, 30, 506.

[9] Ahn, S. T.; Monafo, W. W.; Mustoe, T. A. Arch. Surg**, 1991**, 128, 499.

[10] Sproat, J. E.; Dalcin, A.; Weitauer, N.; Roberts, R. S. Plastic and Reconstructive Surgery, 1992, 90, 988.

[11] Hirotsu, S.; Hirokawa, Y.; Tanaka, T. J. Chem Phys, **1987**, 87, 1392.

[12] Chen, G.; Hoffman, A. S. Macromolecular Rapid Communication, **1995**, 16, 175.

[13] Kim, Y. H.; Bae, Y. H.; Kim, S. W. J. Contr. Rel., **1994**, 28, 143.

[14] Ilmain, F.; Tanaka, T.; Kokufuta, E. Nature, 1991, 349, 400.

[15] Hu, Z.; Zhang, X.; Li, Y. Science, **1995**, 269, 525.

[16] Hu, Z.; Chen, Y.; Wang, C.; Zheng, Y.; Li, Y. Nature, **1998**, 393, 149.

[17] Efros, A. L. Physics and Geometry of Disorder––Percolation Theory. Moscow, Mir Publisher, **1986**.

[18] Treloar, L. R. G. The physics of rubber elasticity. Oxford, Clarendon Press, **1975**.

[19] Zhang, X.; Hu, Z.; Li, Y. J. Appl. Polym. Sci, **1997**, 63, 1851.

[20] Schild, H. G. Prog. Polym. Sci, **1996**, 17, 163

[21] Pickering, J W, Prahl, S A. Vanwieringen, N, Beek, J F, Sterenborg, H J C M and van Gemert, M J C. *Appl. Opt.* **1993**, 32, 339.

[22] Li, Y, Wang, G and Hu, Z. Macromolecules **1995**. 28, 4194.

[23] Tanaka, T. Intelligent gels ACS symp. **1992**, 480, 1.

[24] Schild, H. G. *Prog. Polym. Sci.* **1992**, 17, 163.

[25] Schild, H. G. and Tirrell, D. A. *J. Phys. Chem.* **1990**, 94, 4352.

[26] Taylor, L. D. and Cerankowski, L. D. J. Polym. Sci., Pt. A: Polym. Chem. **1975**, 13, 2551.

[27] Farrell, T. J., Patterson, M. S. and Wilson, B. C. *Med. Phys.* **1992**, 19, 879.

[28] Lin, S P, Wang, L H, Jacques, S L and Tittel, F. K. OSA Technical Digest Series (Optical Society of America, Washington, D. C.), **1996**, 44, 9.

[29] Fujishige, S., Kubota, K. and Ando I. *J. Phys. Chem*. **1989**, 93, 3311.

CHAPTER 6

CONCLUSION

This research includes: the theoretical and experimental studies of polymer gels on swelling kinetics, spinodal decomposition, and convection in gel matrix; applications of polymer gels in wound dressing, tissue-simulating optical phantom and gel display.

In studies on kinetics of gel swelling, Li and Tanaka's theory was extended by including the motions of both the solvent and the gel network. Analytical solutions of solvent and network movement are derived from collective diffusion equations for a long cylindrical and a large disk gel. The motion patterns of solvent have been obtained. It is found that swelling processing is slower than is expected by the pure diffusion theory. From analytical solutions of our generalized gel swelling equations, we can obtain gel-swelling behavior not only at the surface but also in the interior of gels**.** Analysis presented here could be used for many cases where non-spherical gels are used and in many applications such as drug delivery for better understanding.

The equations for gel swelling in pure liquid were modified and extended to gel swelling in polymer solution. Gels have smaller equilibrium diameters in polymer solution (such as PVA) than that in pure liquid (such as water). The equilibrium diameters of gel decrease with increase of polymer concentration. The partial pressure of polymer solution is quadratically related to its concentration in dilute polymer solution. The swelling of gels in polymer solution is slowed down by polymer chains clogging water intake of gels**.** The relaxation times of gels shrinking in polymer solution with various concentrations are not different within experimental error. The experimental results are in excellent agreement with the theory.

Theoretical studies of convection in gel matrix have been given. The convection in gel network is analyzed. The governing equations of the convection were modified to accommodate the convection in gel network. Two network numbers were proposed as new dimensionless parameters in controlling the convection in gel network. The analysis predicts the friction between solvent and gel network is the dominant force against convection. Approaching to spinodal decomposition of a gel would lead to more chance for the convection to occur even though the convection has less chance to happen otherwise. Further theoretically and experimentally researches on the convection in gel network could help for better understanding the interaction between gel network and solvent, and also for applications such as thermal conductivity of gel.

Kinetics of Spinodal decomposition of NIPA polymer gel is investigated using the turbidity and ultrasonic techniques. By probing the movement of domains, a possible time-dependent gel structure in spinodal decomposition region is presented.

NIPA gel undergoes volume phase transition around 34 ^{0}C. The light turbidity

has a jump at that temperature. Usually the opaque remains even after a sample is totally shrunken. Our experiment shown that the turbidity can disappear if the sample stay long enough at that temperature or even never show up at higher temperature if it is heated quite slowly. The kinetics of turbidity reveals the mechanism of the domains induced in phase separation and improves our understanding of both opaque and phase separation at transition stage.

NIPA gel's domain structure is meta-stable. It is induced by quick dynamical process. The free energy is minimized locally by introducing domain structure through spinodal decomposition. Optical turbidity and ultrasonic attenuation are associated with domain structure. Slow heating will suppress the showing up of domains above the transition temperature. Domains could be formed in phase separation only if heating process is quick. And existing domains could disappear if time is long enough. Volume phase transition in polymer gel is very unique phase transition, represented by its global mechanism, which is responsible for spinodal decomposition, turbidity dynamics and slow behavior.

Polymer gels with engineered surface patterns were implemented. NIPA gel deposited on the surface of an acrylamide gel can be used as responsive gel display. A dynamically measurement technique of local shear modulus and swelling ratio of a gel is presented based on an engineered surface pattern as square array.

Polymer gels with engineered surface patterns could be synthesized using different materials combination. In one implementation, non-polymer materials such as metal or dielectric materials could be incorporated onto gel surface with certain pattern. The patterns will always exist after a designed pattern being transferred to a gel surface. Since

a gel is environmentally responsive, and can swell or shrink in response to temperature, polymer solution pressure, and electric field, so gel surface pattern will change accordingly. A gel with such surface pattern can be used as sensors, responsive grating. Another example is gel/gel system where two or more than two types of gels (sometime, one of them could be polymer chains) are incorporated together to designed pattern. The first type of gel is synthesized first, the second (or the rest for multi-gel system) type of gel can be incorporated into the first type of gel in different ways, and the second type of gel could undergo phase transition by environmental changes including temperature, polymer solution pressure, and electric field. The method of photo-induced cross-linking could be used to form the second type gel and a surface pattern will be transferred to the surface of this gel system. The gel system takes advantage of gel phase transition so the refractive indexes mismatch after phase transition, and a built-in pattern will show up. Applications include display, sensor, smart window curtain, and indicator.

The structure of a gel with an engineered surface could include, surface coated and patterned by mask; two types of polymers with interpenetrating structure such as NIPA/PAAM composite gel system shown in this chapter, or the second type gel can be polymer chains which are physically trapped inside of the first type gel; Another possible option for future experiment could be a gel/gel system where the first type gel is a porous gel and the second type gel is trapped inside the porous space of the first type gel only. So the first gel may only function as porous matrix to hold the second gel. If this structure is formed only on surface of the matrix, then such surface patterned gel has a unique application due to its different mechanical characteristics, and swelling mechanism.

To enhance the drug uptake and release capacity of silicone rubber (SR), NIPA hydrogel particles have been incorporated into a SR membrane. This SR/NIPA composite gel has promising attributes for wound dressing and other uses.

The SR/NIPA composite gels combine the strength of the silicone rubber and the wettability of the NIPA gel. The hydrophobic SR provides strong mechanical support, while the hydrophilic NIPA hydrogel enhances the wettability of the system. The NIPA particles form an interconnected network that provides a channel for diffusion of drug solution. The composite membrane could be used to release drug under external stimuli such as temperature and pH and has promising attributes for wound dressing and other uses.

Tissue-simulating optical phantom has been synthesized and analyzed using NIPA solution trapped inside a hydrogel. As a possible candidate for tissue-simulating phantoms, the turbid optical properties of the NIPA/PAAM gel system were investigated using a multi-wavelength oblique-incidence reflectometer. The turbidity of such a system can be easily changed by adjusting the sample temperature and NIPA concentration. It is found that the NIPA plays a crucial role in light scattering while the blue dextran determines the light absorption. The reduced scattering coefficient and absorption coefficient of the NIPA/PAAM gel system can be adjusted to simulate biological tissues by choosing the compositions of NIPA and blue dextran.

REFERENCE LIST

Ahn, S. T.; Monafo, W. W.; Mustoe, T. A. Arch. Surg**, 1991**, 128, 499.

Bansil, R.; Liao, G.; Falus, P. Physica, **1996**, A 231, 346.

Baranoski, S. Home Healthcare Nurse, **1999**, 17, 19.

Bates, F. S.; Wiltzius, P. J. Chem. Phys. **1989**, 91, 3258.

Borchard, W. Ber Bunsen-Ges Phys Chem **1977**, 81, 989.

Borchard, W. Eyr Polym J **1978**, 14, 661.

Cahn, J. W.; Hilliard, J. H. J. Chem. Phys. **1958**, 28, 258; Cook, H. E. Acta Metall. **1970,** 18, 297.

Chen, G.; Hoffman, A. S. Macromolecular Rapid Communication, **1995**, 16, 175.

Cherayil, B. J. et al. Macromolecules **1986**, 19, 2770.

Clugston, P. A.; Vistnes, M. D.; Perry, L. C.; Maxwell, G. P. Annals of Plastic Surgery, 1995, 34, 12.

Dagani, R. Chem Eng News **1997**, 75, 26.

Dhont, J. K. G. J Chem Phys **1996**, 105, 5112.

Dusek, K.; Prins, W. Adv Polym Sci **1969**, 6, 1.

Eck, W.; Wilson, H. R.; Cantow, H. J. Adv Mater **1995**, 7, 800.

Efros, A. L. Physics and Geometry of disorder––Percolation Theory. Moscow, Mir Publisher, **1986**.

Eskinazi, S. Principles of Fluid Mechanics. 2th Edition, Allyn and Bacon, Boston, **1968**.

Farrell, T. J., Patterson, M. S. and Wilson, B. C. *Med. Phys.* **1992**, 19, 879.

Findlay, D. Australian Family Physician, **1993**, 23, 824.

Flory, P. J. Principles of Polymer Chemistry, Cornell University Press, Itaaca, N.Y., **1953**.

Fujishige, S., Kubota, K. and Ando I. *J. Phys. Chem*. **1989**, 93, 3311.

Gehrke, S. H. Adv. Polym. Sci., **1993**, 110,80.

Gemert, M. J. C. *Appl. Opt.* **1993**, 32, 339.

Gold, M. H. Journal of the American Academy of Dermatology, **1994**, 30, 506.

Grabar, K. C., Freeman, G. G., Hommer, M. B. & Natan, M. J. Anal. Chem. **1995**, 67, 735.

Gunton, I. D.; Miguel, M. S.; Sahni, P. S. In Phase Transition and Critical Phenomena, Edited by Domb, C and Lebowitz, J. L. Academic, NY, **1983**, 8.

Hall, C. M. Geriatric Nursing, **1997**, 18, 266.

Hayward, P. G.; Morrison, W. A. Australian Prescriber, **1996**, 19, 11.

Heskins, M.; Guillet, J. E. J. Macromolec. Sci. Chem. **1969**, 2, 1441.

Hirose, H.; Shibayama, M. Macromolrcules **1998**, 31, 5336.

Hirotsu, S. Japn. J. Appl. Phys. **1985**, 24, 396.

Hirotsu, S.; Hirokawa, Y.; Tanaka, T. J. Chem Phys, **1987**, 87, 1392.

Hoffman A. S. Macromol. Symp. **1996**, 101, 443.

Hoffman, A. S. J. Controlled Release, **1987**, 6, 297.

Howle, L.; Behringer, R. P.; Georgiadis, J. G. Nature, **1993**, 362, 230.

Hu, Z.; Chen, Y.; Wang, C.; Zheng, Y.; Li, Y. Nature, **1998**, 393, 149.

Hu, Z.; Zhang, X.; Li, Y. Science, **1995**, 269, 525.

Ilmain, F.; Tanaka, T.; Kokufuta, E. Nature, 1991, 349, 400.

Imisides, M. D., John, R., & Wallace, G. G. Chemtech. **1996**, 26, 19.

Inomata, H.; Yagi, Y.; Saito, S. Macromolecules, **1991**, 24, 3962.

Kajiwara, K. et al. Polymer Gels; Plenum Press: New York and London, 1990.

Kielhorn, L.; Muthukumar, M. J Chem Phys **1999**, 110, 4079.

Kim, Y. H.; Bae, Y. H.; Kim, S. W. J. Contr. Rel., **1994**, 28, 143.

Landau, L. D.; Lifshitz, E. M. Theory of Elasticity; Pergamon press: Oxford, 1986.

Li, C., Hu, Z. & Li, Y. J. Chem. Phys. **1994**, 100, 4645.

Li, Y. Ph. D. Thesis, MIT, unpublished **1989**

Li, Y., Li, C. & Hu, Z. J. Chem. Phys. **1994**, 100, 4637.

Li, Y.; Tanaka, T. Ann. Rev. Mater. Sci. **1992,** 22, 243.

Li, Y.; Tanaka, T. J. Chem. Phys. **1990,** 92, 1365.

Li, Y.; Tanaka, T. J. Chem. Phys. **1990**, 92, 1365.

Li, Y.; Tanaka, T. Polymer Gels; Plenum Press: New York, 1991.

Li, Y.; Tanaka, T. Springer Proceedings in Physics, Heidelberg, **1990,** 52, 44.

Li, Y.; Tanaka, T.; J Chem Phys. **1989**, 90, 5161.

Li, Y.; Wang, G.; Hu, Z. Macromolecules, **1995**, 28, 4194.

Liao, G.; Xie, Y.; Ludwig, K. F.; Bansil, R.; Gallagher, P. Phys Rev E: Stat Phys Plasmas Fluids Relat Interdiscip Top **1999**, 60, 4473.

Lin, S P, Wang, L H, Jacques, S L and Tittel, F. K. OSA Technical Digest Series (Optical Society of America, Washington, D. C.), **1996**, 44, 9.

Matsuo, E. S.; Tanaka, T. J. Chem. Phys., **1988**, 89,1695.

Merkle G. et al., Macromolecules **1993**, 26, 2736.

Mills, N. J. In Encyclopedia of Polymer Science and Engineering; Mark H. F., Ed., Wiley: New York, **1988**, 10, 493

Onuki**,** A. Dynamics and Statistics of Patterns; World Science, 1989.

Onuki**,** A.; Adv. Polym. Sci. **1993**, 109, 97.

Onuki, A.; Puri, S. Phys Rev E: Stat Phys Plasmas Fluids Relat Interdiscip Top **1999**, 59, 1331.

Osada, Y.; Okuzaki, H.; Hori, H. Nature **1992**, 355, 242.

Otake, K.; Inomata, H.; Yagi, Y.; konno, M.; Saito, S. Polym Commun **1989**, 30, 203.

P. K. Pathria, Statistical Mechanics, Pergamont Press, New York, **1989**.

Palmieri, B.; Gozzi, G. International Journal of Dermatology, **1995**, 34, 506.

Papadakis, E.P. In Methods of Experimental Physics: Ultrasonic; Edmonds, P. D., Ed.; Academic: New York, **1981**, 19, 237.

Peppas, N. A. & Langer, R. Science **1994**, 263, 1715.

Peters, A.; Candau, S. J. Macromolecules **1986**, 19, 1952.

Peters, A.; Candau, S. J. Macromolecules **1988**, 21, 2278.

Pickering, J W, Prahl, S A. Vanwieringen, N, Beek, J F, Sterenborg, H.; and van

Ryan, T. J. Dermatologic Therapy, **1993**, 11, 207.

Sato Matsuo, E.; Tanaka, T. J Chem Phys **1988**, 89, 1695.

Sato-Matsuo, E. & Tanaka, T. Nature, **1992**, 358, 482.

Schild, H. G. and Tirrell, D. A. *J. Phys. Chem.* **1990**, 94, 4352.

Schild, H. G. Prog. Polym. Sci, **1996**, 17, 163

Sedlacek, B. Collect Czech Chem Commun **1967**, 32, 1308.

Shattuck, M. D.; Behringer, R. P.; Jonson, G. A.; Georgiadis, J. G.; Phys. Rev. Lett., **1995**, 73,1934.

Shibayama, M.; Nagai, K. Macromolrcules **1999**, 32, 7461.

Shibayama, M.; Tanaka, T. Adv. Polym. Sci. **1993,** 109, 1.

Silberberg-Bouhnik M. et al., J. Polym. Science **1995**, 33, 2269

Sproat, J. E.; Dalcin, A.; Weitauer, N.; Roberts, R. S. Plastic and Reconstructive Surgery, 1992, 90, 988.

Suzuki, A., Yamazaki, M. & Kobiki, Y. J. Chem. Phys. **1996**, 104, 1751.

Tanaka, H.; Sigehuzi, T. Phys. Rev. Lett. **1995**, 75, 874.

Tanaka, T. Am. Chem. Soc. Symp. **1992**, 480, 1.

Tanaka, T. Phys. Rev. Lett. **1978**, 40, 820.

Tanaka, T., Sun, S. T., Hirokawa, Y., Katayama, S., Kucera, J., Hirose, Y. & Amiya, T. Nature **1987**, 325, 796.

Tanaka, T.; Fillmore, D. J. Chem. Phys. **1979**, 70, 1214.

Tanaka, T.; Hocker L.; Benedek, G. J. Chem. Phys. **1973**, 59, 5151.

Tanaka, T.; Ishiwata, S.; Ishimoto, C.; Phys. Rev. Lett., **1977**, 38, 14.

Taylor, L. D. and Cerankowski, L. D. J. Polym. Sci., Pt. A: Polym. Chem. **1975**, 13, 2551.

Tokita, M. Adv. Polym. Sci., **1992**, 110, 27.

Treloar, L. R. G. The physics of rubber elasticity. Oxford, Clarendon Press, **1975**.

Tritton, D.J. Physical Fluid Dynamics, 2nd ed. Oxford, Oxford University Press, England, **1989**.

Vasilevskaya, V. V. Macromolecules **1992**, 25, 384.

Vink, H. Europ. Polym. J. **1971**, 7, 1411.

Vink, H. Europ. Polym. J. **1974**, 10, 149.

W. Nisch, J. Bock, U. Egert, H. Hammerle, and A. Mohr, Biosensors & Bioelectronics. **1994**, 9, 737.

Wang, J. & Chen, Q. Anal. Chem. **1994**, 66, 1007.

Weissman, J. M., Sunkara, H. B., Tse, A. S. and & Asher, S. A. Science. **1996**, 274, 959.

Weissman, J. M.; Sunkara, H. B.; Tse, A. S.; Asher, S. A. Science, **1996**, 274, 959.

Wiltzius, P.; Bates, F. S.; Heffner, W. R. Phys. Rev. Lett. **1988**, 60, 1538.

Yuan, K.; Hu, Z.; Li, Y. Appl Phys Lett **1999**, 74, 2233

Zhang, X.; Hu, Z.; Li, Y. J. Appl. Polym. Sci, **1997**, 63, 1851.

Zrinyi, M.; Rosta, J.; Horkay, F. Macromolecules **1993**, 26, 3097**.**